Democratic and Popular Republic of Algeria

Ministry of Higher Education and Scientific Research

University Mohamed Khider of Biskra

Faculty of Exact Sciences and Science of Nature and Life

Department of Material Sciences

Thesis

Presented to obtain the degree of

Doctorate

Speciality: Physics

Entitled:

Elaboration and characterization of undoped and doped titanium dioxide thin layers by sol gel (spin coating) for photocatalytic applications.

Presented by:

MESSEMCHE RADHIA

Publicly defended on: **11 / 03 / 2021**

To the Jury composed by:

M^{r} .N.Attaf	Professor	University of Constantine	President
M^{me}. H. Saidi	Professor	University of Biskra	Supervisor
M^{r}. A. Attaf	Professor	University of Biskra	Co-Supervisor
M^{r}. E. Belbacha	Professor	University of Batna1	Examiner
M^{r}. S. Rahmane	Professor	University of Biskra	Examiner

Acadymic year 2020-2021

Dedication

I dedicate this thesis

To my father and my mother

To my Husband who supported me to make this work easier

To my son dhiyaeddine

To all my sisters

To all my friends

Radhia

Acknowledgements

It was for me a great chance to be able to prepare this thesis with laboratory of the thin films of our university, which I have to achieve it thanks to the contribution of a great number of persons, and that no matter what I say, I will never be able all as much them to thank. But before that I thank GOD the whole powerful for having agreed his infinite kindness, courage, the force and patience to complete this modest work.

I express my deep gratitude has Mister **Nadhir Attaf** Professor at university of Constantine for the honor that makes to me by accepting the presidency of this jury. After that, I make a point of profoundly thanking to my director for thesis **M^me^ Hanane Saidi**, Professor at the Department of sciences of matter at Faculty of Exact Sciences and Sciences of Nature and Life in Mohamed KHIDER University, Biskra, for his confidence that he testified to me during this work, for her support and its councils, accompanied me with the daily in the preparation by this work with greatest assiduity, and to devote necessary time to discussions and human remarkable qualities, and his daily presence was a major asset for the realization of this work, as well from a scientific point of view as moral, thanks to him my efforts was leaded. I make a point of deeply thanking to **M^r^. Abdallah Attaf**, Professor at the Department of sciences of matter at Faculty of Exact Sciences and Sciences of Nature and Life in Mohamed KHIDER University, Biskra, for his support in the preparation of this work as a co-director

My sharp thanks to:

M^r^. Belbacha Eldjemai Professor at university of Batna1who agreed to agree to belong to the jury and to examine my work..

M^r^. Saäd Rahmane Professor at the Department of sciences of matter in Med university of Biskra, who agreed to accept to belong to the jury and to examine my work.

I address to my sincere thanks to all the teachers of the department of sciences of matter especially the teachers of physics, everyone by his name, for all for their advised councils and their continuous encouragement. I to also thank my friends in the laboratory of thin films whom with them I have realized this work.

Contents

General introduction

General introduction

The effect of titanium dioxide was discovered in 1967 by Professor Fujishima unexpectedly when an electrode of titanium dioxide in an aqueous solution was exposed to strong light. Fujishima observed bubbles coming out of the surface of the electrode, and these bubbles do not come out when there is no light. It was later found that these bubbles consist of oxygen gas. He also confirmed the generation of hydrogen gas on the opposite electrode, which was composed from platinum element. Thus, it was concluded that the water is decomposed to an oxygen gas and hydrogen gas. The phenomenon which happened on the surface of titanium dioxide was photocatalysis. This phenomenon was known later as the Honda-Fujishima effect. These results were published in a scientific research in 1972 and the results of this research attracted the attention of many scientists around the world. [1] Japanese scientists used this phenomenon to produce hydrogen from water using sunlight to obtain a clean source of energy.

Fujishima proved an experiment for producing hydrogen from photocatalysis phenomenon, where he painted the roof of his house with a thin layer of titanium dioxide in the presence of sun light, and he was succeed to produce hydrogen.

In 1989, he experimented with painting the ceiling and walls of an operating room in a hospital by titanium dioxide thin film and the result was a decrease in the amount of bacterial contamination in that room and that became the material has since been used as an anti-bacterial and in air purification systems [2]. The removal of dangerous organic contaminants derived from human productive activities which present in the environment and particularly in water sources. This has become an important research topic aimed toward the development of sustainable water treatment strategies and processes [3]. TiO_2 is one of the promising materials in the field of photocatalysis owing to its unique physicochemical properties such as low-cost, non-toxicity, photostability, and biocompatibility [4].

Using titanium dioxide as a water purifier powder is an effective method, but there are problems after the purification process which lies to purification the water from the powder. The solution to this problem was to use titanium dioxide (TiO_2) as a thin film.

There are number of methods have been employed to fabricate TiO_2 thin films, including reactive sputtering, chemical vapor deposition, and sol–gel process. The sol-gel technique offers many advantages over other deposition techniques due to the use of very simple and inexpensive equipment. Novel morphologies can be obtained and novel physical properties may be expected depending on the structures which are not produced by the usual

processes. This simple method has also advantages to produce TiO_2 thin films in a relatively shorter processing time at lower temperatures. The morphological properties of sols and gels can give rise to the formation of films and thus considerably increase the anisotropy of the material and its chemical reactivity [5]. However, it is very important to study the evolution of different physical and chemical properties of TiO_2, prepared by a suitable technique which is effective for controlled modification [5, 6, 7].

In this thesis, synthesis of TiO_2 thin film by spin coating method is studied. The influence of the parameters to the structural, optical and photocatalysis properties is investigated. The effect of the structural and optical properties of TiO_2 thin films to the photocatalysis in the degradation of methylene blue which used as a model of organic pollution is investigated.

Chapter one presents a review of thin films and growth modes. In addition, it talks about titanium dioxide (TiO_2), defects types, the structural, optical and electronic properties and doping of TiO_2 Photocatalysis application, photocatalysis mechanism and organic pollution is discussed in the last part.

Chapter two presents a review of sol-gel (spin-caoting) method and the characterization techniques of films.

Chapter three contains an explanation of the effect of the solution concentration on the structural, optical and morphological properties of TiO_2. As well as, it was confirmed that the prepared thin films can used as a photocatalyst by the studied their efficiency in degradation of methylene blue solution.

Chapter four talks about the effect of rotation speed of substrate on the structural, optical, and morphological properties of TiO_2 thin films which were used to produce hydrogen gas through photocatalysis application.

In chapter five, the effect of the molar ratio between the tetranium (IV) isopropoxide concentration and acetyl acetone concentration on the properties of thin films TiO_2 and its influence on the photocatalytic property by calculating the photodegradation rate of methylene blue solution was studied in the first part. In the last part, the influence of Ga doping concentration on TiO_2 thin films structural, optical, and photocatalysis properties was examined. Finally we move general conclusion and future work.

The objective of this work is to study the structural, optical and photocatalytic properties of TiO_2 thin films prepared by sol- gel (spin-coating) process. To obtain the optimal conditions to produce a best TiO_2 thin films used as a photocatalyst in removing organic pollutants with highest photodegradation rate.

Chapter I

Titanium dioxide Thin Films (TiO_2) and Photocatalytic activity Applications

I.1 Introduction

Titanium is a metal, so by definition is a reduced simple body, its usual oxide is chemically speaking titanium dioxide TiO_2 which is one of the most used materials in our everyday life. It is a harmless white material.

Many industries, such as dye, textile, cosmetic, leather, paper, foods, plastics and pharmaceuticals industries, use dyes to color their products. Many of these dyes could pose a serious threat to living organisms and they should be removed or degraded prior to discharge to the environment [3]. Air and water pollution is a major risk to human health and the environment. To remove these pollutants, titanium dioxide thin films are a good photocatalyst in the application of photocatalysis. Its anatase form appears to be the most photoactive.

This chapter is concerned with thin films and some general properties of titanium dioxide and Photocatalytic activity Application.

I.2 Thin films

I.2.1 Thin films growth process

Thin films are deposited on a substrate by thermal evaporation, chemical decomposition, and/or the evaporation of source materials by the irradiation of energetic species or photons. Any thin-film deposition process involves three main steps:

1. Production of the appropriate atomic, molecular, or ionic species.
2. Transport of these species to the substrate.
3. Condensation on the substrate, either directly or via a chemical and/or electrochemical reaction, to form a solid deposit.

The unit species, on impacting the substrate, lose their velocity component normal to the substrate (provided the incident energy is not too high) and are physically adsorbed on the substrate surface. The adsorbed species are not, initially, in thermal equilibrium with the substrate initially and move over the substrate surface. In this process, they interact among themselves forming bigger clusters.

The clusters or the nuclei, as they are called, are thermodynamically unstable and may tend to desorb in time, depending on the deposition parameters. If the deposition parameters are such that a cluster collides with other adsorbed species before getting desorbed, it starts growing in size. After reaching a certain critical size, the cluster becomes thermodynamically

stable and the nucleation barrier is said to have been overcome. This step involving the formation of stable, chemisorbed, critical-sized nuclei is called the nucleation stage.

The critical nuclei grow in number as well as in size until a saturation nucleation density is reached. The nucleation density and the average nucleus size depend on a number of parameters such as the energy of the impinging species, the rate of impingement, the activation energies of adsorption, desorption, thermal diffusion, and the temperature, topography, and chemical nature of the substrate. A nucleus can grow both parallel to the substrate by surface diffusion of the adsorbed species, and perpendicular to it by direct impingement of the incident species. In general, however, the rate of lateral growth at this stage is much higher than the perpendicular growth. The grown nuclei are called islands. The next stage in the process of film formation is the coalescence stage, in which the small islands start coalescing with each other in an attempt to reduce the substrate surface area. This tendency to form bigger islands is termed agglomeration and is enhanced by increasing the surface mobility of the adsorbed species,

Larger islands grow together, leaving channels and holes of uncovered substrate. The structure of the films at this stage changes from discontinuous island type to porous network type. Filling of the channels and holes forms a completely continuous film [8].

I.2.1 Growth modes

In the early stage of research on thin films, it soon became clear that it was imperative to understand the mechanisms, which control and define the growth of thin films to achieve good control over these novel materials. Hence the huge effort of the scientific community to characterize, optimize and understand film growth.

Evidently, thin films are composed of atoms, which are their zero-dimensional building blocks. Extending this concept, nanoparticles (also termed 'nano-crystals') can also serve as zero-dimensional building blocks which by self-assembly may form two-dimensional thin films or three-dimensional crystals (so-called 'nanoparticle super-lattices'), analogous to atomic films and crystal lattices[8].

Atomic thin film growth is understood to occur in form of three basic growth modes, which result from competing energy terms during the film deposition, i.e. Frank van der Merwe, Stranski-Krastanov, and Volmer-Weber growth. Various processes occur when atoms arrive at a substrate during thin film growth. That is adsorption, desorption, diffusion, finding or leaving

of equilibrium positions. These processes occur simultaneously averaged over the ensemble of arriving atoms [9, 10, 11].

As in the case of atoms, the interplay of various free energy terms determines the way on how the nanoparticles (NPs)films will grow. These are in detail [12]: an entropic contribution E_{TS}, an inter-particle energy term E_p, summing up all relevant types of interactions between NPs[13], and a NP-to-substrate interaction energy E_s. A further important factor is the diffusion energy barrier, E_d, which can be overcome by 'thermal' energy $k_B T_s$. Hereby T_s is a quantity comparable to a substrate 'temperature', which precise physical meaning still needs to be understood for NP systems.

Depending on the relative magnitudes of E_d and $k_B T_s$ the NPs will either stay fixed at one place once they are attached to the substrate or move freely to seek energetically more favorable locations considering the two extreme cases.

From a comparison of these free energy terms one finds [11, 12] that three different growth modes follow: in the case where NP-to-substrate energy, Es, dominates a layer-by-layer growth is found, viz. the so-called Frank-van-der-Merwe growth mode (FvdM). Once a stable cluster (or 'nucleus') of NPs is formed, the following NPs prefer to attach at the periphery of the nucleus in contact with the substrate.

Accordingly this leads to the advancement of planar film growth. Depending on the ratio of Ed and $k_B T_s$ (i.e. the mobility of NPs) one will either obtain polycrystalline or single-crystalline superlattices. In the first case, the immobility of NPs leads to the nucleation of many independent superlattice crystallites, while, in the other case, the large mobility enables the NPs to seek equilibrium positions and hence promotes single-crystal growth. [8]

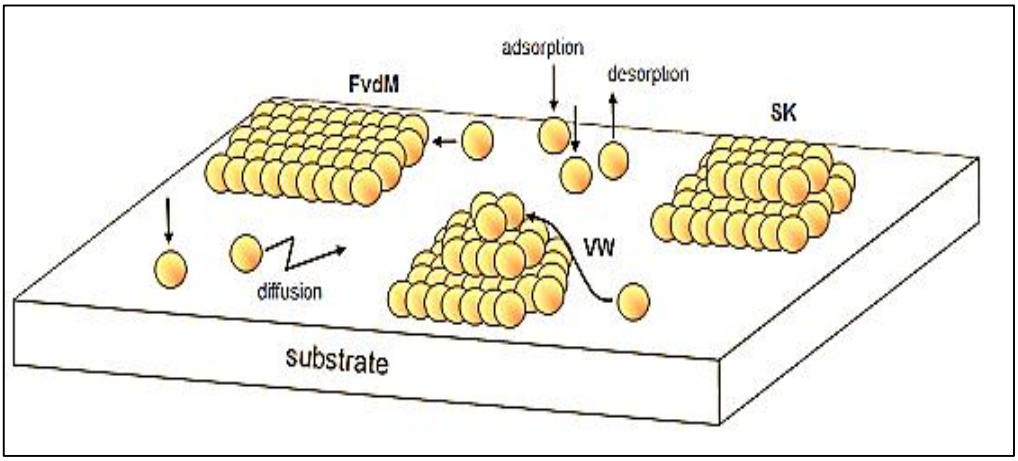

Fig.I.1 Schematic representation of the three known film growth modes [11].

I.3 Titanium dioxide (TiO_2)

I.3.1 Different phases of titanium dioxide (TiO_2)

TiO_2 materials naturally occur in three available crystal forms, known as anatase, rutile and brookite, in which well crystallized anatase and rutile have been widely studied owing to their practical uses[14].

a. Anatase phase

The crystal structure of the anatase is much more complex than that of rutile, the octahedral have been "deformed". The anatase mesh is shown in Figure I.2.TiO_2 has a band gap around 3.2 eV [1, 3]. This phase has not been studied much, although it interests many researchers, because of its use in photocatalysis and solar cell technology. Recently, individual Anatase crystals have been made and their studies have shown completely different electrical properties than rutile. These observations are consistent with the study of the electronic and optical properties of Anatase thin films [15].

b. Rutile phase

The rutile TiO_2 structure, whose elementary mesh is quadratic (figure I.2), is described as a compact hexagonal stack of oxygen atoms of which one octahedral site out of two is occupied by Ti^{4+} ion.In its stoichiometric form, the Bravais network is tetragonal and contains six atoms per unit cell. It is the densest form of titanium dioxide, stable at high temperatures and high pressures.When stoichiometric, rutile TiO_2 is insulating with a band gap of approximately 3 eV. However, deviations from the stoichiometry can be obtained by annealing at high temperature (> 500 ° C) under ultrahigh vacuum or under a reducing atmosphere and by interaction with a beam of charged particles (electrons or ions)[16].

c. Brookite phase

The third metastable crystalline form of TiO_2 is the brookite of orthorhombic structure (figure I.2).The synthesis of pure brookite is very difficult to carry out. Most studies on the synthesis of TiO_2 brookite show the simultaneous presence of the brookite phases and rutile and / or anatase. At high temperatures, from 750 ° C, the brookite turns into rutile [16].

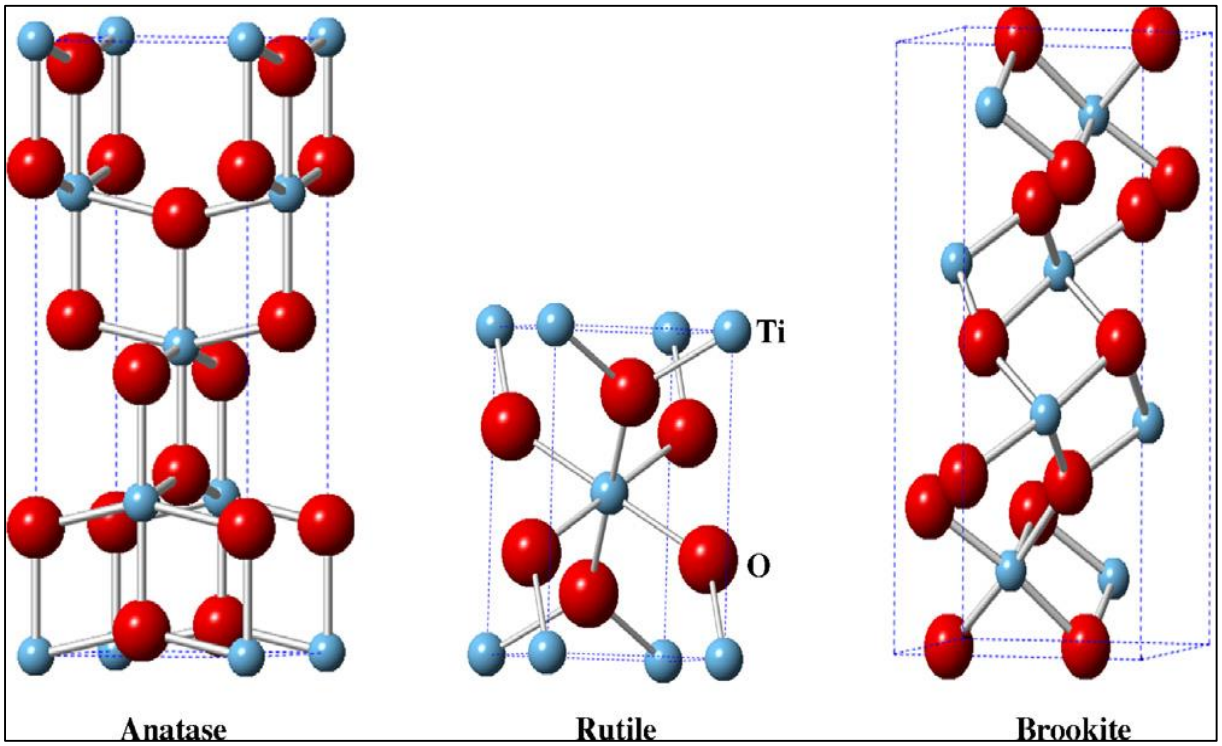

Fig.I. 2 Crystal structure of anatase, rutile and brookite [17].

Table I. 1 Crystal structure data of TiO_2 [18].

Phase	Rutile	Anatase	Brookite
Crystal structure	Tetragonal	tetragonal	orthorhombic
Lattice constants (Å)	a=4.5936 c=2.9587	a=3.784 c=9.515	a=9.184 b=5.447 c=5.145
Molecule/cell	2	4	8
Volume/molecule ($Å^3$)	31.2160	34.061	32.172
Density (g/cm3)	4.13	3.79	3.99
***Ti–O* bond length (Å)**	1.949 (4) 1.980 (2)	1.937 (4) 1.965 (2)	1.87~2.04
***O–Ti–O* bond angle**	81.2° 90°	77.7° 92.6°	77°~105°

I.3.2 Surface energies

The calculated surface energies of low index surfaces of anatase structure are listed in Table I.1 by using a self consistent ab initio (from the beginning) method [8,9,10]. (101) surface was calculated to be the most thermaldynamic stable surface with lowest surface energy among different low index surfaces, followed by (100), (001) and (110). Based on the relative value of surface energies of facets, the Wulff shape of anatase structure was proposed, as shown in Fig.I.4, being in excellent agreement with shape of matrually grown samples. In anatase, (101) plane is the predominent facet in anatase phase TiO_2 materials and other planes are also observed.

Since bulk rutile is more stable thermodynamically than anatase at all temperatures and pressure due to its lower total free energy (bulk and surface), metastable anatase phase can easily transfer to rutile upon heating accompanied by a thermal generation [11,12]. Comparing Table I.1, however, we can see the average surface energy of equilibrium shape anatase crystal is lower than that of rutile crystal. In the case of crystallites of extremely small sizes below a critical value, anatase has a lower total free energy on account of their correspondingly high surface areas [13,14]. This means the nanometre sized TiO_2 particles could be more stable in anatase phase compared to rutile.

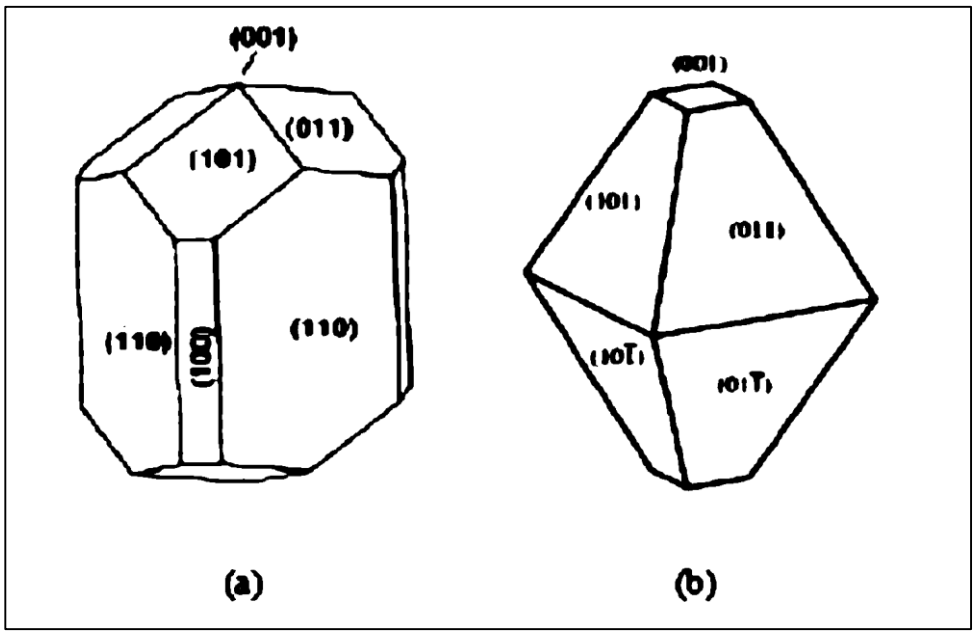

Fig.I.3 The equilibrium shape of TiO_2 in rutile crystal (a) [4] and anatase crystal (b) [9,10].

I.3.3 Types defects in TiO_2

Defects are often crucial in governing the physical and chemical properties of solids. These defects, at the surface and in the bulk, control chemical properties as well as electronic properties of the crystal [19].

Defects in TiO_2 have drawn much attention in the wide applications of TiO_2 in the fields of catalysis, photocatalysis and photoelectronics [20, 21]. During catalytic processes, defects in TiO_2 can modify the TiO_2 electronic structure, change the interaction between reactants or metal clusters with the TiO_2 support, and participate in surface reactions. During photon-related processes, the presence of defects can change the quantum yield of photonic excitation by tuning the energy band structure and modifying electron-hole separation and transport in TiO_2. Based on the dimensions of defect structures, defects in solids can be divided into four types: 0D defects (point defects), 1D defects (line defects), 2D defects (interfacial defects), and 3D defects (bulk defects) [22].

Point defects are in the size range of single atomic sites. Figure I.4 schematically lists the possible types of point defects in TiO_2:

Interstitial Defect: This can be produced when an atom occupies an extra site in the crystal which is normally not occupied by atoms in the perfect lattice. The extra atom can be the same type of atom comprising the crystal (self-interstitial) or an alien atom (impurity interstitial). The presence of interstitial defects may cause the distortion of lattice structure, which produces a high energy configuration. Usually, small atoms (positive ions) are energetically favored to occupy the interstices without requiring the expenditure of high energy. In TiO_2, Ti interstitials are common species and have been recognized as being important in surface reactions. Although theoretical results [23, 24] suggested the existence of oxygen interstitials, there is not too much experimental evidence for these until recent isotopic self-diffusion measurements [25] indicating the presence of O interstitials. There are many other elements that may form interstitial defects in TiO_2, such as H [26, 27], B [28, 29, 30, 31], C [32], N [33–38], Al [39], V [40, 41], Fe [42], Co [43], and Nb [44].

Vacancy Defect: This can be produced when an atom is missing from a normally occupied lattice site. In TiO_2, there are either oxygen vacancies or Ti vacancies. There is overwhelming evidence about the existence of oxygen vacancies in reduced TiO_2, which makes TiO_2 n-type. Oxygen vacancies exist together with Ti interstitials. The presence of Ti vacancies in a p type TiO_2 single crystal with prolonged oxidation at elevated temperature (>1,100 K) has

also been discovered. The concentration of Ti vacancies increases with decreasing TiO_2 crystallite size in TiO_2 prepared by sol-gel methods under oxygen-rich conditions [22].

Substitution Defect: This can be produced when the host atom in a lattice site is substituted by different atoms. In TiO_2, usually, Ti sites are substituted by positive ions, such as P [45, 46, 47], S [48], Fe [49, 50], V [22], Cr [51], Ni [52], and Pt [53]. O sites are substituted by negative ions, such as N [54,55,56], F [57, 58], C [59, 60], S [61, 62], B [63], and P [47].

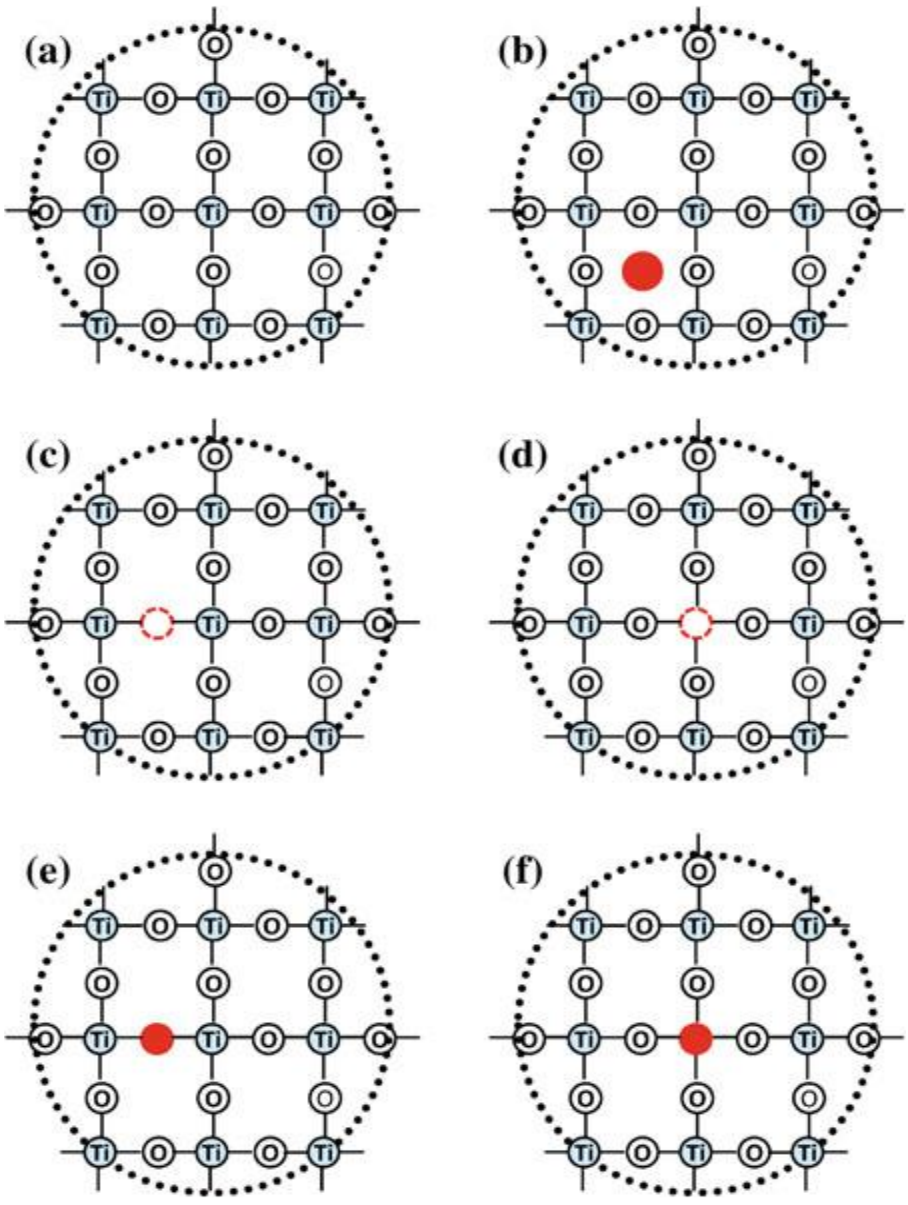

Fig. I.4 Types of point defects. (a) Perfect lattice. (b) Interstitial defect. (c) Oxygen vacancy. (d) Ti vacancy. (e) Substitution of O by a foreign atom. (f) Substitution of Ti by a foreign atom [22].

Line defects in a solid are called dislocations; these can be classified in two basic types: edge dislocations and screw dislocations. In a real crystal, most dislocations are hybrids of the two types. The formation of an edge dislocation can be viewed as the insertion of an extra half plane of atoms into the perfect crystal. The edge dislocation line is at the end of the extra plane of atoms (fig.I.5) [22].

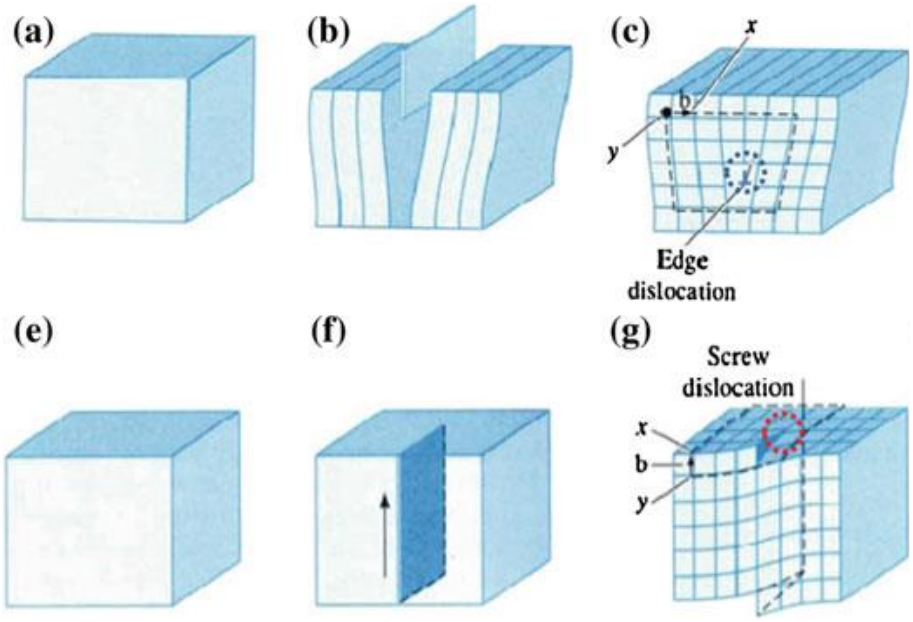

Fig. I.5 a–c Schematic diagram of formation of edge dislocations in TiO_2. e–g Schematic diagram of formation of screw dislocation in TiO_2 [22].

2D defects in solids include stacking faults and grain boundaries. The crystal can be treated as a sequence of atomic planes stacking together in an orderly fashion. A one or two layer interruption of the stacking sequences of atom planes is called a stacking fault. In Fig. I.6a, the correct stacking sequence is …ABCABCABC…, where A, B and C designate the in equivalent atomic planes. The presence of a stacking fault changes the stacking sequence to …ABC/BCABC…, and "/" (red dashed lines in Fig. I.6 a, b) indicates the stacking fault Stacking faults have been discovered in TiO_2. Figure I.7b shows a stacking fault of crystalline anatase TiO_2 [22].

Polycrystalline materials composed of many small single crystals or grains with the size from nanometers to millimeters are widely used technologically. The interfaces between crystals or grains are called grain boundaries. In TiO_2, the grain boundaries can be the interfaces between TiO_2 particles and other substances (such as metal, metal oxide), TiO_2 particles with

different phases or TiO_2 particles with the same phase but different orientations. Figure I.7d shows the TEM images of grain boundaries between anatase and rutile of P25 titanium dioxide (P25 TiO_2 is a common powdered TiO_2 produced for industrial purposes.) [64,22].

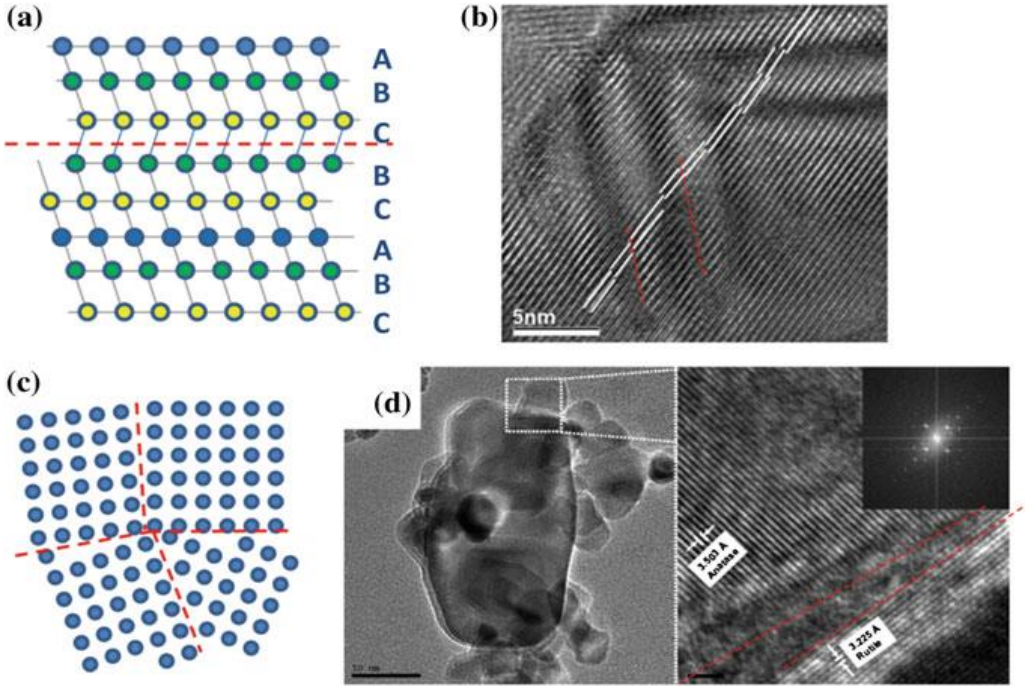

Fig. I.6 Types of 2D defects in TiO_2: a, b stacking faults; c, d grain boundaries. b and d are TEM images of stacking faults and grain boundaries from respectively[64].

I.3.4 Electronic structures of TiO_2

In the energy view, electrons in the crystalline semiconductors are confined to certain energy levels, which are also known as electron movement orbitals, and forbidden from other region, as shown in Fig. I.7. The highest range of energy levels which electrons occupy at absolute zero degree is called valence band and the range of energy levels, higher than that, is called conduction band. Each energy band has a large number of quantum states. The valence band describes a state of electrons tightly bound to the atomic nuclei and the conduction band reflects the electrons escaped from the materials to move entirely free in crystal lattice. As for TiO_2, the bottom of the conduction band (CB) is dictated by the Ti 3d electron states and the top of the valence band (VB) is dominated by the oxygen 2p electron states. The energy difference between the top of valence band and the bottom of conduction band is dubbed as band gap (Eg). Therefore, the band gap determines the specific minimum amount of energy in order for an electron to jump from valence band to conduction band. When a semiconductor is illuminated with light of energy higher than the band gap, electrons receive the energy from

incident photons and jump from the valence band to the conduction band leaving as many positive holes in the valance band. This process is equivalent to the movement of electrons from bonding orbital to anti-bonding orbital. In most cases, the excited electrons are unstable and can easily jump back into the valence band and recombine with holes quickly with the release of heat. There are two kinds of band gaps, direct band gap which means carriers at the highest point of valence band and the lowest point of conduction band have the same momentum and electrons can directly jump into conduction band without changing momentum, and indirect band gap which means electrons must pass through an intermediate state to reach conduction band and transfer momentum to crystal lattice. Rutile phase TiO_2 has a band gap of 3.0 eV while anatase phase has a band gap of 3.2 eV [15]. TiO_2 anatase thin films can have a direct or indirect band gap depending of defects proportion.

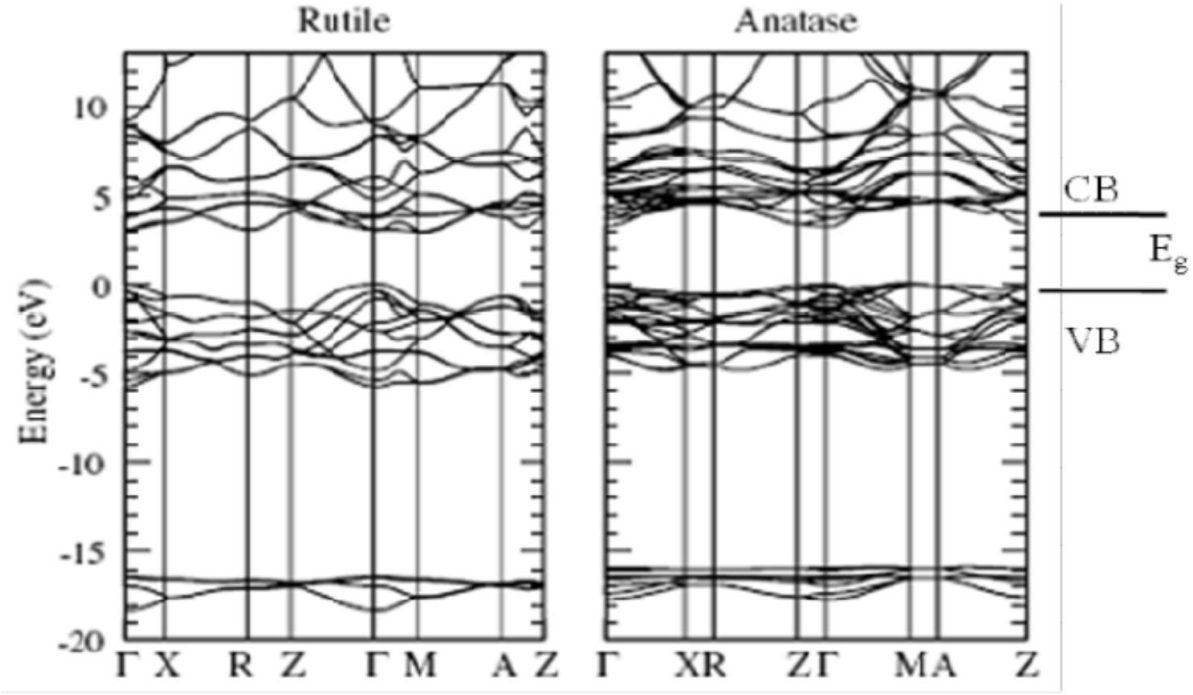

Fig.I.7 Energy band structures of TiO_2 [15].

I.3.5 Optical properties

TiO_2 is presented as a semiconductor material with a wide forbidden band (band-gap). The gaps in Rutile, Anatase and Brookite are 3 eV, 3.2 eV and 3.1 eV respectively. The band gap (Eg) is between the valence band (corresponding to the O 2p orbital) and the conduction band (corresponding at orbital Ti 3d)). These gap values give rise to transitions corresponding to photons located in the ultraviolet range.

The transparency of TiO_2 in the visible, associated with an absorption edge around 0.42 µm leads to a strong absorption in the ultraviolet, which gives it excellent properties, such as protection against UV radiation [65, 66].

The different varieties of titanium oxide have a high refractive index n in the visible range. Among the three stable crystalline phases, Rutile has the highest index (n ~ 2.66) higher than that of the anatase variety (n ~ 2.54). This combined with a diffusion coefficient of the high visible light, make the Rutile phase a white pigment of choice for industry (paints, food or pharmaceutical coloring, etc.) [67, 68].

I.3.6 Doping of TiO_2

The main objective of metal ions doping on band gap narrowing is to shift up valence band or shift down conduction band of intrinsic TiO_2 or create shallow intermediate band levels into forbidden band through substituting Ti atoms by dopants in TiO_2 lattice, since deep intermediate band levels would predicatively act as recombination centre and thereby arouse significant electron and hole recombination. On the ground of this, various single metal ions have been widely studied to address the optical limitation of TiO_2 materials, including transition metal such as V [69,70,71,72], Cr [73,74,75,76,77], Mn [78] , Fe [79], Co [80], Ni [81], Cu [82], Zn [83], Zr [70], Mo, Ru, Rh, Ag[84,85], Pt, rare earth metals, such as Ce, Pr, Sm, Eu, Gd and Er, other metals such as Mg, Sr, Ba, Ca, Pb and so on. Albeit a great deal of theoretical and experimental works have been focused on doping TiO_2 with single metal ions, the exploitation of TiO_2 with doping still has profound prospective because the chemical states of doping ions determined by fabrication method play a crucial role on the doping effect [22].

In this thesis, the doping effect of titanium dioxide by gallium (Ga-TiO_2) on the photocatalysis properties is studied.

I.3.6.1 Gallium properties

Gallium is a chemical element with the symbol Ga and atomic number 31. Elemental gallium is a soft, silvery blue metal at standard temperature and pressure It is in group 13 of the periodic table, Gallium does not occur as a free element in nature, but as gallium(III) compounds in trace amounts in zinc ores and in bauxite. (**Table I.2).**

Table I.2 Gallium properties

Gallium properties

Atomic number	31
Atomic weight	69.72
Melting point	29.78 °C (85.6 °F)
Oxidation state	+3
Electronic configuration	[Ar] $3d^{10}4s^{2}4p^{1}$

I.3.6.2 Gallium doped of TiO_2 thin films

LIU Gui-Ang and all found a good photocatalysis activity degradation rate of 71.8 % for methylene blue after 8 hours under low power UV lamp (15 W)[86].

The Ga-doped TiO_2 powders elaborated by mild hydrothermal method exhibit better photocatalytic activity reaching up to 82% compared to un-doped TiO_2 when decolorizing methylene orange under 420–780 nm visible light irradiation [87].

I.4 Photocatalytic activity application

I.4.1 Why was titanium dioxide chosen?

Titanium dioxide (TiO_2) is the most widely used photocatalyst in the treatment of industrial waste water, due to:

- The low energy required for its activation (E_{act} = 3.2 eV).
- Its biologically and chemically inert
- Its stable (in acidic and basic medium), insoluble, non-toxic and less expensive than other catalysts such as ZnO, CdS or ZnS
- Its anatase form appears to be the most photoactive.
- It promotes the photodegradation of a wide range of indoor pollutants at room
- Temperature [88].

I.4.2 Photocatalysis mechanism

Photocatalysis is defined as ‘capture of the sun light or any incident light to turn organic matter to carbon dioxide and water’ by the presence of as semiconductor photocatalyst.

To better understand the mechanism of photocatalysis, oxidative and reductive reaction procedures of TiO_2 are depicted in Fig.I.8, in which the energy band diagram of TiO_2 in

PH = 7 solution is proposed by Fujishima [1,2], together with redox potential of various radials and molecules versus standard hydrogen electrode (SHE)[15].

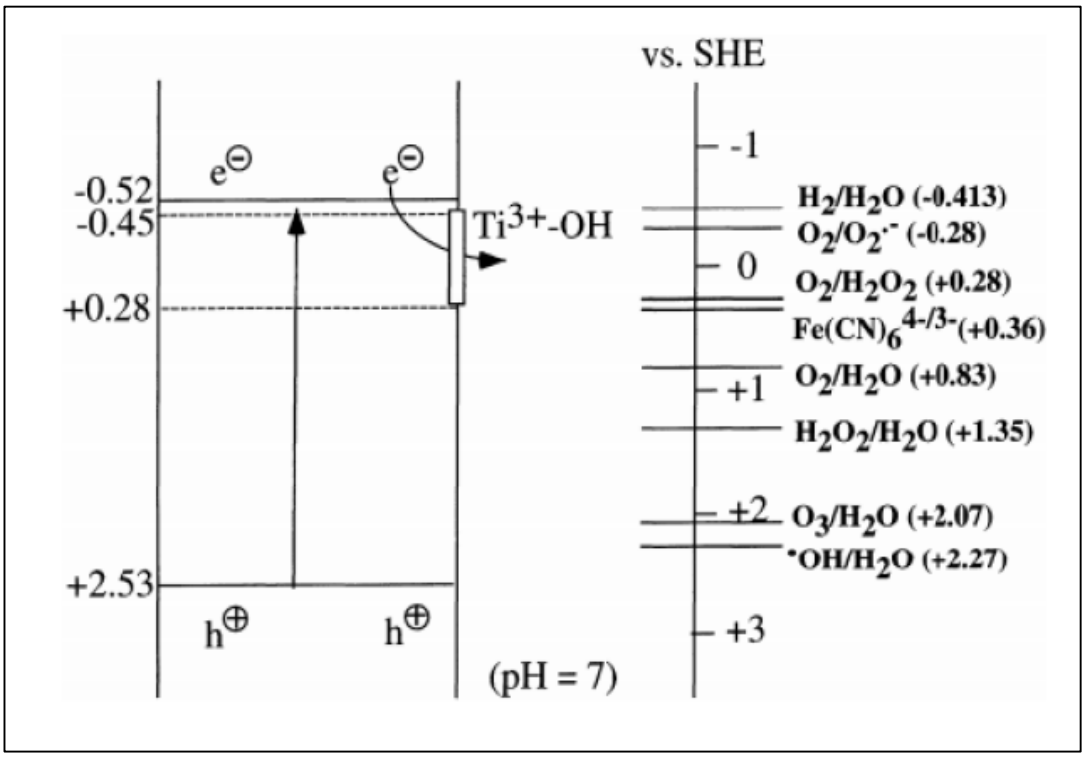

Fig. I.8 Schematic diagram of photocatalysis process of TiO_2 [15].

The photocatalysis process is based on the excitation of TiO_2 by a light radiation of wavelength less than 385 nm, corresponding to an energy greater than or equal to the width of the forbidden band of 3.2 eV. The initial step in this photocatalytic process is the absorption of UV radiation leading to the formation of electron-hole pairs according to the equation I.1. The electrons (e-) of the valence band (BV) of TiO_2 pass towards the conduction band (BC), leaving a positive charge or hole (h^+) in the BV [89].

$$TiO_2 + h\nu \rightarrow e^-_{CB} + h^+_{VB} \qquad \text{(I.1)}$$

These electron / hole pairs can recombine by releasing heat (I.2), or react separately with other molecules present in the medium on the surface of the catalyst, In the presence of water, the holes can react with electron donors (H_2O, HO^-) to produce oxidizing species such as the hydroxyl radicals $HO^\bullet$ (equation II.3 and II.4).

$$e^-_{CB} + h^+_{VB} \rightarrow heat \qquad \text{(I.2)}$$

$$HO^- + h^+_{VB} \rightarrow HO^\bullet \qquad \text{(I.3)}$$

$$H_2O + h_{VB}^{+} \rightarrow HO^{\bullet} + H^{+} \quad \text{(I.4)}$$

In the presence of a pollutant in aqueous solution, the latter can yield an electron to a hole and oxidize in the primary form of a cation radical. The oxidation of the latter species will continue until complete mineralization thanks in particular to the active oxygen species ($HO^{\bullet}$,$HO_2^{\bullet-}$,H_2O_2) generated by reactions I.3 to I.8 [90].

$$O_2 + \text{é} \rightarrow O_2^{\bullet-} \quad \text{(I.5)}$$

$$\text{é} + O_2^{\bullet-} + 2H^{+} \rightarrow H_2O_2 \quad \text{(I.6)}$$

$$O_2^{\bullet-} + H^{+} \rightarrow HO_2^{\bullet-} \quad \text{(I.7)}$$

$$H_2O_2 + HO^{\bullet} \rightarrow HO_2^{\bullet-} + H_2O \quad \text{(I.8)}$$

The adsorption of organic pollutants (P) do according to [91]:

$$Site + P \rightarrow P_{ads} \quad \text{(I.9)}$$

Hydroxyl radicals attack organic pollutants generating intermediates (INj) first [91, 92].

$$HO^{\bullet} + P_{ads} \rightarrow IN_{jads} \quad \text{(I.10)}$$

The hydroxyl radicals attack the intermediaries generating other intermediaries:

$$HO^{\bullet} + IN_{ads} \rightarrow IN_{(j+1)ads} \quad \text{(I.11)}$$

Photocatalysis seems very suitable not only for changing aqueous liquid waste, but also for its degradation which can go as far as the formation of mineralization products CO_2, H_2O, NO^-_3, SO^-_4 [93].

The speed of formation of electron-hole pairs under the impact of photons depends mainly on the intensity of the incident light and the optical and physical properties of the photocatalyst. If the light intensity is too high, it has been shown that an electron-hole recombination phenomenon occurs, inhibiting the photocatalytic phenomenon [91]. The reactions that occur in photocatalysis are illustrated in Fig I.9.

.

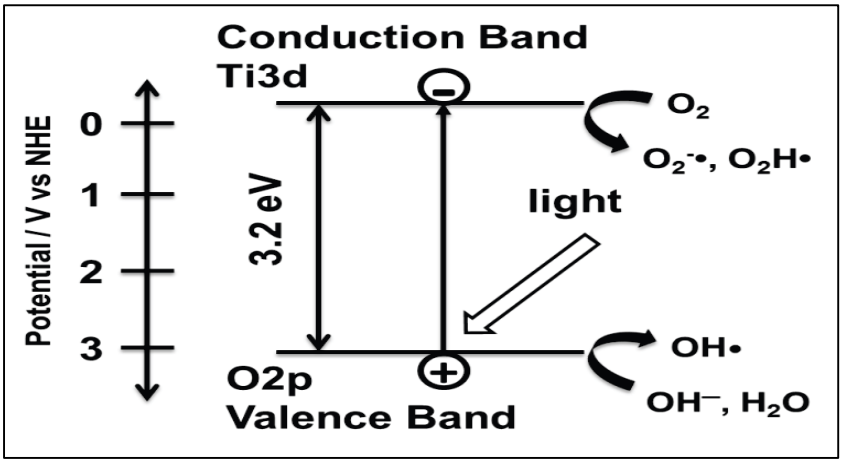

Fig.I.9 Scheme of photocatalytic reaction with TiO_2 photocatalyst [15].

I.4.3 Role of hydroxyl radicals

In order to confirm that the hydroxyl radicals are indeed the primary oxidizing species formed, Muruganandha and Swaminathan (2005) have shown that the addition of isopropanol, known as an HO • inhibitor, decreases the photocatalytic degradation of Reactive Orange 4. For dyes Azoic, an azolinkage type reaction occurs with hydroxyl radicals, which oxidize carbons to the azo double bond. The fragments produced by the breaking of the azo bond of the molecule then correspond to the primary intermediates of the reaction. The analyzes of the intermediates resulting from the photocatalytic degradation of the dye Acid Blue 25 and of the yellow Metanil also showed that they were indeed by-products having the same basic structure as the dye of departure [91].

I.4.4 Factors affecting photocatalysis degradation rate (PDE)

The photocatalysis degradation rate of TiO_2 thin films is largely affected by the following factors:

- The first critical factor is the light absorption properties of TiO_2 thin films, including absorption region and coefficient, which decide the maximum amount of photons that can be converted into electrons and holes from incident light.
- The surface area of TiO_2 photocatalyst, the larger surface area means more molecules can adsorb onto TiO_2, leading to faster photocatalytic rates.
- The electron and hole recombination rate, normally determined by defect levels, is also central to the photocatalytic activity. The interface is generally a defective site for

carriers to recombine, as the lifespan of photogenerated carriers are approximately 10 ns [88].

I.4.5 Effect of the allotropic phase of TiO_2 on photocatalytic activity

The difference in forbidden bandwidth of anatase (3.2 eV) and rutile (3.0 eV) allows us to understand why H^+ is reducible on anatase while on rutile it is thermodynamically impossible. From a thermodynamic point of view, anatase and rutile are able to initiate photocatalytic oxidation reactions because the position of the valence band is similar. However, in several scientific studies, anatase has been identified as the more effective variety of the two in photocatalysis .

This difference in efficiency can be attributed to different parameters. The mobility of the charges created in the matrix of the TiO_2 semiconductor under the impact of photons, the grain size, the specific surface, the OH content of the surface, the adsorption of the species to decompose, the absorption of photons UV (affected by particle size and texture) are parameters whose effect plays a key role in the difference in activity between the two Allotropic varieties.

Studies on the comparative photoconductivity between anatase and rutile have shown at the lifetime of charge carriers, electrons and positive holes, is longer for anatase than for rutile. The charge carrier recombination rate is significantly higher for rutile. This recombination slows down the photodegradation of pollutants because it limits the formation of oxidizing species, necessary for the mineralization of organic matter adsorbed on the surface of the grains [88].

I.4.6 Photocatalytic activity of doped TiO_2

As it was mentioned above, the band gap of TiO_2 can be tuned through suitable doping to shift valence band up or conduction band down; or introduce intermediate states for effective absorption under visible light illumination. Nevertheless, photocatalytic activities, of some doped catalysts, were hardly improved despite red shift of optical absorption edges was indeed observed. In doped TiO_2, high doping level could induce electronic defect states, crystal defects or even ions oxides separated out from TiO_2 crystal, to act as carrier recombination centres, whereas low doping level could act as charge transfer mediator to prolong lifespan, when carriers migrated from the inside of the photocatalyst to the surface [15].

Durgam Komaraiah and all found of the photocatalytic activity (PCA) of TiO_2: x % Fe^{3+} (x=0, 1, 3, 5, 7 and 10) catalysts were determined by the decomposition of methylene blue (MB) under irradiation of visible light. The observed results revealed that the optimized Fe^{3+}

doped TiO_2 film displayed high PCA. The enhancement of PCA of the films is due to the effect of Fe doping [94].

I.5 Organic pollution

I.5.1 Water Pollution Due to Organic Dyes

For various industrial applications, a number of diverse dyes are used and significant proportions are spilled into the environment which comes out in the form of effluent wastewater. Among various dyes, azo dyes due to their versatility and chemical stability are the major class of colorants used in consumer products, printing, cosmetics, tattooing as well as in textile industries. However, their durability and non-biodegradability cause pollution once these dyes are released into the water bodies. Some of the azo dyes are very toxic, carcinogenic and mutagenic [95]. Wastewater discharge of dyes contains a large number of toxic pollutants. Among all the dyestuffs, the azo dyes account for about 70% by weight. Azo dyes intermediates, *i.e.*, aromatic amines, are much carcinogenic and mutagenic, which cause a serious health hazard to human beings [96].

Reactive dyes are an important class of the commercially available synthetic dyes. Reactive dyes are mainly characterized due to their excellent binding capability initiated due to the formation of a covalent bond between the reactive groups of dyes and the surface groups present on the textile fibers. Reactive dyes are extensively used in textile industries, and their discharge in the ecosystem represents rising environmental pollutions, nowadays, because of their non-biodegradability, carcinogenicity, toxicity, and mutagenicity.Reactive dyes are the most problematic dyes among others, as they tend to pass unaffected through conventional treatment systems. Examples of contaminated dyes :

Congo red (CR) is the most commonly used azo dyes worldwide. CR is a diazo benzidine based anionic dye containing double azo (-N=N-) linkage. CR is very toxic and carcinogenic and is metabolized well by known human carcinogen benzidine in many organisms. Due to health concerns, CR dye has been banned by various countries, but it is also still widely used in many countries. The complex aromatic molecular structures of CR dye provide them optical, thermal and physicochemical stability, which make them difficult to biodegrade. Thus, the existence of CR dye in water is highly undesirable even in dilute concentration [95].

Janus Green B **(**JGB) dye has been used for oxidation-reduction capability of different tissues study. JG-B is synthesized by conjugating dimethyl aniline to diethyl safranine dye through azo (-N=N-) linkage. The color of JG-B is blue while diethyl safranine is red. It has been shown that leukosafranine reduced cytochrome *c* and leukosafranine is oxidized to diethyl safranine. The cytochrome oxidase, within mitochondria, prevents JG-B reduction. This cytochrome oxidase enzyme system is cyanide-sensitive and oxygendependent. Dye JG-B is used for mitochondrial staining and its oxidation-reduction shows the alteration in the electron transfer chain. The alteration in mitochondrial in the electron transfer chain is linked to the formation of free radical [97].

A cationic dye Methylene blue (MB) has a number of applications and widely used in dyeing cotton, paper, coloring, wools, silk leather, and coating of paper stock. MB is not too much toxic, although it causes some harmful effects, such as cyanosis, vomiting, increase in heartbeat, quadriplegia, shock, jaundice, and tissue necrosis in human being [98].

I.5.1 Degradation of Dye Pollutants

The majority of pollutants (organic/inorganic) present in aquatic environments are due to the release of wastewaters from households as well as from the industrial sectors. These pollutants, organic molecules could be found in the ground and surface water. The removal of carcinogenic, non-biodegradable organic dyes and other chemicals from the environment is a central ecological problem. Dye molecules are not degraded easily due to the complex aromatic structure and xenobiotic properties [99]. Thus, it is necessary to develop different effective treatment methods and techniques for the removal of these toxic dye contaminants from water bodies. Traditional methods used for wastewater treatment include flocculation, coagulation, membrane separation, waste materials adsorption, adsorption on activated carbon, air floatation processes, chemical oxidation, including Fenton's reagent, electrochemical process, aerobic-anaerobic two-stage biochemical process, advanced oxidation process (AOPs), foam flotation, or combined coagulation like the use of potash alum [100]. Physical methods such as reverse osmosis, flocculation, adsorption on activated charcoal and membrane filtration are nondestructive and simply transfer the organic pollutant molecules to other media, thus causing secondary pollution. Chemical methods for removal of dyes pollutants are cost-effective due to the requirement of large amounts and production of high dosages of sludge. Resistance to aerobic decolorization makes the bio-treatment of dyes pollutants ineffective. Furthermore, anaerobic treatment of azo dyes may produce carcinogenic aromatic amines [101]. All these

practices are nondestructive and produce secondary pollutants. Due to the ineffectiveness of the aforementioned techniques in one way or the other, the present situation requires improved and better methods for wastewater treatment [99]. Thus, it is necessary to develop more ‘‘ideal’’ alternative methods, having low cost, high adsorption capacity, be relatively easily handled, and easily recycled [94].

Recently semiconductor photocatalysts also termed as heterogeneous photocatalysts have been used as a promising method for the removal of carcinogenic contaminants from industrial effluents since they not only degrade but also cause complete mineralization of pollutants to H_2O, CO_2 and mineral acids. Metal oxide nanoparticles have been used as a promising method for the removal of carcinogens and persistent pollutant molecules without generating any toxic secondary materials from industrial wastewater because they not only cause degradation but also their complete mineralization of water and carbon dioxide. Different semiconductor metal oxides have been used, including TiO_2, ZnO, Fe_2O_3, PbO_2, SnO_2, Sb_2O_5, *etc.* [94].

I.5.3 Dangers of organic pollutants.

The most commonly used classification of dyes is based on the chemical structures of synthetic dyes and the methods of application to different substrates (textiles, paper, leather, plastics, etc.).

The accumulation of organic matter in watercourses induces the appearance of bad tastes, bacterial proliferation, pestilential odors and abnormal coloring. A coloration could be perceived by the human eye from 5 x 10^{-6} g / L [102]. Besides the unsightly appearance, coloring agents have the ability to interfere with the transmission of light in water, thereby blocking photosynthesis in aquatic plants.

Synthetic organic dyes are compounds that cannot be purified by natural biological degradation [103]. This persistence is closely related to their chemical structure

I.5.4 Methylene blue properties

In this thesis, methylene blue was chosen as a model for organic pollutants. Methylene blue, a bright greenish blue organic dye belonging to the phenothiazine family. The methylene blue properties are shown in the table

The chemical structure of methylene blue is illustrated in figure I.10 [104].

Table I.3 Methylene blue properties

Methylene blue properties

Molar mass	319.85 g/mol
Molecular Formula	$C_{16}H_{18}ClN_3S$
Other names	Basic blue 9 Methylthioninium chloride
Ionicity	Cationic
Absorption l_{max} (nm)	664 nm

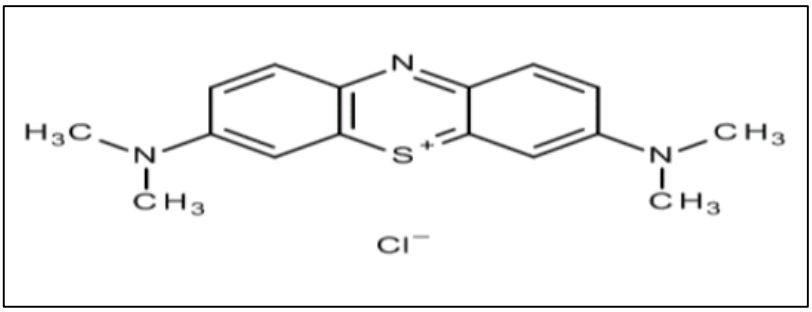

Fig. I.10 The chemical structure of methylene blue [105].

I.6 Photocatalysis parameters

I.6.1 Intensity of absorption (A)

Absorption intensity is obtained using the UV-Vis spectroscopy technique. UV-Visible Spectroscopy is a quantitative analytical method that involves measuring the absorbance or optical density of a given chemical in solution. The more this species is concentrated the more it absorbs light within the limits of the proportionality stated by the law of Beer _ Lambert.

When a substance absorbs light in the ultraviolet and visible range, the absorbed energy causes disturbances in the electronic structure of atoms, ions or molecules. One or more electrons use this energy to jump from a low level to a higher energy level. These electronic transitions are in the visible range, from 350 to 800 nm and the ultraviolet between 200 and 350 nm.

A homogeneous medium traversed by light absorbs part of it; the different radiations constituting the incident beam are absorbed differently according to their wavelength and the radiation transmitted is then characteristic of the medium [106].

Let a monochromatic light ray of wavelength λ passing through a homogeneous medium of thickness 1. The decrease in light intensity as a function of the thickness of the absorbing medium is given by Lambert's law:

$$A = \text{Log}\frac{I_0}{I} \qquad \text{(I.12)}$$

I_0: initial intensity of the light passed through.

I: intensity of transmitted light.

A : absorbance.

The optical density of the solutions is determined by a spectrophotometer previously calibrated over the absorption wavelength of the chemical species.

If the homogeneous medium is a solution of a compound at the molar concentration C (expressed in mol.L-1) absorbing in a transparent solvent, we then have:

$$K = \varepsilon.C \qquad \text{(I.13)}$$

K: the absorption coefficient, the ratio I_0 / I is the transmission coefficient.

The intensity of the transmitted radiation is given by Beer-Lambert law:

$$A_\lambda = \varepsilon_\lambda.C.l \qquad \text{(I.14)}$$

A_λ: absorbance of the solution at wavelength.

C: ($mol.L^{-1}$) the concentration of the absorbent species.

l: the optical path. (l being expressed in cm).

ε_λ: ($mol^{-1}.l.cm^{-1}$) is the molar extinction coefficient, it is an intrinsic quantity of a compound under the given conditions. ε depends on the wavelength used, the temperature and also the nature of the solvent.

The analysis of our samples was performed with a SAFFAS double beam UV / Visible spectrophotometer controlled by a computer. Measurements are made in quartz tanks with an optical path of 1 cm.

UV / Visible spectroscopy makes it possible to follow the discoloration of the solutions thanks to the absorbances which change as a function of the treatment time [106,107].

I.6.2.Kinetic constant (K_{app})

Generally, the degradation kinetics of a compound follow the Langmuir-Hinshelwood model confirming the heterogeneous nature of the photocatalytic system [108]. This model makes it possible to assess the rate of degradation of an organic pollutant at different concentrations. This model was originally developed to describe heterogeneous reactions in the gas phase [109]. It was subsequently used for the first time by Ollis [110] to describe liquid-solid reactions.

The assumptions on which this model is based are as follows:

- At equilibrium, the number of adsorption sites is fixed.
- Only one molecule of substrate is adsorbed per adsorption site (adsorption in monolayer)
- The adsorption energy is identical for all the adsorption sites and independent of the surface covering rate.
- Adsorption is rapid compared to the secondary reactions of the substrate in solution.
- Only the molecules adsorbed on the surface of the catalyst react.

If these hypotheses are verified, the rate of photocatalytic degradation is proportional to the rate of covering of the surface of the catalyst by the pollutant, that is to say to the amount of substrate adsorbed on the surface of catalyst [111].

$$V = \frac{dC}{dt} = k\theta = \frac{k\,Q_e}{Q_{max}} \qquad \text{(I.15)}$$

The amount of substrate adsorbed at equilibrium Q_e depends on the concentration of solution at equilibrium C_e:

$$Q_e = \frac{KQ_{max}\,C_e}{1+kC_e} \qquad \text{(I.16)}$$

The recovery rate θ is written:

$$\theta = \frac{KC_e}{1+kC_e} \qquad \text{(I.17)}$$

The expression speed is therefore written

$$V = \frac{KkC_e}{1+kC_e} \qquad \text{(I.18)}$$

V: reaction speed (μmol / L / min)

θ : Rate coverage of the catalyst surface by the substrate

k : Kinetic degradation constant (μmol / L / min)

K : Substrate adsorption constant (L / mmol)

C_e: Steady state concentration of pollutant (mmol / L)

For low pollutant concentrations, KC_e becomes negligible compared to 1 ($KC_e \ll 1$), the reaction speed becomes directly proportional to the pollutant concentration, The reaction is then first order, It is written according to the equation [108,112]:

$$V = KkC_e = K' C_e \quad \text{(I.19)}$$

$$V = -\frac{dC}{dt} = K' C_e \quad \text{(I.20)}$$

In this situation, an integral form of the L-H model would be more feasible, which can be expressed with an approximation as follows:

$$\int_{C_0}^{C_t} \frac{dC}{C} = -K' \int_0^t dt \quad \text{(I.21)}$$

$$-ln\left[\frac{C_t}{C_0}\right] = K' t = Kkt = K_{app}\, t \quad \text{(I.22)}$$

$$-ln\left[\frac{C_t}{C_0}\right] = K_{app}\, t \quad \text{(I.23)}$$

$where, K_{app}$ is the first-order rate constant (kinetic constant). The rate constants (k) have been calculated by linear fitting to the $-ln\left[\frac{C_t}{C_0}\right] = f(t)$ versus plots.

I.6.3 Photocatalytic degradation rate (PDR)

The photocatalytic degradation rate (PDR) of thin films for the photocatalytic degradation of organic pollution dye solution was calculated with the formula [113].

$$PDR\ (\%) = \frac{C_0 - C_t}{C_0} \times 100 \quad \text{(I.24)}$$

Where, C_0 is the absorbance of organic pollution dye solution before the illumination and C_t is the absorbance of organic pollution in the solutions after sun light exposure time *t*.

Chapter II

Sol-gel (spin-coating) and characterization methods

II.1 Introduction

Generally any thin film deposition follows the sequential steps: a source material is converted into the vapor form (atomic/molecular/ionic species) from the condensed phase (solid or liquid), which is transported to the substrate and then it is allowed to condense on the substrate surface to form the solid film [114]. Depending on how the atoms/molecules/ions/clusters of species are created for the condensation process, the deposition techniques are broadly classified into two categories: physical methods and chemical methods [115].

Modern techniques employed in the characterization of electronic thin-film materials and devices. Among their characteristics are the unprecedented structural resolution and chemical analysis capabilities over small lateral and depth dimensions. Some techniques only sense and provide information on the first few atom layers of the surface. Others probe more deeply, but in no case are depths much beyond a few microns accessible for analysis. Virtually all of these techniques require a high or ultrahigh vacuum ambient. Some are nondestructive, others are not. In common, they all utilize incident electron, ion, or photon beams. These interact with the surface and excite it in such a way that some combination of secondary beams of electrons, ions, or photons are emitted, carrying off valuable structural and chemical information in the process. A rich collection of acronyms has emerged to differentiate the various techniques. These abbreviations are now widely employed in the thin-film and surface science literature [116].

In this chapter, the first part is explained the technique of Sol-Gel (spin coating) to prepare thin films. As for the second part of this chapter includes different techniques and different relationships, which are used to describe films.

II.2 Thin films depositions techniques

The properties of thin films are extremely sensitive to the method of preparation, several techniques have been developed (Depending on the desired film properties) for the deposition of the thin films of the metals,alloys,ceramic,polymer and superconductors on a variety of the substrate materials.Each methods has it's own merits & demerits and of course no one technique can deposit the thin films covering all the desired aspects such as cost ofequipments, deposition conditions and nature of the substrate material etc.

Various deposition methods have been employed to get TiO_2 in thin film form, such as plasma enhanced chemical vapor deposition, sol-gel methods, chemical vapor deposition and DC reactive magnetron sputtering, RF reactive magnetron sputtering, electron-beam evaporation, ion-beam assisted deposition [117].

The Sol-Gal method was chosen to precipitate thin films because it is simple and inexpensive.

II.3 Sol-Gel method

The sol-gel method is a wet-chemical synthesis technique for preparation of oxide gels, glasses, and ceramics at low temperature. It's based on control of hydrolysis and condensation of alkoxide precursors. As early as the mid-1800s, interest in the sol-gel processing of inorganic ceramics and glass materials has begun with Ebelman and Graham‟s studies on silica gels. The investigator recognized that the product of hydrolysis of tetraethoxysilane (TEOS) under acidic conditions is SiO_2. In the 1950s and 1960s Roy and co-workers used sol-gel method to synthesize a variety of novel ceramic oxide compositions with very high levels of chemical homogeneity , involving Si, Al, Zr, etc, which couldn‟t be made using traditional ceramic powder methods . It's possible to fabricate ceramic or glass materials in a variety of forms, such as ultra-fine powders, fibers, thin films, porous aerogel materials or monolithic bulky glasses and ceramics. Since then powders, fibers, thin films and monolithic optical lens have been made from the sol-gel glass [115].

II.3.1 Sol-gel process

The sol-gel process, as the name implies, involves transition from a liquid "sol" (colloidal solution) into a "gel" phase. Usually inorganic metal salts or metal organic compounds such as metal alkoxide are used as precursors. A colloidal suspension or a "sol" is formed after a series of hydrolysis and condensation reaction of the precursors. Then the sol particles condense into a continuous liquid phase (gel) [118]. Generally three reactions are used to describe the sol-gel process: hydrolysis, alcohol condensation and water condensation. Because water and alkoxides are immiscible, alcohol is commonly used as co-solvent. The two phases which describe the sol-gel process are defined as follows [115]:

Sol: a stable suspension of colloidal solid particles or polymers in a liquid.

Gel: porous, three-dimensional, continuous solid network surrounding a continuous liquid phase.

a. Solution based on an inorganic precursor

The aqueous solution of a mineral salt is used. In this solution, the cations M^{z+} are captured by polar molecules H_2O. A bond $(M-OH)^{(z-1)+}$ is formed when an electron from a saturated orbital σ is transferred to a lower energy orbital and not saturated. This results in fact in the following two partial reactions:

$$M^{z+} + (OH)^{-} \leftrightarrow (M-OH)^{(z-1)+} \quad \text{(II-1)}$$

$$(M-OH)^{(z-1)+} \leftrightarrow (M=O)^{(z-2)+} + H^{+} \quad \text{(II-2)}$$

We know that according to the aforementioned reactions that in an acid medium, by increasing the PH of the solution, one of the following two types of ligands can form:

- Ligand hydroxo : $(M-OH)^{(z-1)+}$
- Un ligand Oxo : $(M=O)^{(z-2)+}$

Condensation reactions involving the hydroxo ligands: $(M-OH)^{(z-1)+}$ lead to the formation of (M – OH – M) or (M – O – M) bonds. Note, however, that colloidal solutions and stable gels can be obtained by keeping the PH constant. This route is mainly used in industrial powder manufacturing processes [119].

b. Solution based on an organic precursor:

The most used organic precursors are metal alkoxides of generic formula M $(OR)_z$ where M denotes a metal of valence z and R denotes a radical of an alkyl chain - $(C_n H_{2n+1})$. The metal alkoxides must be of high purity and have high solubility in a wide variety of solvents. This condition of high solubility can generally only be achieved in organic solvents. The main advantage of using organic precursors is to allow a homogeneous and intimate molecular mixture of different precursors in order to produce glasses and ceramics with several components [120].

II.3.2 Reaction mechanisms of the sol-gel method

The chemical transformation mechanism breaks down into two stages:

• Hydrolysis, which corresponds to the activation reaction.

• Condensation-polymerization which is the stage of chain growth.

a. Hydrolysis reaction

It is a chemical reaction where a hydroxyl group $(OH)^-$ binds to a molecule $M(OR)_n$ of the metal alkoxide to form a bond $M(OR)_{n-x} - (OH)_x$.

$$M(OR)_n + xH_2O \longrightarrow M(OR)_{n-x} - (OH)_x + x\ ROH \qquad \text{(II-3)}$$

The hydrolysis reaction is accompanied by consumption of water and release of alcohol. After this step, the precursors are functional with respect to the condensation step [121].

b. The condensation

A condition for condensation is generally at least partial hydrolysis of the precursors. This hydrolysis generates a much better nucleophilic hydroxyl group than the alkoxide group. It follows that the hydroxyl group reacts by nucleophilic substitution with a mechanism analogous to hydrolysis. A "metalloxane" (M-O-M) bridge will form with a temporary increase in the coordination of the metal. Two mechanisms compete: alkoxolation and oxolation.

i) Alcoxolation:

This reaction takes place between two metal alkoxides, only one of which has been partially hydrolyzed. Its reaction mechanism is similar to that of hydrolysis.

$$(OR)_{n-x}M(OH)_n + M(OR)_n \longleftrightarrow (OR)_{n-x}(OH)_{n-x}\ M-O-M(OR)_{n-1} + ROH \qquad \text{(II.4)}$$

ii) Oxidation

This mechanism occurs between two partially hydrolyzed alkoxides. The mechanism remains the same, except that the leaving group is a water molecule.

$$M(OH)_n(OR)_x\ (OR)_{n-y} + M(OH)_2 \longleftrightarrow (OR)_{n-x}(OH)_{x-1}M-O-M(OR)_{y-1} + (OR)_{n-x} + H_2O \qquad \text{(II.5)}$$

In the majority of metal alkoxides, the hydrolysis reactions quickly lead to the condensation of particles of insoluble oxides and hydroxides, which means that the solution cannot be used to deposit thin layers. To avoid this condensation of non-hydrolyzed solutions, hydrolysis occurs either through the humidified atmosphere or by adding water to it in the form of an alcoholic solution [121].

c.Polycondensation

The reaction takes place between two metal alkoxides, only one of which is partially hydrolyzed. Its reaction mechanism is similar to that of hydrolysis growing polymer chains which agglomerate by polycondensation to form clusters. This reaction constitutes the actual polymerization of the precursors. The size of the clusters increases with

an increase in the viscosity of the solution. When all the bonds have been used, the gel is formed. The transformation of the solution into a solid gel is then called the sol-gel transition. From this moment the infinite cluster, called gel fraction, continues to incorporate the smaller polymeric groups, and the elastic constant of the gel increases [121].

II.3.3 Different sol-gel methods

Several techniques can be used for the deposition of thin films on a given substrate: the "spin-coating", the "drain-coating" and "dip-coating". Each having their own characteristics, the choice of method of deposition depends on the characteristics of the substrate such that its geometry or size. The two methods presented below are the most commonly used.

II.3.3.1 Spin-coating

This method involves depositing a small puddle of a fluid resin onto the center of a substrate. Then spinning the substrate at high speed. This technique has the advantage of being easily implemented, for moderate investments. It gives excellent results on planar substrates with dimensions of the order of cm^2. This deposition method can be divided into four phases, shown schematically in figure II. 1:

1) The deposition of the solution.

2) The start of rotation: the acceleration step causes the flow of liquid outwardly of the substrate.

3) Rotating at a constant speed allows the ejection of excess liquid in the form of droplets and the reduction of the thickness of the film uniformly.

4) Evaporation of the more volatile solvent which increases the reduction of the thickness of the deposited film [119]. Final film thickness and other properties depend on the parameters chosen for the spin process.

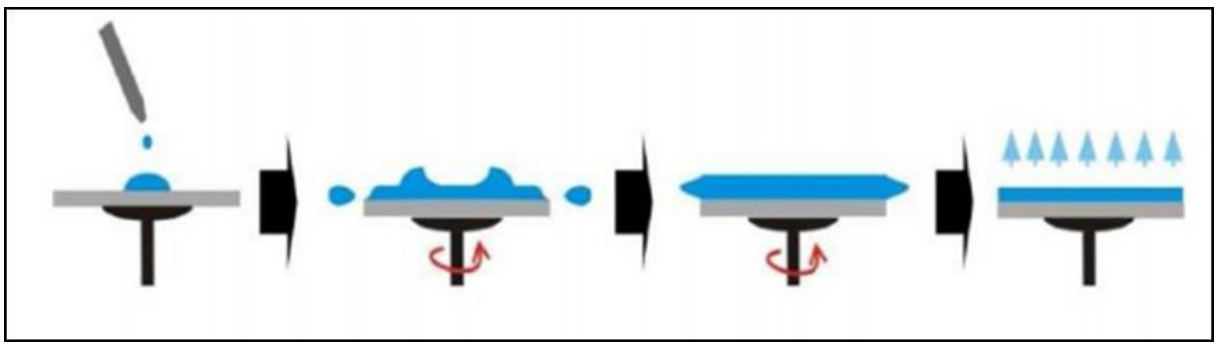

Fig.II.1 The four steps of spin coating [115].

II.3.3.2 Dip-coating:

The dip-coating technique can be described as a film deposition process where the substrate to coated is immersed in a liquid and then withdrawn with a well-defined speed under controlled temperature and atmospheric conditions [115,119].

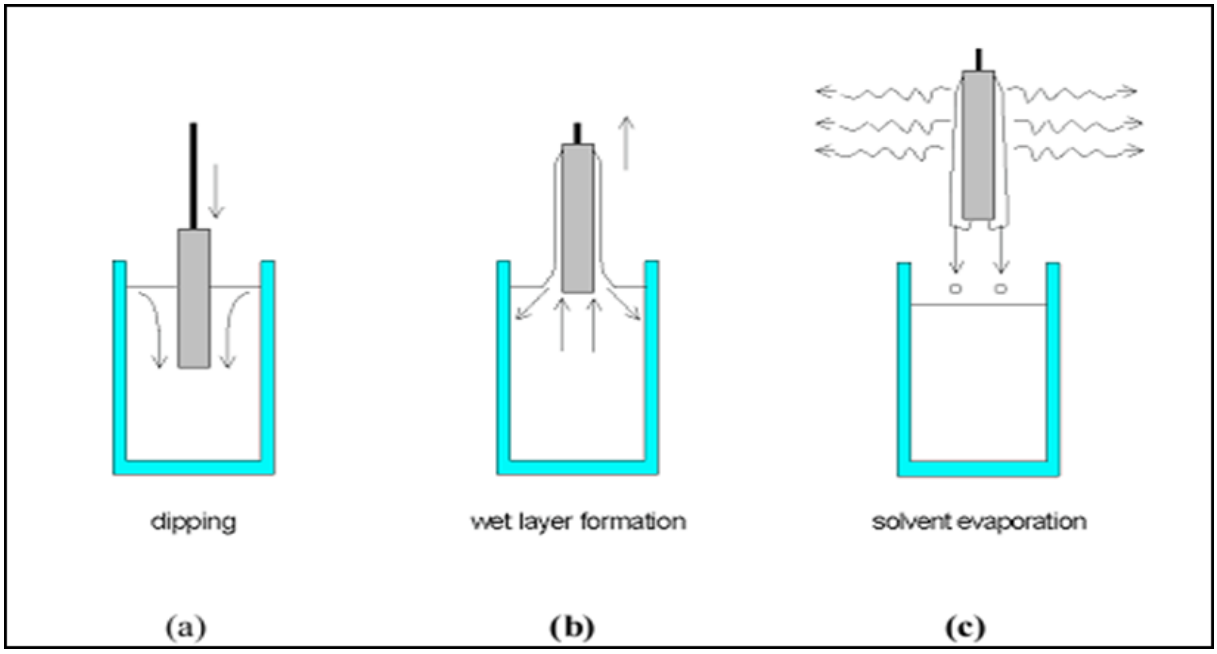

Fig.II.2 Stages of the dip-coating process: a) dipping of the substrate into the coating solution; b) wet layer formation by withdrawing the substrate; c) gelation of the layer by solvent evaporation [122].

II.4 Characterization methods

A measurement of thin-film properties is indispensable for the study of thin film materials and devices. The chemical composition, crystalline structure, and optical, electrical, and morphological properties must be considered in evaluating thin films.

II.4.1 X rays diffraction (XRD)

The X rays diffraction is carried out to study the crystalline quality of the TiO_2 thin films. It is a simple and non-destructive analysis technique, which provides means to identify different phases and their distribution in the sample, texture, evaluate average grain size, internal stress, etc [8].

X-rays are electromagnetic waves with wavelength (0.5-50 Å) comparable to atomic separation distances. When propagating through a crystal, the X-rays interact with the lattice and are diffracted according to the Bragg's law [8]:

$$2d_{hkl}\sin\theta = \lambda \qquad (II.6)$$

d_{hkl}:The atomic spacing.

θ: The scattering angle..

λ: The wavelength.

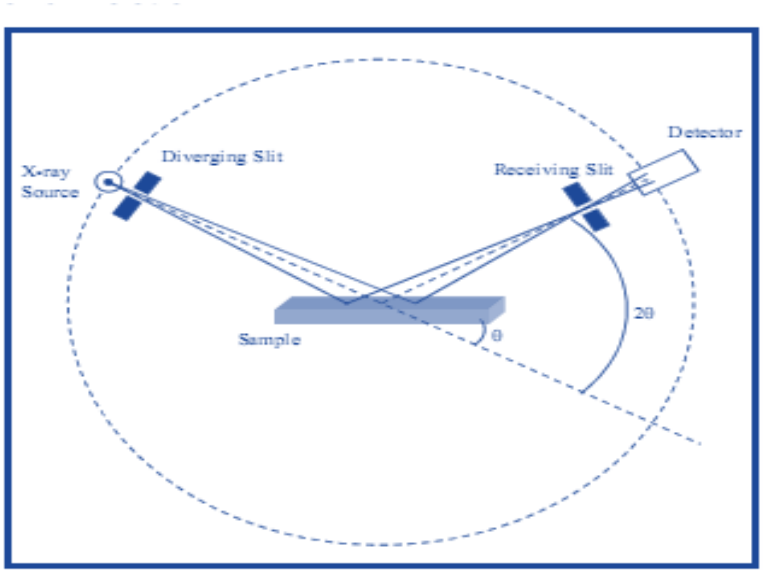

Fig.II.3.Schematics of X-ray diffractometer [8].

In this technique, the diffracted radiation is detected by the counter tube, which moves along the angular range of reflections. The intensities are recorded on a computer system. The X-ray diffraction data thus obtained is printed in tabular form on paper and is compared with Joint Committee Power Diffraction Standards (JCPDS) data to identify the unknown material. The sample used may be powder, single crystal or thin film. The crystallite size of the elaborated sample is estimated from the full width at half maximum (FWHM) of the most intense diffraction line by Scherrer's formula as follows [8]:

$$D = \frac{0.9\,\lambda}{\beta\,cos\theta} \qquad (II.7)$$

D: The crystallite size (nm).

λ : The wavelength of X-ray (nm).

β:The full width at half maxima of the peak (FWHM) in radians,

θ:TheBragg's angle (rd.).

It can be calculate the dislocations density using the grains size values according to the following relationship [8]:

$$\delta = \frac{1}{D^2} \qquad \text{(II. 8)}$$

The micro-strain are calculated using, a Williamson-Hall plot method [123]

$$\beta \cos\theta = \frac{0.9\,.\lambda}{D} + 4\,\varepsilon \sin\theta \qquad \text{(II.9)}$$

The lattice parameter values for Tetragonal system can be calculated from the following equations using the (hkl) parameters and the interplanar spacing d [115].

$$\frac{1}{d^2} = \frac{h^2+k^2}{a^2} + \frac{l^2}{c^2} \qquad \text{(II.10)}$$

II.4.2 Scanning electron microscope (SEM)

The scanning electron microscope (SEM) is a type of electron microscope that images the sample surface by scanning it with a high-energy beam of electrons in a raster scan pattern. The electrons interact with the atoms to make the sample producing signals that contain information about the surface of the sample, composition and other properties of the TiO_2 thin films. The SEM uses electrons instead of light to form an image. A beam of electrons is produced at the top of the microscope by heating of a metallic filament. The electron beam follows a vertical path through the column of the microscope. It makes its way through electromagnetic lenses which focus and direct the beam down towards the sample. Once it hits the sample, other electrons such as backscattered or secondary are ejected from the sample (see Figure II.4). The SEM gives information on the surface morphology of the sample, which can help us check whether the growth has taken place or not. The SEM produces 2D images and reveals topographic features of the sample, which allows us to examine the diameter, length, shape and density of the TiO_2 nanostructures. However, the images from the SEM cannot definitively prove that the obtained nanostructures actually consist of TiO_2 [8].

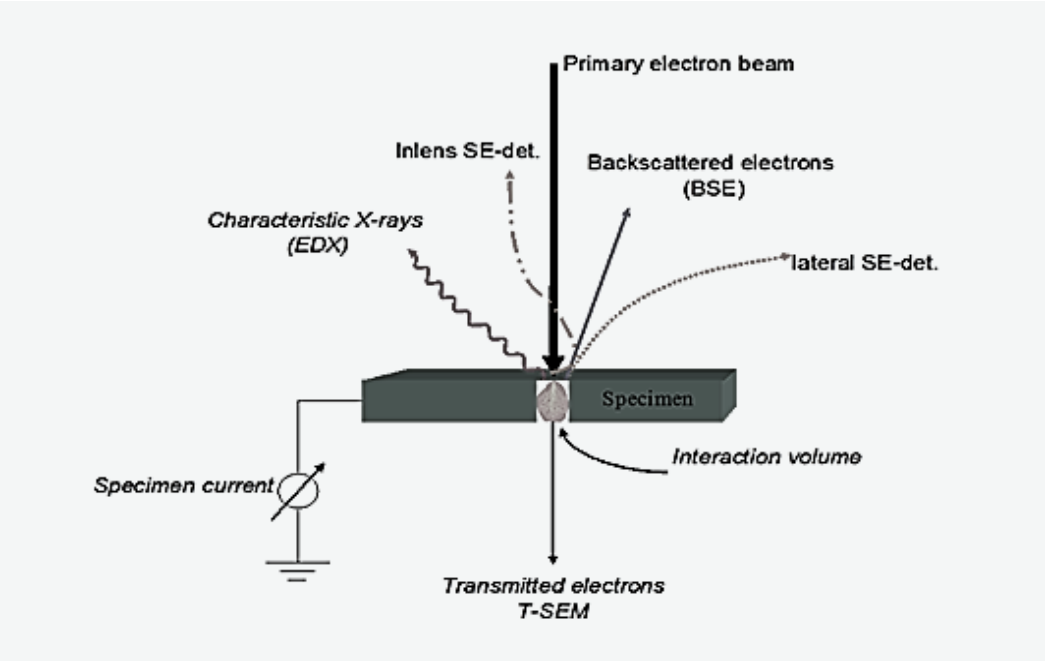

Fig.II.4 Illustration of electron-specimen interactions in SEM [8].

II.4.3. Energy dispersive X-ray spectroscopy (EDS or EDX)

EDX is a chemical microanalysis technique used in conjunction with SEM. EDX can provide elemental analysis on areas as small as nanometer in diameter and it is used to determine the elemental composition of individual points or to map out the lateral distribution of elements from the imaged area. When an incident electron beam hits atoms of the sample, secondary and backscattered electrons are emitted from the sample surface. However, these are not the only signals emitted from the sample. When the incident beam bounces through the sample creating secondary electrons, it leaves thousands of the sample atoms with holes in the electron shells where the secondary electrons used to be. If these "holes" are in inner shells, the atoms are not in a stable state. To stabilize the atoms, electrons from outer shells will drop into the inner shells, however, because the outer shells are at a higher energy state, to do this the atom must lose some energy. It does this in the form of X-rays. The X-rays emitted from the sample atoms are characteristic in energy and wavelength to, not only the element of the parent atom, but which shells lost electrons and which shells replaced them, this permits the elemental composition of the sample to be measured. An EDX spectrum not only identifies the element corresponding to each of its peaks, but also the type of X-ray to which it corresponds as well. For example, a peak corresponding to the amount of energy possessed by X-rays emitted by an electron in the L-shell going to the K-shell is identified as a K-alpha peak. The peak corresponding to X-rays emitted by M-shell electrons going to the K-shell is identified as K-beta peak [119] (Figure II.5).

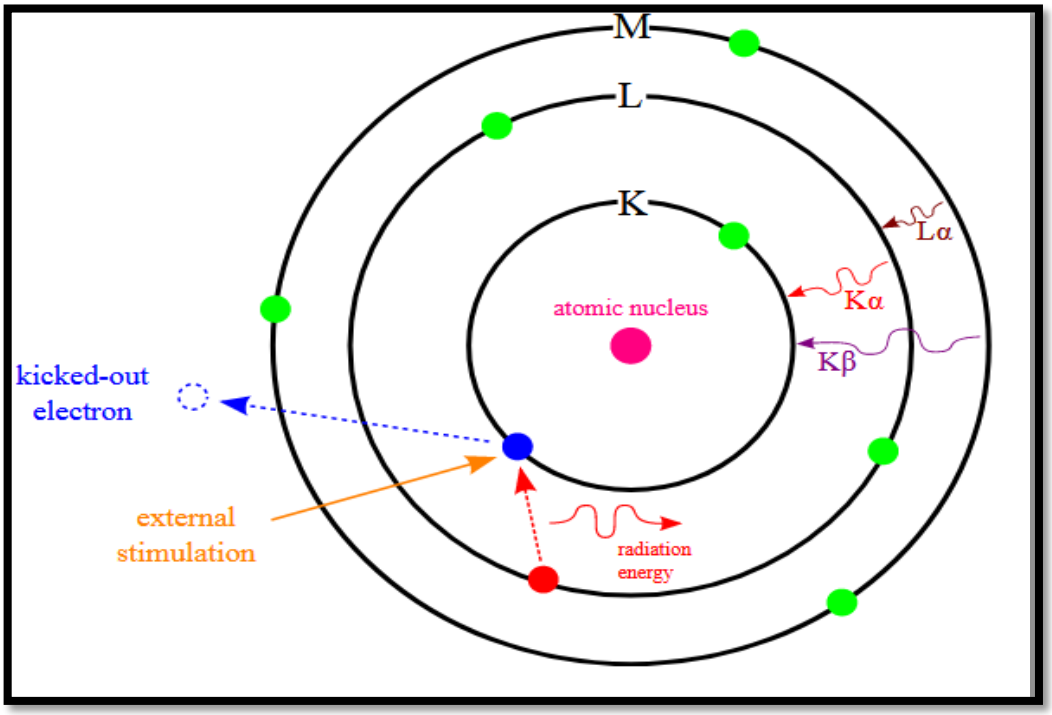

Fig.II.5 Scheme of X-ray excitations in EDX analysis [119].

II.4.4 Photoluminescence spectroscopy

The spontaneous emission of light from a material under optical excitation is known as photoluminescence (PL). Photoluminescence spectroscopy is a nondestructive method to probe the electric structure of materials. PL spectroscopy can be used to characterize a variety of material parameters. It provides electrical characterization and information on the quality of surfaces and interfaces. It is a direct method to measure various important material properties such as band gap, impurity levels, and defect detection and recombination mechanism. The schematic diagram of the PL measurement set-up is shown in Figure II.6.

When light of sufficient energy is incident on a material, photons are absorbed. Electrons are excited due to the energy of absorbed photons and goes to the excited state.

Eventually, such excited electrons reach to the ground state with emitting radiations in the form of light. This emitted light can be collected and analyzed to get information about the material. After analyzing the signals, transition energies and electronic energy levels can be determined [119].

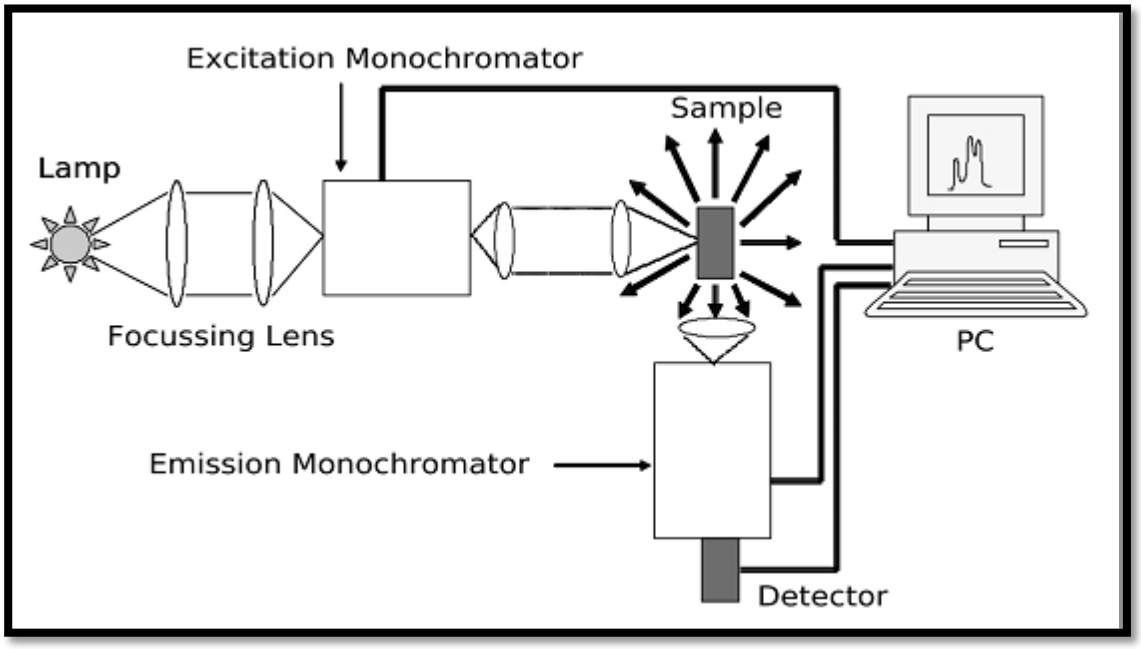

Fig.II.6 Schematic diagram showing elements used to measure photoluminescence spectra [124].

II. 4.5 Fourier Transform Infrared (FTIR)

The FTIR is mostly used to identify chemicals that are either organic or inorganic. We can also use it to get information of some compounds of an unknown mixture. The FTIR can be applied to the analysis of solids, liquids and gases. Today, the FTIR is computerized and it has become more sensitive than the other dispersive instruments.

The FTIR not only identify chemicals but also identify the types of chemical bonds (functional group). To get absorption spectrum of material it absorbs the wavelength of light. By interpreting the IR absorption spectrum, we can able to determine the chemical bonds in the molecule. We can obtain unique FTIR spectra of pure compounds like a molecular fingerprint. The spectrum of unknown materials can be identified by comparison to a library of known compounds.

West coast analytical service (WCAS) has several IR spectral libraries including online computer libraries. A schematic diagram of FTIR is as shown in Figure II.7 [125].

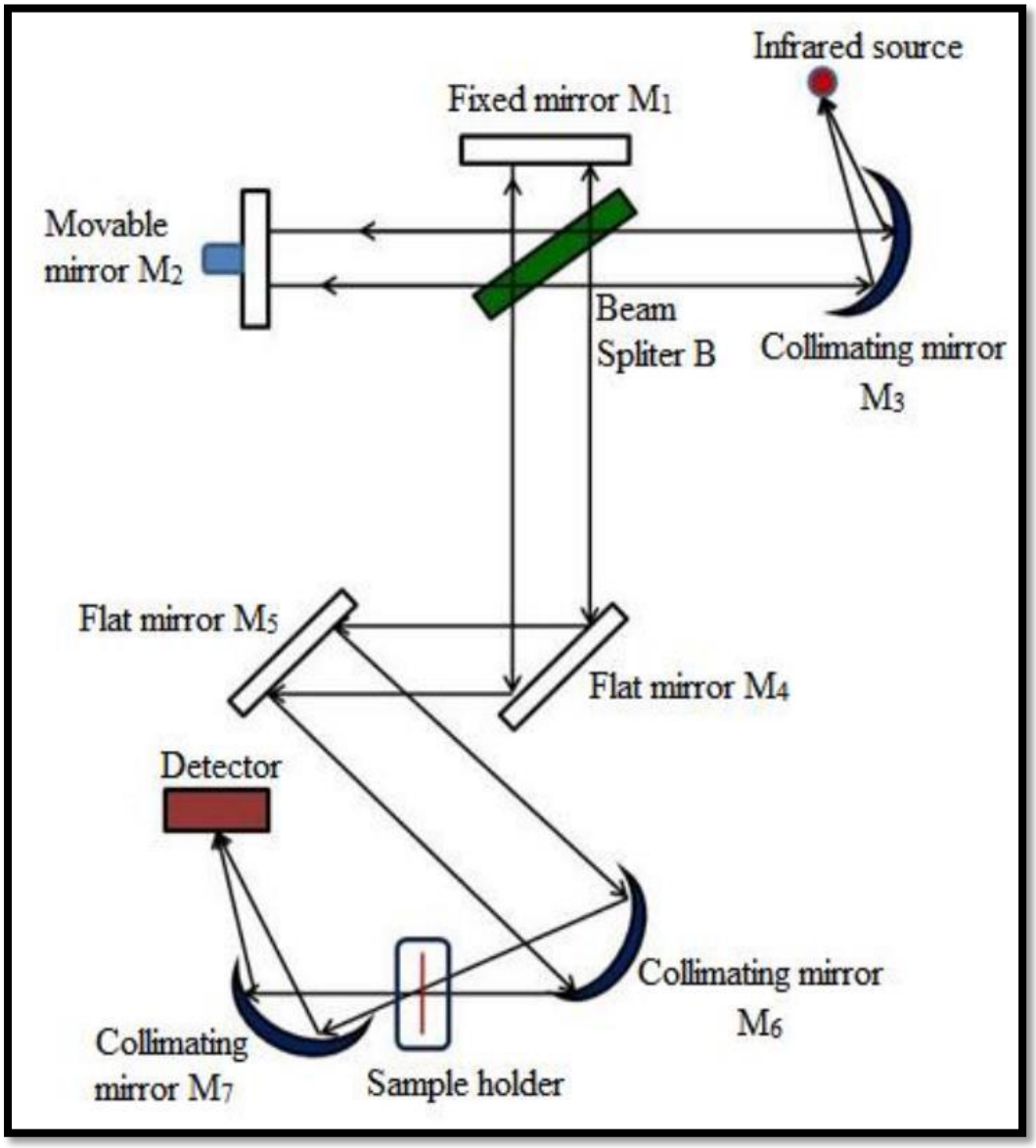

Fig.II. 7 Schematic diagram of a Fourier transform infrared spectrometer [125].

II. 4. 6. Raman spectroscopy

Raman spectroscopy is a spectroscopic technique based on inelastic scattering of monochromatic light, usually from a laser source. Inelastic scattering means that the frequency of photons in monochromatic light changes upon interaction with a sample. Photons of the laser light are absorbed by the sample and then reemitted. Frequency of the reemitted photons is shifted up or down in comparison with original monochromatic frequency, which is called the Raman Effect. This shift provides information about vibrational, rotational and other low frequency transitions in molecules (to determine the crystalline phases). Raman spectroscopy can be used to study solid, liquid and gaseous samples. A Raman system typically consists of

four major components: excitation source (Laser), sample illumination system and light collection optics, wavelength selector (Filter or Spectrophotometer) and detector (Photodiode array, CCD or PMT).

A sample is normally illuminated with a laser beam in the ultraviolet (UV), visible (Vis) or near infrared (NIR) range. Scattered light is collected with a lens and is sent through interference filter or spectrophotometer to obtain Raman spectrum of a sample [115].

II.4.7 UV-Visible spectroscopy

Ultraviolet-visible spectrophotometer involves the spectroscopy of photons in the ultraviolet region (200–400 nm) and visible region (400–800 nm). It is a type of absorption spectroscopy in which the excitation of the electrons takes place from ground state to excited state while fluorescence measures transitions from excited state to ground state. The method is most often used in a quantitative way to determine concentrations of an absorbing species in sample using the Beer-Lambert law. The principle involved in UV-VIS Spectroscopy states that, when a beam of monochromatic light is passed through a homogeneous medium of an absorbing substance, the rate of decrease in intensity of radiation with respect to thickness of the absorbing medium is directly proportional to the intensity of incident radiation as well as the concentration of the medium [119].

$$I = I_0\ e^{-\alpha d} \qquad \text{(II. 11)}$$

where α is the absorption coefficient, d is the thickness of the film, I_0 and I are the intensity of the incident and the transmitted beams, respectively.

The absorption coefficient (α) can be calculated using the following expression:

$$\alpha = \frac{1}{d}\ln\frac{100}{T\ (\%)} \qquad \text{(II. 12)}$$

where T(%) is the transmittance (quantity of the transmitted light), and can be directly measuredby [119]:

$$T\ (\%) = \frac{I}{I_0} \times 100 \qquad \text{(II. 13)}$$

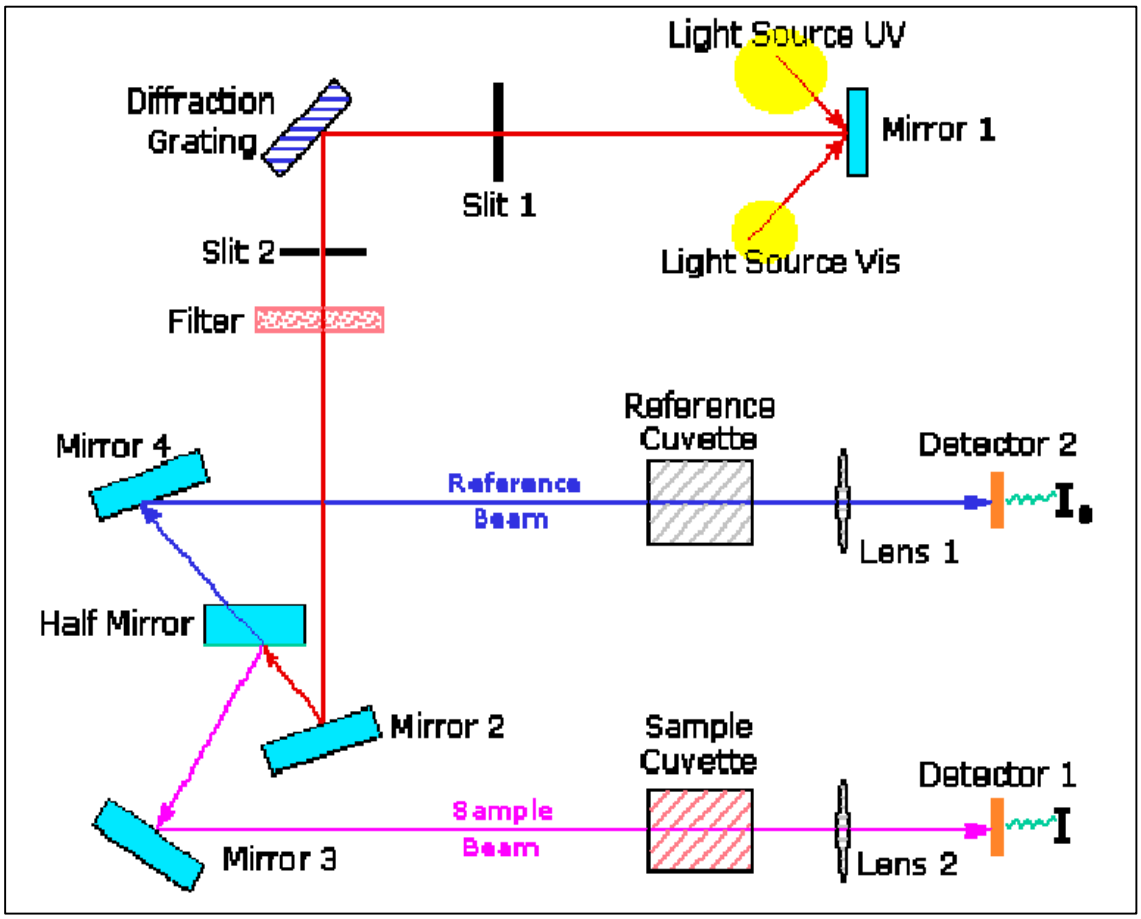

Fig.II.8 Schematic representation of UV-Visible Spectrophotometer [126].

II.4.7.1 Film thickness *d* (Swanepoel method):

$$d = \frac{\lambda_1 \lambda_2}{2(\lambda_1 n_2 - \lambda_2 n_1)} \qquad \text{(II. 14)}$$

Where: n_1 and n_2 are the refraction index of the film for the wavelength λ_1 and $\lambda_2$respectively, we can calculate n_1 and n_2 from the following relation:

$$n_{1,2} = \left[N_{1,2} + \left(N_{1,2}^2 + s^2\right)^{1/2}\right]^{1/2} \qquad \text{(II.15)}$$

Where: s is the refraction indexes of the substrate and $N_{1,2}$ can be obtained using this relation:

$$N_{1,2} = \frac{2s(T_M - T_{m1,2})}{T_M T_{m1,2}} + \frac{s^2+1}{2} \qquad \text{(II.16)}$$

With: $T_{m1,2}$ is the minimum transmittance corresponds with $\lambda_1(\lambda_2)$ and T_M is the maximum transmittance confined between T_{m1} and T_{m2} [127].

II.4.7.2 Optical bad gap Eg

In high energy, absorption results from electronic transitions between wide states of band to band. It is usually described by Tauc law [128]:

$$(\alpha h\nu)^n = A\left(h\nu - \mathrm{E_g}\right) \qquad \text{(II.17)}$$

Where: $h\nu$ is the photon energy, Eg is optical gap n and A are constants, n characterizes the optical type of transition and takes the values 2, 1/2 (2 for allowed direct transitions or 1/2 for allowed indirect transitions). In order to determine the nature of the transition from the films produced in this study, we will plot the curves $(\alpha h\nu)^n = f\ (h\nu)$ [129]. We can obtain E_g value as it showing in figure (II.9):

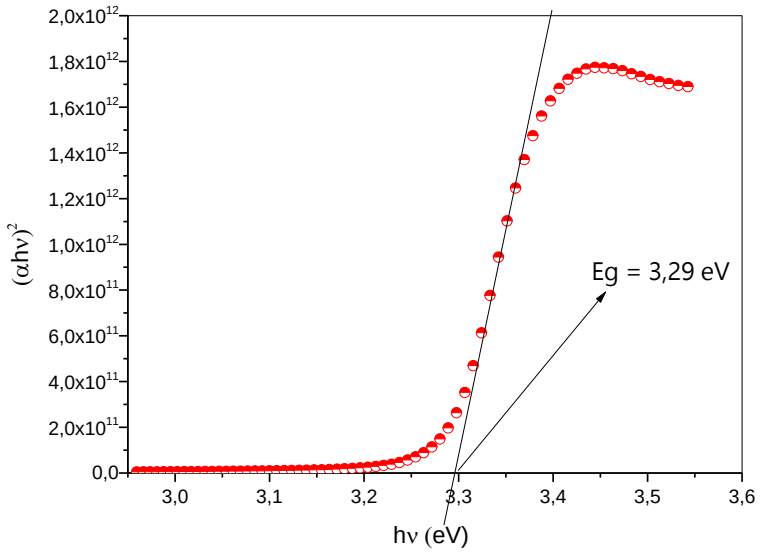

Fig.II.9. Curve represent the function $(\alpha h\upsilon)^2 = f(h\upsilon)$[8].

II.4.7.3 Urbach energy (E_u)

Urbach energy is usually used to describe the width of the localized states in the band gap (but not their positions). Pankove [130] has shown that the value of Eu is related to the impurity concentration. However, Redfield [131] has shown that all defects (point, line and planar defects) lead to local electric fields that cause band tailing. Thus, the Urbach energy can be considered a parameter that includes all possible defects. The relation between the Urbach energy and absorption coefficient is described by [132]:

$$\alpha = \alpha_0 exp\left(\frac{h\nu}{E_u}\right) \qquad \text{(II.18)}$$

where α_0 is a constant and E_u is Urbach energy.

By drawing (α) versus $h\nu$ we can determine Eu value as the reciprocal of the linear part slope (Figure II.10) [119]:

$$Ln\ \alpha = Ln\ \alpha_0 + \frac{h\nu}{E_u} \qquad \text{(II.19)}$$

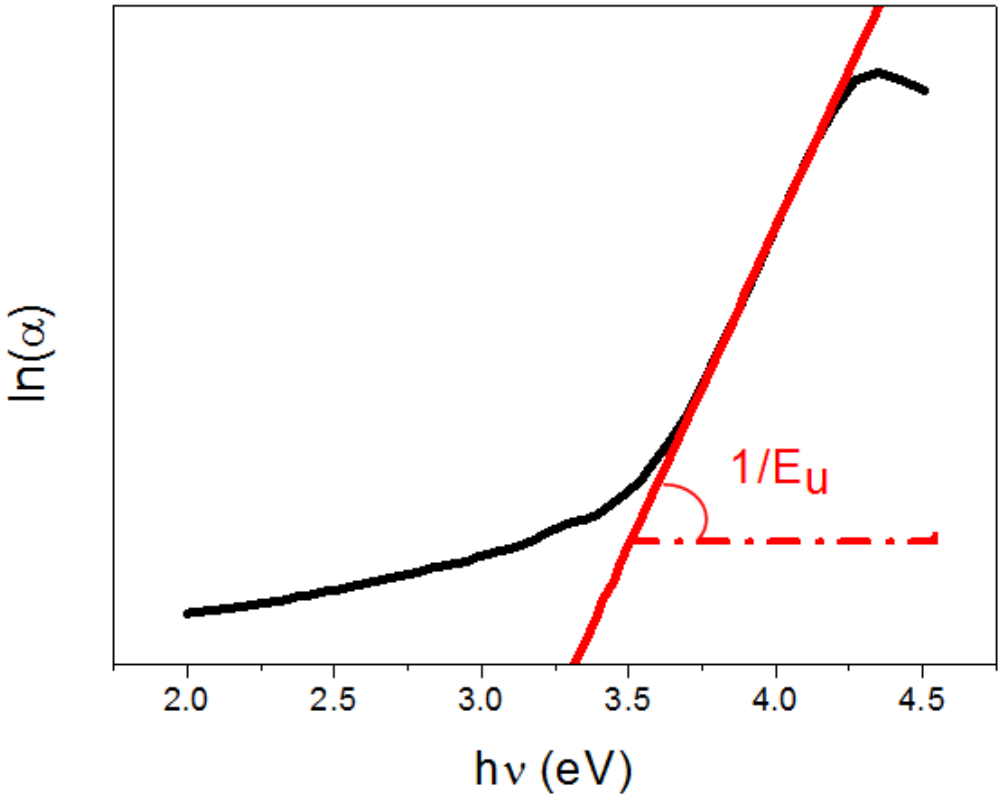

Fig.II. 10 Determination of Urbach energy (Eu) [119].

II.4.7.4 Refractive index (n) and porosity

The refractive index (n) was determined from the reflectance (R) data using [133]:

$$n = \frac{(R+1)^2}{(R-1)^2} - \sqrt{\frac{4R}{(R-1)^2} - k^2} \qquad \text{(II.20)}$$

And $k = \frac{\alpha\lambda}{4\pi}$ (k: extinction coefficient).

The porosity of elaborated films was calculated using the following relationship [134]:

$$Porosity = \left(1 - \frac{n^2-1}{n_d^2-1}\right) \times 100\ \% \qquad \text{(II.21)}$$

Where n_d is the refractive index of pore-free anatase TiO2 (nd = 2.52), and n is the refractive index of the samples at 550 nm as a wavelength.

Chapter III

Solution concentration C_s effect on Anatase TiO_2 thin films Properties

III.1. Introduction

In this chapter, TiO_2 thin films were elaborated by gel sol (spin coating) using titanium (IV) isopropoxide as a precursor. In the first part, structural, optical and morphological properties of TiO_2 as a function of the solution concentration C_S are examined. Whereas in the second part, the photocatalytic properties of TiO_2 thin films are studied.

III.2. Experimental details

III.2.1. Used apparatus (Spin coater):

The spin coater which was used to deposit the TiO_2 thin films has the following shape and characteristics (Fig.III.1):

Fig.III.1 Holmarc Spin coater.

III.2.2.Preparation of the substrate:

III.2.2.1. Choice of substrate:

The studied films were deposited on substrates of solid glass which have a length of 2.5cm and a width of 2.5cm; the choice of glass like substrate of depot was adopted because of the following reasons:

- The thermal compatibility with TiO_2 which minimize the stress in the interface film/substrate.

- For their transparency which adapts well for the optical characterization of films in the visible one.
- For economic reasons.

III.2.2.2. Cleaning of the substrate

The adherence and the quality of the depot repose on purity and the state on substrate thus the cleaning of the substrate is one of the most important steps, the cleaning of our substrates surfaces is as follows:

- The substrates are cut using a pen with diamond point.
- Cleaning with soap solution.
- Rinsing with the water distilled and then with acetone during 5 min.
- Rinsing with distilled water.
- Rising with methanol during 5 min at ambient temperature.
- Cleaning in water distilled bath.
- Drying using a drier.

III.2.3.Preparation of the solution

At room temperature, TiO_2 thin films were deposited as a function of concentration solution using sol gel (spin coating) process. The solution was prepared by mixing tetranium (IV) isopropoxide (Ti [OC-H $(CH_3)_2]_4$) which was used as precursor and acetyl acetone (CH_3COCH) used as a stabilizer and ethanol (C_2H_5OH) used as a solvent, where the ratio of Titan Tetra (IV) isopropoxide and acetyl acetone 1:1. The solution concentration C_S varied from 0.1M to 0.5M with the step of 0.1M.

The solution put on stirrer at 50 ° C for 3 hours. Titanium dioxide thin films (TiO_2) deposited on the glass substrate. The films were dried at 250 ° C for 10 min followed by annealing at 500 ° C for 2 houre. The deposition of TiO_2 layers by sol-gel route comprises the following two stages: the hydrolysis and the polycondensation of titanium alkoxides according to the following reactions [135]: ($R = C_3H_7$)

$$C_2H_5OH \longrightarrow C_2H_4 + H_2O \qquad \text{(III.1)}$$

$$Ti(OR)_4 + H_2O \longrightarrow Ti(OR)_3(OH) + ROH \qquad \text{(III.2)}$$

$$Ti(OR)_4 + Ti(OR)_3(OH) \longrightarrow Ti_2O(OR)_6 + ROH \qquad \text{(III.3)}$$

The reaction stops with the inclusion of two water molecules:

$$Ti(OR)_4 + 2H_2O \longrightarrow TiO_2 + 4\ ROH \qquad (III.4)$$

III.2.4.Depositing of thin films

The precursor solution mentioned previously was dropped on glass substrate until the covering of all the surface (the sufficient quantity is V= 0.25 ml). The substrate was rotated by using spin coater; the spinner reached 4000 rpm after 10 s which was maintained for 30 s. After each coating, the coated film was dried at 250 °C for 10 min . the preheat-treatment temperature of 250 °C is required for the evaporation of organic solvents and the initiation of formation and crystallization of the TiO_2 film. After the deposition and drying of the five layer, the resulting thin films were inserted into a furnace and annealed in 500°C for 2 h. The adhesion test was used to confirm the adhesion of the TiO_2 layers. The preparation of TiO_2 thin films is shown in figure III.2.

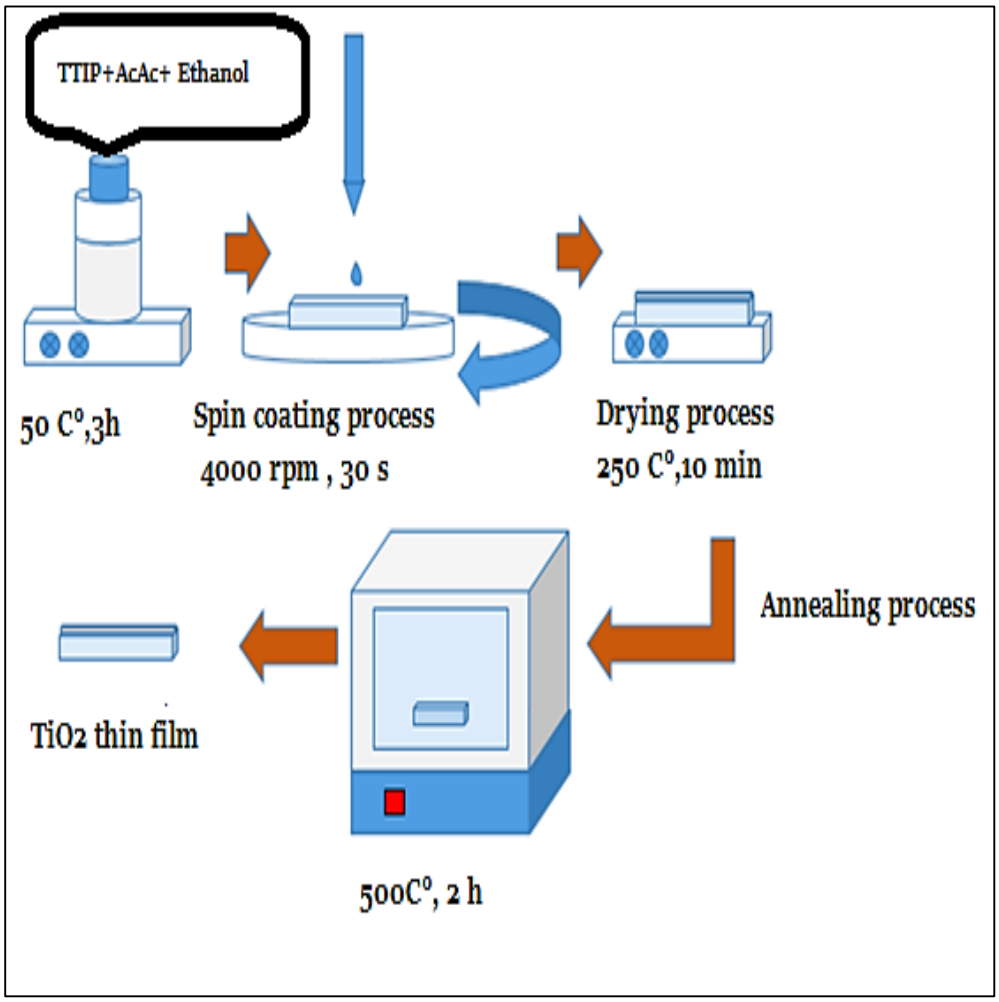

Fig.III.2 Schematic represents the experimental procedure.

III.3 Results and discussion

III.3.1 Film thickness

Fig.III.3 illustrates the evolution of the thickness of the titanium dioxide (TiO_2) films as a function of solution concentration C_S. It can be noted that the thickness of the elaborated thin films increases with the increasing concentration of the solution. This is explained by the increase in the amount of material deposited on the surface of the substrate [136].

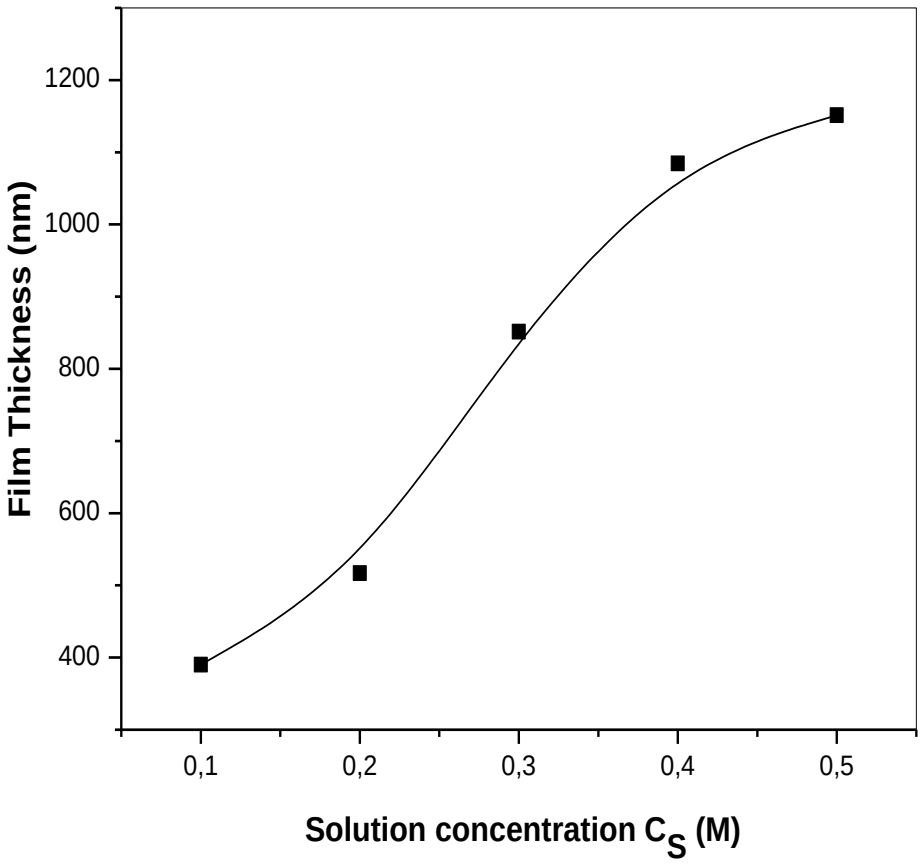

Fig.III.3 Titanium dioxide (TiO_2) films thickness as a function of solution concentration.

III.3.2. Structural characteristics

The structural characterization is carried out by X-ray diffraction. The diffractometer used for the characterization of the samples is of type XPERT-PRO with copper anode having an X-ray beam of wavelength Kα (Cu) = 1.5418 Å.

III.3.2.1.X.ray diffraction

The XRD diffraction spectra of TiO_2 thin films deposited by different concentrations of solution C_S under T = 500 ° C as a annealing temperature are shown in figure.III.4. The XRD diffractions peaks around 2θ = 25.41, 37.94 °, 48.05 °, 54.13 °, 55.39 °, 70.24 ° and 75.14 ° which correspond to the planes (101), (004), (200), (105), (211), (220) and (215). These reflections peaks correspond to the anatase phase of TiO_2 according to (JCPDS 21-1271). This pase has a tetragonal structure with cell parameters corresponding to a = 3.7852 A ° and c = 9.5139 A ° [137].

The presence of these orientations in X-ray spectra indicates that the films are polycrystalline. Moreover, there are many possible orientations for the growth of TiO_2 crystallites. It may be noted that the films are oriented preferentially along to the plane (101) because this orientation has a minimum energy for the growth of the TiO_2 thin films [138, 139].

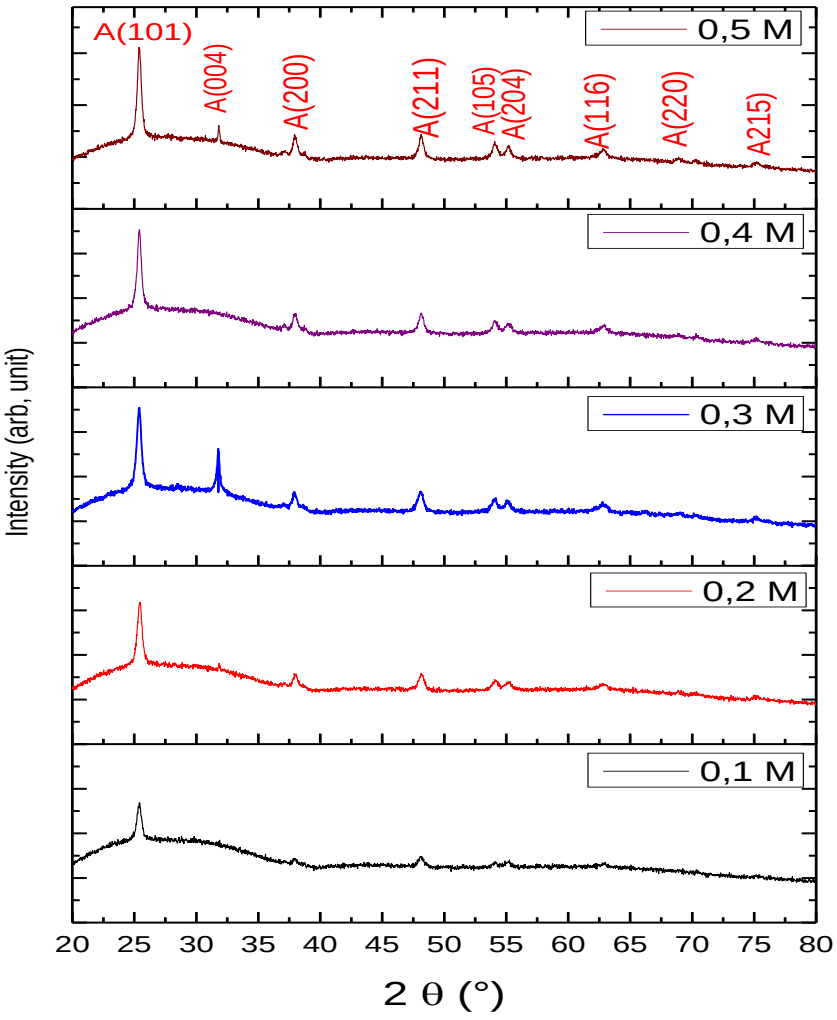

Fig.III. 4 XRD spectra of TiO_2 thin films with different solution concentration.

It can be noted that the crystalline state of the samples will be improved with increasing of the solution concentration C_S. This is attributed to the increase in nucleation sites due to the increased of mater deposited on the surface of the substrate [140]. The disappearance of the plane (004) at the sample level of 0.4 M could be due to the change of symmetry groups.

III.3.2.2.Grain size (D)

The grain size D of the samples was estimated using the Scherer formula (equation II.7). It is generally known that the grain size measured by this method is generally lower than the actual value. This is the consequence of internal stresses and defects in the deposited thin films [141]. It may be noted that the size of the grains increases as a function of the concentration of the solution (see figure.III.5).

It is noted that there are two modes of change in increasing the grain size: The first mode, we notice a slight increase in the grain size when the solution concentration is less than 0.4 M. This means that a change in the solution concentration has a slight effect on the grain size. A slight increase in the grain size can be explained by the reaction kinetics where they are increased in the number of nucleation sites due to the rise of the material deposited in one part. On the other hand, large grains absorb small grains to form large grains (coalescence step) but this step is slow.

The second mode, we notice a considerable change in the grain size when the solution concentration is greater than 0.4 M .The increase in grain size is attributed to the increase in the number of nucleation sites due to the rise of the material deposited in one part. On the other hand, large grains absorb small grains to form large grains (coalescence step) but this step is rapid. [142, 143].

III.3.2.3. Internal strain (ε)

The strain values (ε) of the TiO_2 films are calculated by a Williamson-Hall formula (equation II.9). The variation of the strain is illustrated in Fig.III.5. It can be observed that the strain is reduced with the increase of the concentration of the solution. This behavior can be explained by the improvement of the crystalline state of the films. The dislocation density (δ) is defined by the length of the dislocation lines per unit volume of the crystal. Table .III.1 shows the dislocation density values (δ) calculated using the following formula (equation II.8).

Table.III.1 structural properties of TiO_2 vs solution concentration C_S.

Solution concentration C_S (M)	Film thickness (nm)	Grain size D_{ave} (nm)	Dislocation density (δ_{ave}) × 10^{14}(line /m^3)	Internal strain ×10^{-3}
0.1	389.9	34.773	8.27	5.37
0.2	516.9	35.558	7.91	2.7
0.3	851.6	37.441	7.133	2.23
0.4	1084.4	37.445	7.131	1.89
0.5	1151.3	48.674	4.220	1.22

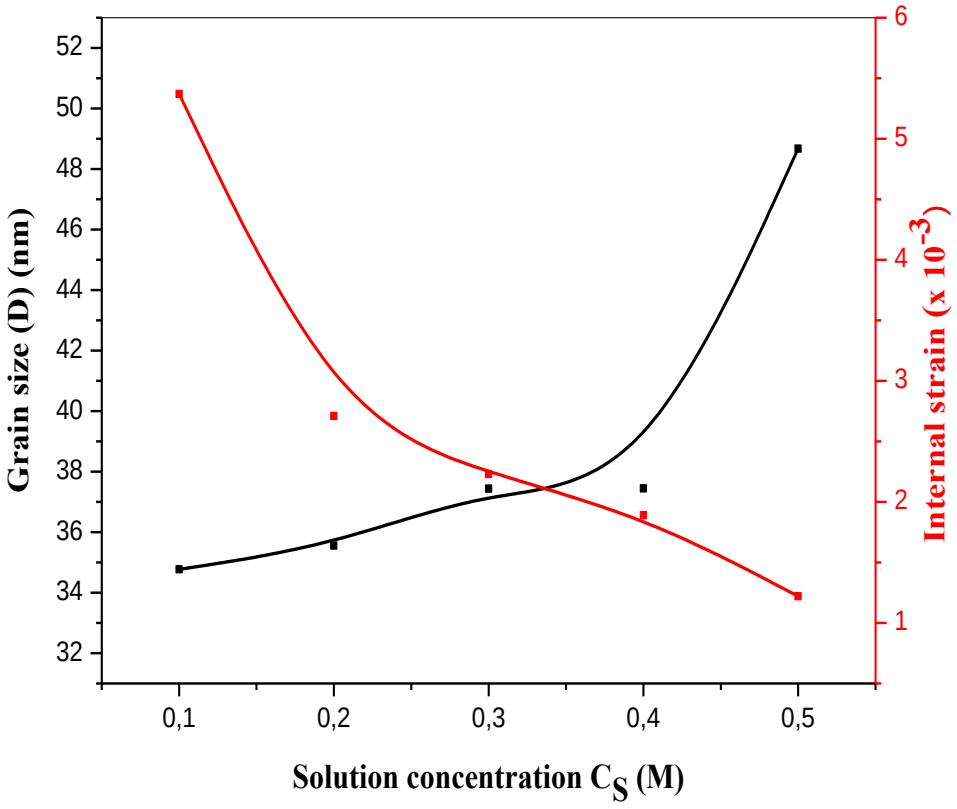

Fig.III.5 Grain size and internal strain as a function of solution concentration.

III.3.2.4 Lattice parameters

Anatase phase has a tetragonal structure with cell parameters were calculated (equation II.10) Table III.2 shows the cell parameters a and c experimental and theoretical. It is noted that the experimental cell parameters are less than the theoretical cell parameters, which indicates the presence of compression in the cell.

Table.III.2 The experimental and theoretical cell parameters on TiO_2 thin films.

Solution concentration (M)	**a_{exp} (A°)**	**c_{exp} (A°)**	
0.1	3.7804	9.4916	a_{the} = 3.7852 A° c_{the} = 9. 5132 A°
0.2	3.7792	9.4492	
0.3	3.7832	3.4968	
0.4	3.7812	9.5016	
0.5	3.7842	9.4992	

III.3.3. Fourier Transform Infra-Red (FTIR) spectra

Fig.IV.5 shows the Fourier transform infrared (FTIR) spectra of anatase titanium dioxide (TiO_2) synthesized by sol-gel spin coating. It can be observer a peak between 340 cm^{-1} and 500 cm^{-1} which characterizes the Ti-O-Ti bond with a stretching mode of vibration [144, 145]. Another peak between 500 cm^{-1} and 600 cm^{-1} corresponds to the stretching vibration of the Ti-O bond [144]. It can be seen that the height of Ti-O peak increases with increasing concentration of the solution. This indicates that the crystalline state of TiO_2 thin films is improving and the defects of the crystal lattice are reduced. This result has been correlated with the results obtained from the XRD spectra.

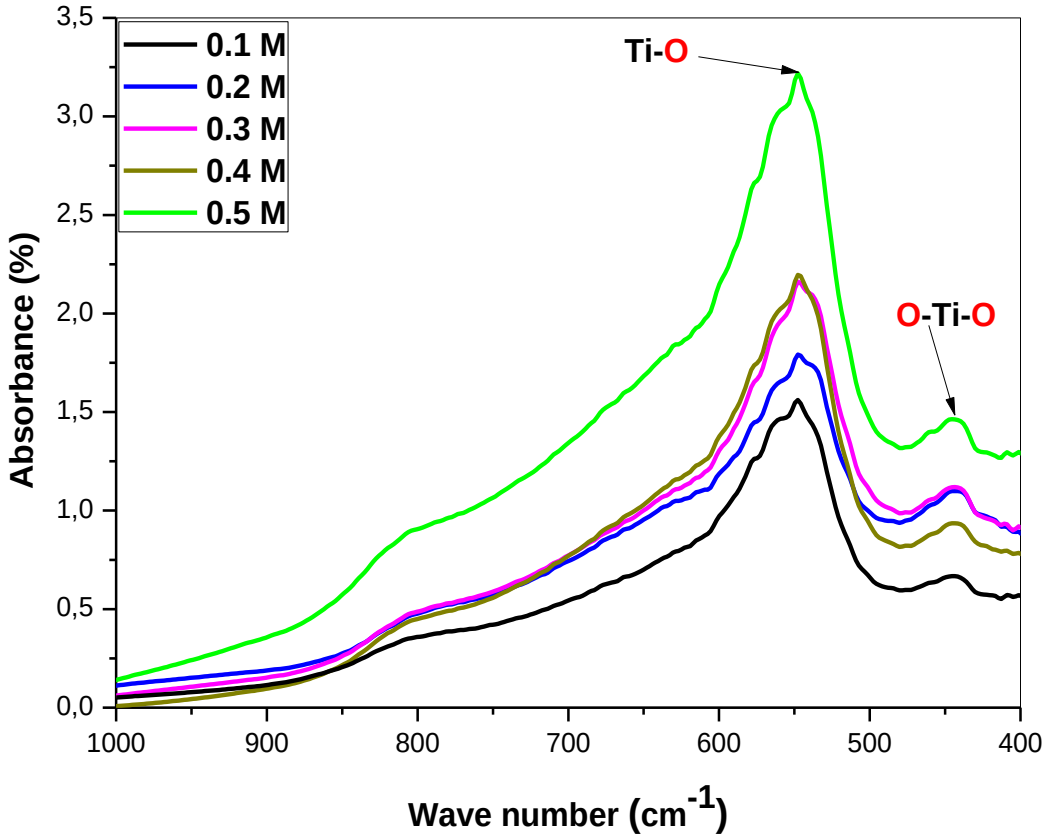

Fig.III.6 FTIR spectra of TiO_2 versus solution concentration.

III.3.4. Surface morphology

Scanning electron microscopy (SEM) is performed to study the morphology of thin films. Figure.III.7 shows SEM images of TiO_2 deposited at deferent solution concentration. It can be observed that TiO_2 deposited at low solution concentration has a smooth surface with a few small grains located on the surface of the substrate. At a higher solution concentration, as can be seen, the surface of the TiO_2 film has changed to a granular surface. The evolution of the film surface as a function of the concentration of the solution concentration as a function of the deposition rate can be explained as follows; at low deposition rate, this means that a few amounts of titanium dioxide have been deposited, a smooth surface is then formed. Increasing of TiO_2 amount leads to increase the grain size, which provoke the increase in film thickness.

This result reinforces DRX observations indicating the reduction of FWHM with increasing thickness [146].

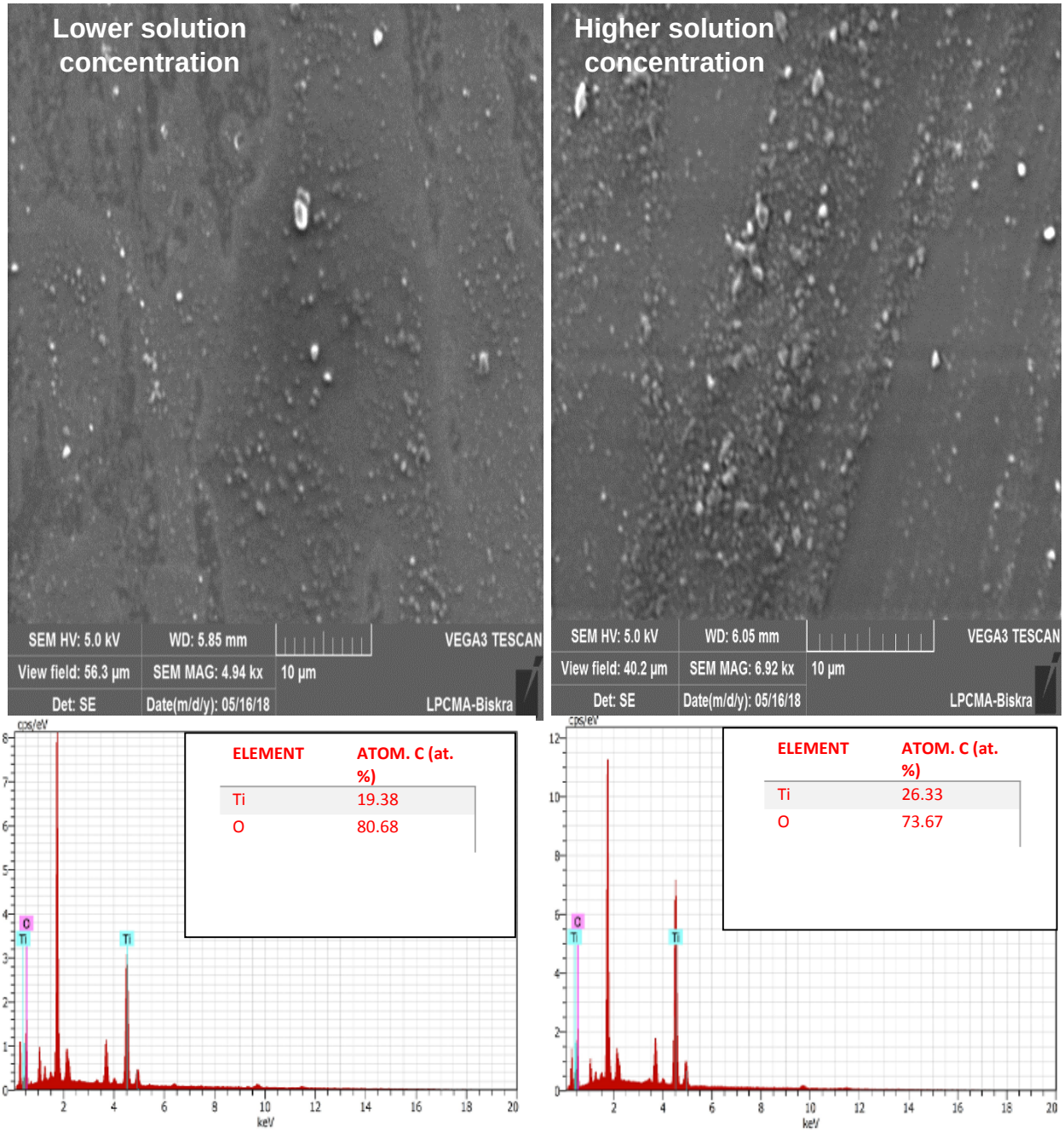

Fig.IV.7 SEM images and EDS spectra of TiO_2 thin films.

III.3.5. Optical properties

III.3.5.1. Transmittance and reflectance spectra

The transmittance and reflectance spectra of TiO_2 thin films as a function of solution concentration C_S are shown in Fig.III.8. It can be seen, the TiO_2 thin films have good transmittance in the visible range about 90 %. According to the interferences fringe, the elaborated films have a smooth surface.

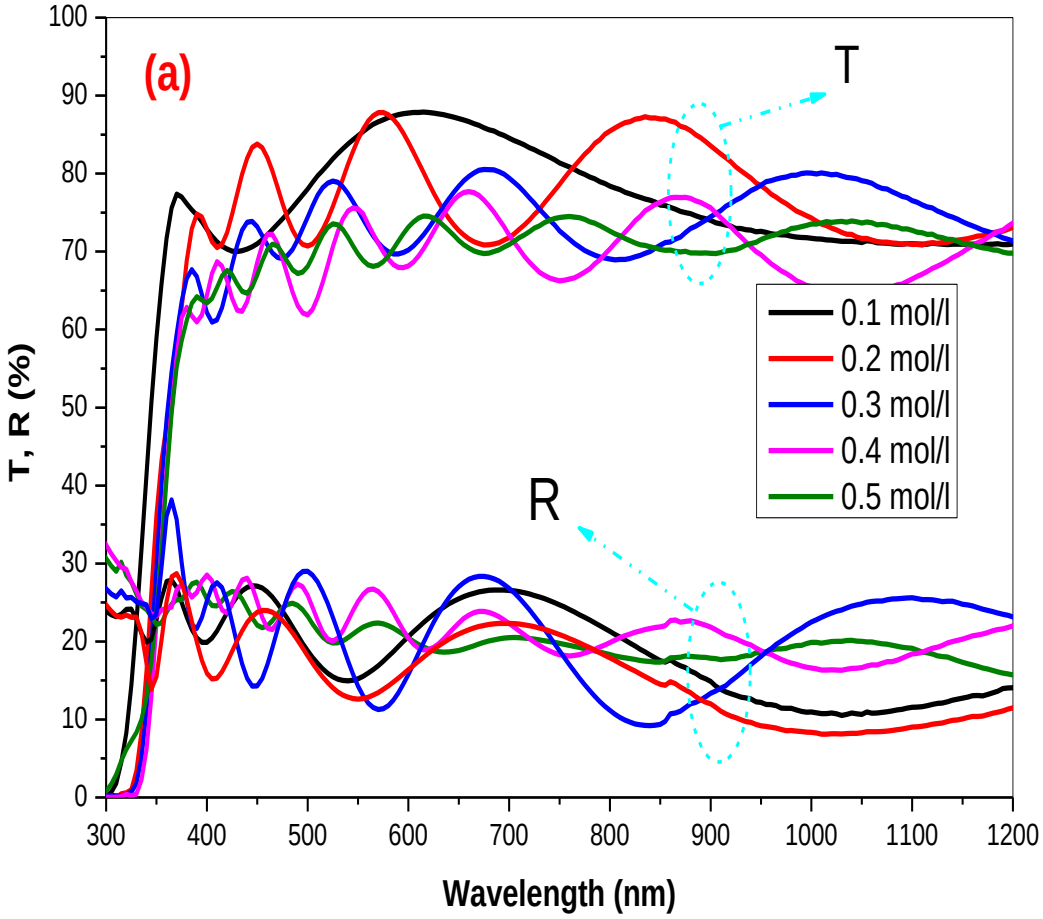

Fig.IV.8 Transmittance and reflectance spectra of TiO_2 thin films as a function of solution concentration.

III.3.5.2. Optical band gap

The absorption edge corresponds to the electronic excitation of the valence band at the conduction band, which determines the value of the direct optical band gap. The incident photon energy $h\nu$ and absorption coefficient α are related through the well-known equation [147]. The direct optical band gap values of thin films are calculated by extrapolating the straight line portion of the $\alpha h\upsilon^2 = f\ (h\nu)$ graph (Fig.III.9).

The indirect optical band gap values of thin films are calculated by extrapolating the straight line portion of the $\alpha h\upsilon^{1/2} = f\ (h\nu)$ graph (Fig.III.10).

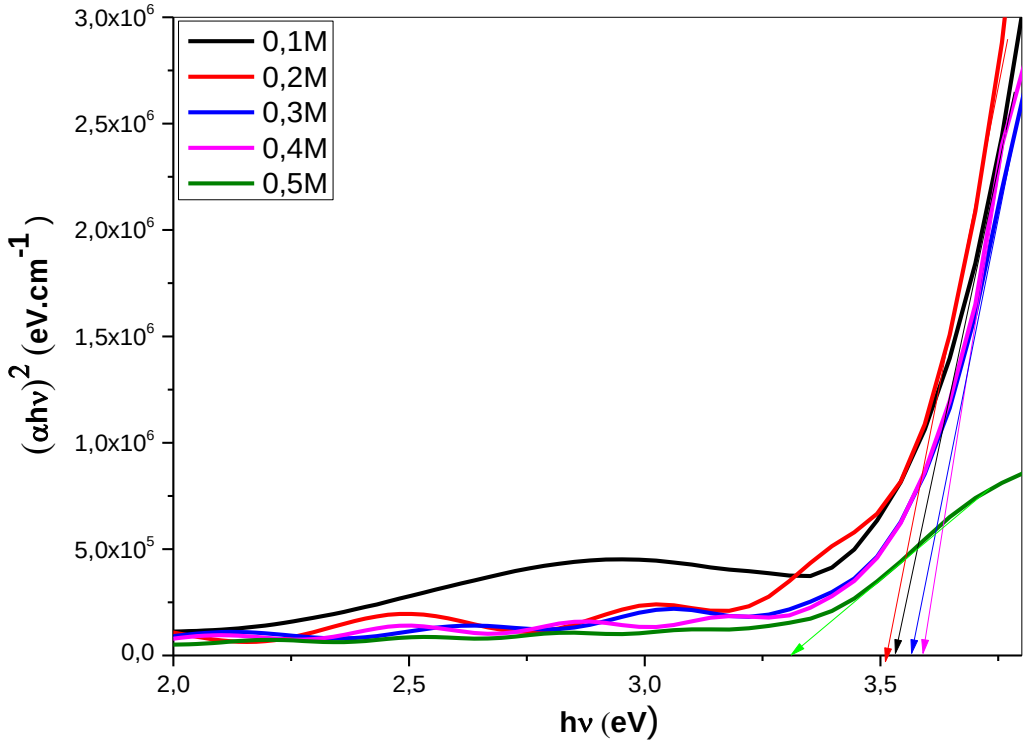

Fig.III.9 $(\alpha h\upsilon)^2$ versus hν of TiO_2 thin films as a function of solution concentration CS.

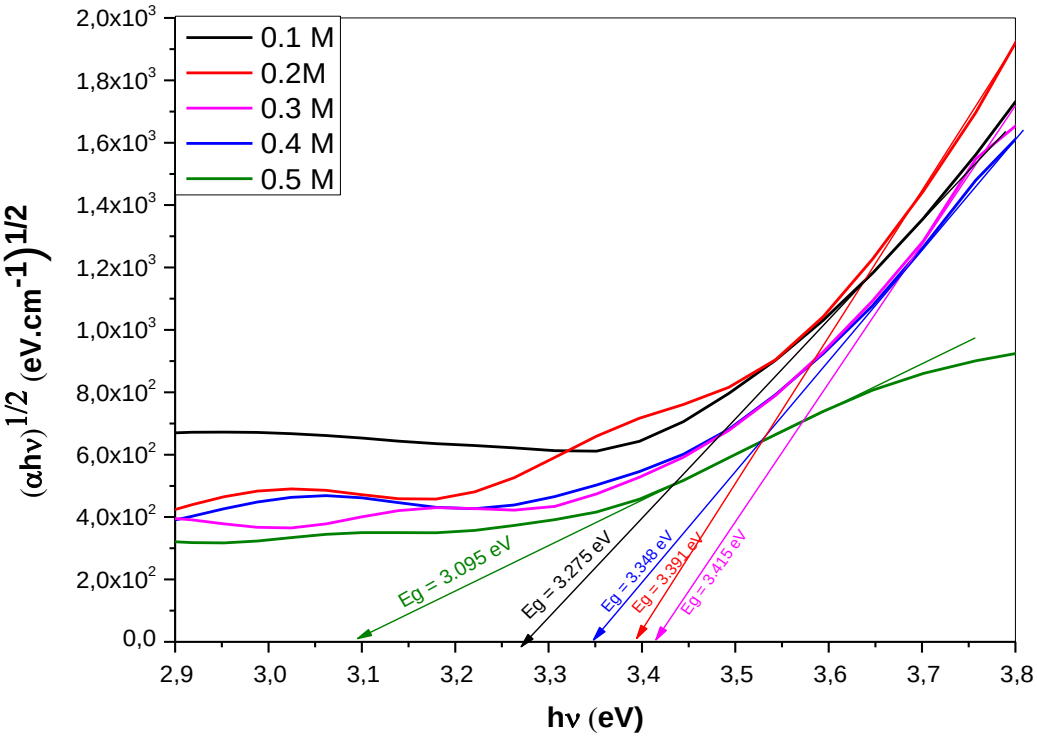

Fig.III.10 $(\alpha h\upsilon)^{1/2}$ versus hν of TiO_2 thin films as a function of solution concentration C_S.

The direct and indirect optical band gap values of thin films are shown in the table III.3

Table III.3 Direct and indirect band gap values of TiO_2 thin films.

solution concentration C_S (M)	Direct optical band gap (eV)	Indirect optical band gap (eV)
0.1	3.52	3.275
0.2	3.50	3.391
0.3	3.56	3.416
0.4	3.59	3.348
0.5	3.30	3.095

It is observed that the values of the direct optical band gap of the thin films change from 3.30 eV to 3.59 eV. It is found that the indirect band gap increases from 3.275eV to 3.415eV and then decreases to 3.09 eV. Increasing the film thickness up to 0.3 M could explain the increase in optical band gap [136].

The reduction of the optical band gap in films could be explained by increasing the grains size of the as a function of the quantum confinement effect [148].

III.3.5.3 Refractive index and porosity

The refractive index n and the extinction coefficient k of the TiO_2 films were determined using equations II.20, II.21 [149]. Figure IV.10 displays the variation of refractive index "n" versus of wavelength ranged from 350 nm to 800 nm (equation II.20). It can be seen, a decrease in refractive index with increasing concentration solution. This is dependent on the crystalline state of films and surface roughness. The improvement of crystallinity leads to the decrease of light scattering. The latter produces the decline of refractive index of elaborated films. Figure.III.11 shows the variation of film porosity as a function of solution concentration C_S. The porosity of elaborated films was calculated using the following relationship (equation II.21).Where n_d is the refractive index of pore-free anatase TiO_2 (n_d = 2.52 [134]), and n is the refractive index of the samples at 550 nm as a wavelength. As seen, the porosity of the films increases with increasing concentration of the solution. It can be explain by the formation of the clusters of TiO_2 takes place in a thin surface layer, which leads to increase of the elaborate films porosity [150].

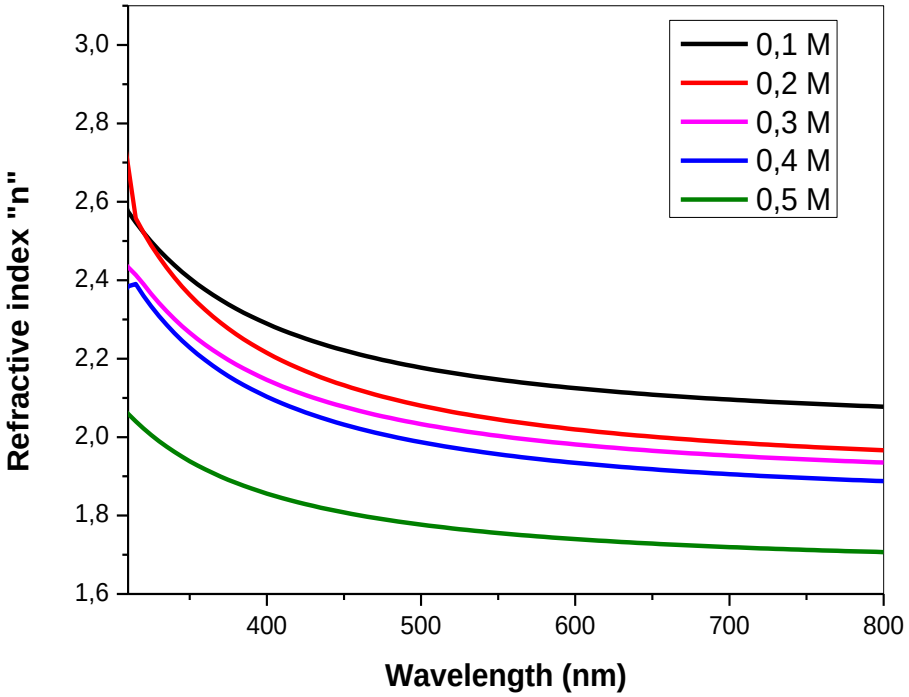

Fig.III.11 Refractive index "n" of TiO_2 thin films as a function of solution concentration.

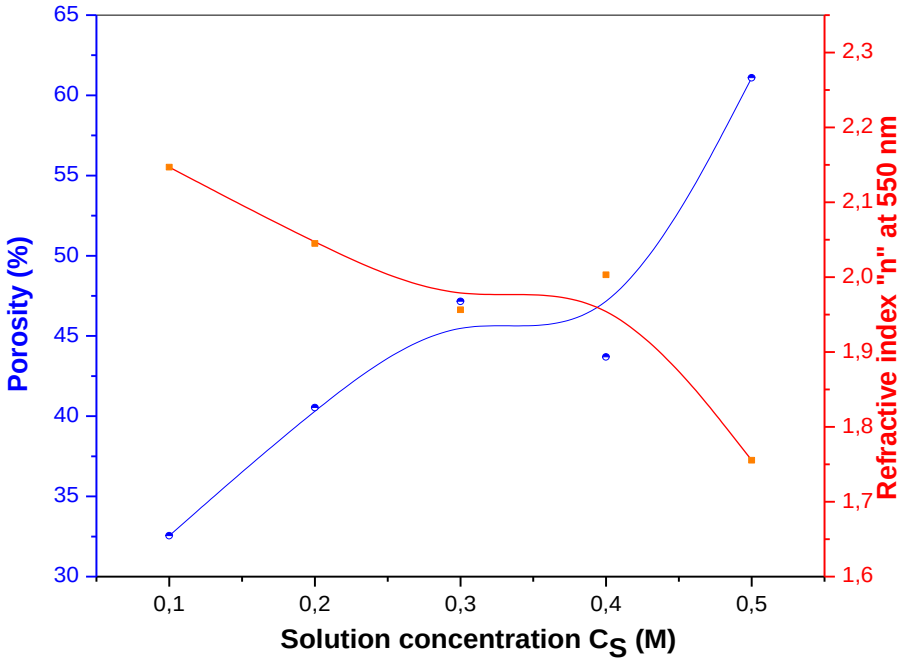

Fig.III.12 Refractive index at 550 nm and porosity of TiO_2 thin films as a function of solution concentration.

III.4.Photocatalytic activity properties

III.4.1. Why was the sample chosen with a concentration of 0.2 M?

For supported photocatalytic, a similar relationship exists between the reaction rate (or reaction constant k) and the thickness of the photocatalytic film. The optimal thickness 500 nm [151, 152] of the anatase photocatalytic depends exclusively on the microstructural characteristics of the film: crystallite size, crystallinity, porosity.

For photocatalytic applications, we must therefore determine optimal thickness. The grain size increases with thickness. Beyond a certain size, the recombination of electron-hole pairs becomes very important and limits the effectiveness of the TiO_2 thin films.

The porosity of the layer, which influences the specific surface and therefore the number of available and active sites of the catalyst, no longer changes significantly beyond a critical thickness.

From the previous results, a sample with a concentration of 0.2 M was selected because:

1-Its thickness is equal to 516 nm. After this thickness, the photocatalytic does not change.

2- The grain size is appropriate. After this grain size, recombination of electron - hole pairs reduces the effectiveness of photocatalytic [153].

D.Komaraiah and all found the maximum photo-degradation of MB dye obtained for 0.2 M film. The photocatalytic performance of TiO_2 thin films indicates that the photo degradation efficiencies decreased with an increase in the precursor concentration for the degradation of MB under visible light illumination [154].

III.4.2.Why was methylene blue selected?

Methylene blue (BM) molecules were chosen for the following reasons:

- The decrease in the concentration of these molecules is easy to follow by photocolorimetry.
- Methylene blue was used in a process to standardize the photocatalytic test because it is the molecule already proposed as a model in the standardized test [88].

III.4.3.Photocatalytic degradation of methylene blue solution by TiO_2/sunlight

The methylene blue (MB) dye was selected as a model pollutant for the investigation of the photocatalytic activity. MB solutions were prepared by dissolving the MB powder in deionized water concentrated (C_0) 15 mg/l. Titanium dioxide (TiO_2) thin film was immersed in methylene blue solution. Before irradiation, the solution was kept in the dark for 30 min to ensure adsorption equilibrium between the dye and the photocatalyst. After that, it was exposed to sunlight for two hours.The absorption of a methylene blue solution was measured (A_0) by the UV-Visible spectra.

III.4.3.1 UV-Vis Absorption Analysis of MB Solution.

The aqueous solution of MB molecules exhibited a double-peak feature at 664 and 615 nm, which correspond to monomers and dimers, respectively [155].Upon irradiation, the peak at 664 nm has a progressively blue shift to shorter wavelength because of hypsochromic effect [156, 157]. The absorption of a methylene blue solution containing a thin layer of titanium dioxide was measured after exposure to sunlight (A) the UV-Visible spectra (see figure.III.13).

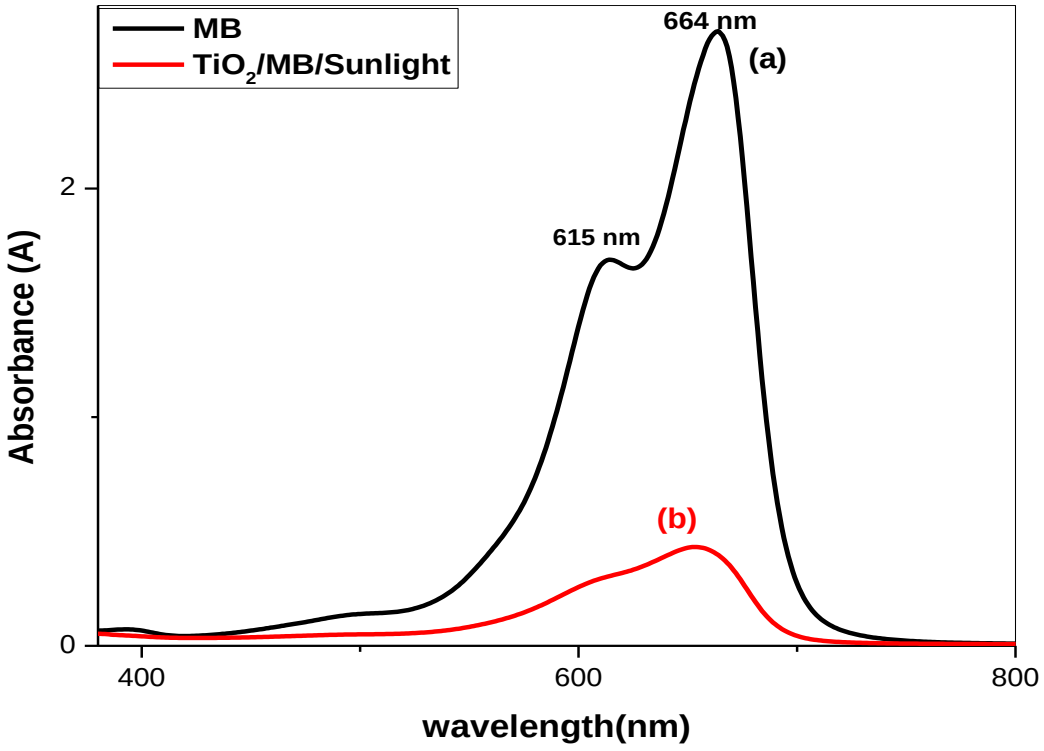

Fig.III.13 (a) The absorption spectrum of MO, (b) The absorption spectrum of MB which has been degraded by TiO_2 thin film.

A decrease in the height of the methylene blue peak is observed at the wavelength of 664 nm from 2.6 to 0.4. This decrease indicates that the thin layers of TiO_2 in the presence of sunlight are effective in degrading the methylene blue dye. The photodegradation rate was calculated using the relationship (I.24) and found 84%.

III.4.4.The effect of sunlight exposure time on the the photodegradation rate.

III.4.4.1 UV-Vis Absorption Analysis of MB Solution.

Glass bottles containing MB solution and TiO_2 thin layers are exposed to sunlight for estimated time periods of 30min, 60min, 120min, 180min and 240 min. Figure III.14 shows the absorption spectrum of the methylene blue solution in previous time periods.

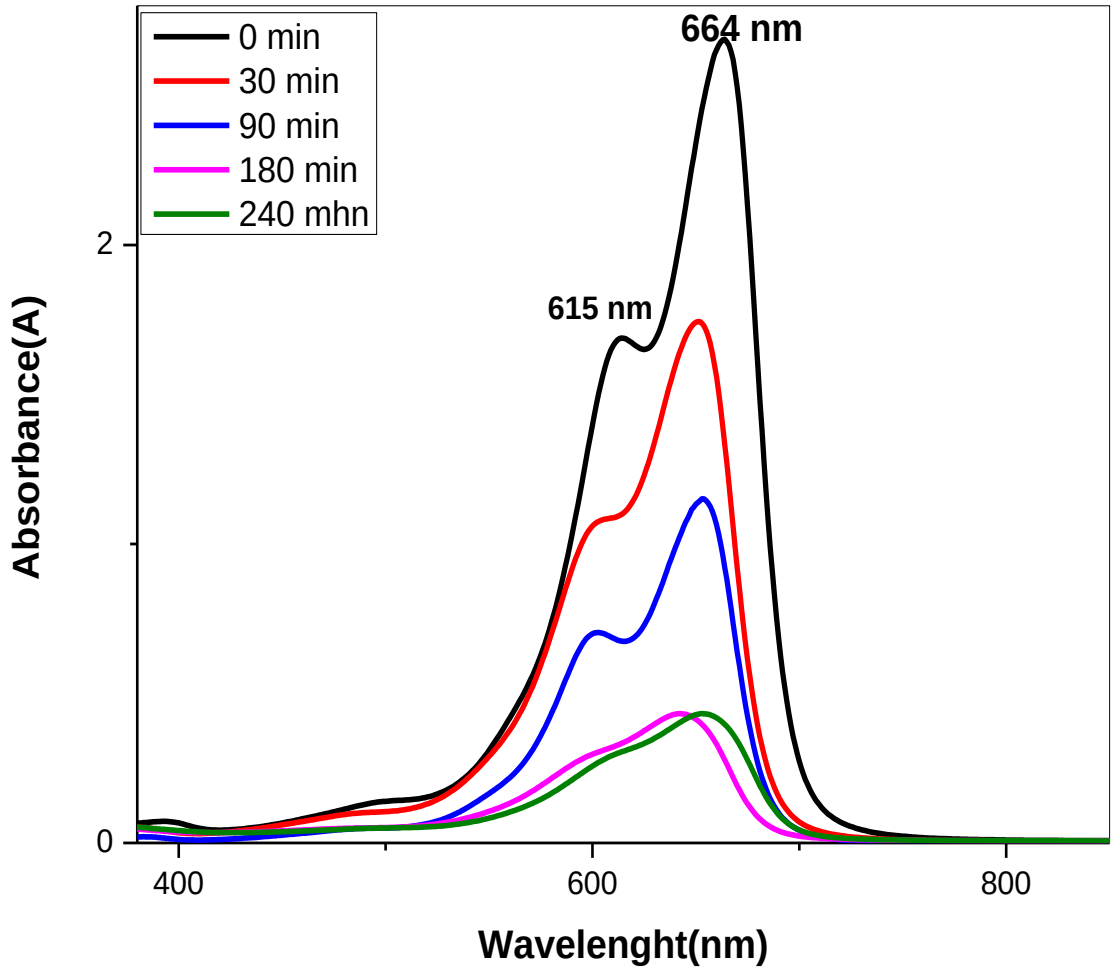

Fig.III.14 Absorption spectra of MB solution and MB solution /TiO_2 thin films which exposed at sunlight in different time periods**.**

It observed a decrease of absorption peak height of methylene blue with increasing in the sunlight exposure time from 2.69 to 0.4 at 180 min and then fixed.

III.4.4.2 Photodegradation rate

Figure III.15 shows a variation of photodegradation rate as a function of sunlight exposure time.It is observed that the photodegradation rate increases with increasing sunlight exposure time up to 180 minutes. Then it is 84% proven. It can be interpreted as follows:

For $t \leq 180$ min, an increase in the sunlight exposure time leads to a rise in the number of hole-electron pairs, which raise the concentration of hydroxyl radicals. An increase in the concentration of hydroxyl radicals leads to an increase in the concentration of dissolved methylene blue (MB) molecules.

For $t > 180$ min, unchanged photodegradation rate is explained by the surface area of TiO_2 thin films and the initial concentration of methylene blue (C_0).

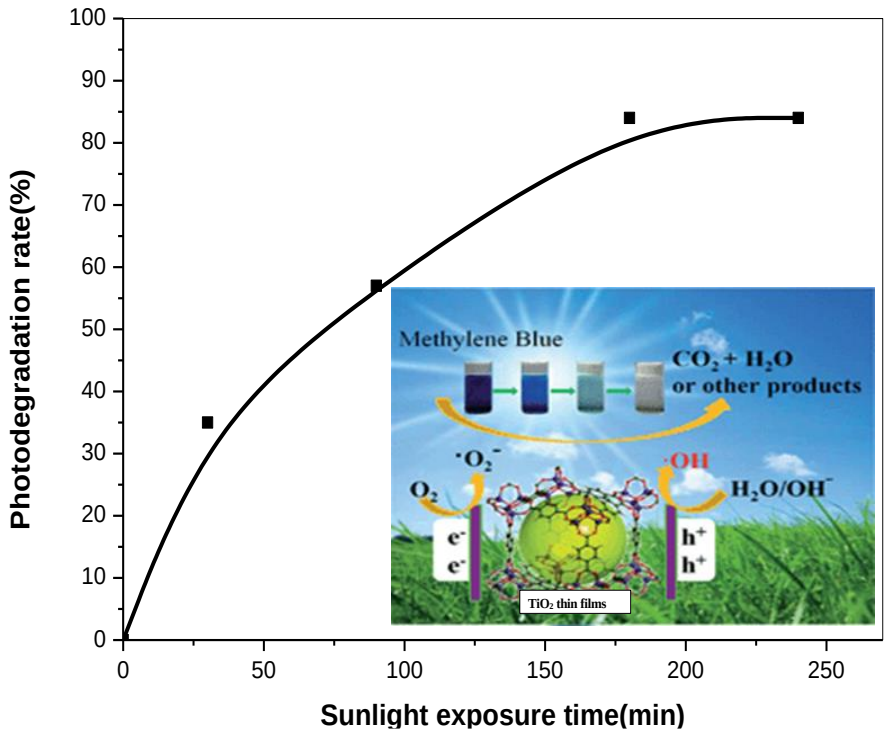

Fig.III.15 Photodegradation rate as a function of sunlight exposure time.

III.4.5 The photocatalytic reaction rate constant (k_{app})

The photocatalytic reaction rate constant (k_{app}) was determined from the plots represented in Fig. III.16 and using the pseudo-first-order reaction (equation I.23).

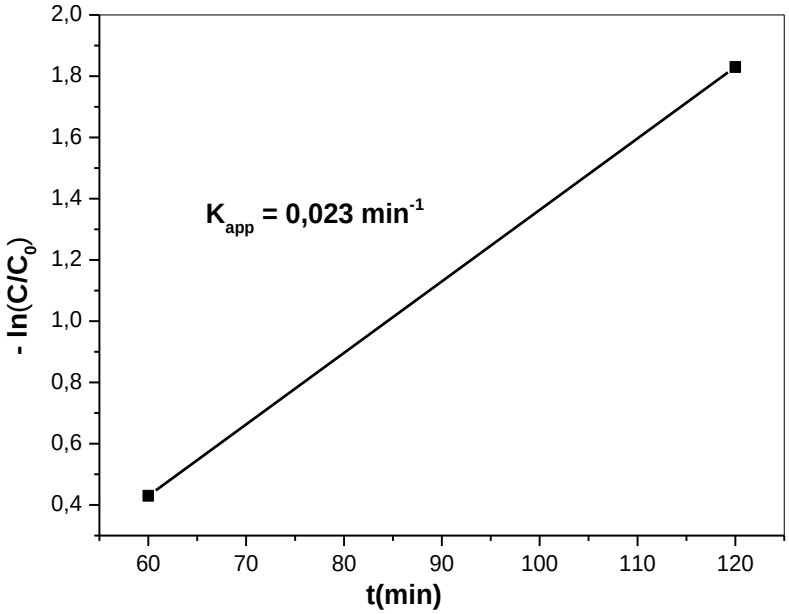

Fig.III.16 variation of $\left[-ln(^{C_t}/_{C_0})\right]$ as a function of sunlight exposure time.

III.5 Conclusion

Thin films of TiO_2 were prepared by sol-gel (spin coating). The effect of the concentration of the CS solution on the properties of titanium dioxide was studied. The results obtained show that the deposited films were crystallized in an anatase phase oriented along to (101) plane. The surface morphology of the films has been modified with increasing concentration of the solution C_S. Good transparency in the visible area.

The indirect optical band gap ranged from 3.09 eV to 3.415 eV. It can be concluded that the concentration of the solution has a significant impact on the structural, morphological, optical and electrical properties of TiO_2 thin films. Through the obtained results, it can be said that the titanium dioxide thin films prepared by sol gel (spin coating) technique are applicable in the photocatalysis application**.** From the obtained results, it was found that TiO_2 thin films with a solution concentration of 0.2 M have a good photocatalytic property and the best photodegradation rate of methylene blue is 84 % within 3 hours. It can be conclude that the TiO_2 thin films are applicable as a photocatalytic to remove the organic pollutants.

Chapter IV

Rotation speed influence on the properties of TiO_2 thin films.

IV.1.Introudction

Hydrogen gas is characterized by a number of important characteristics that qualify it to be the "fuel of the future", it is a clean fuel, environmentally safe and does not release harmful gases when burned, and possesses high energy, so it is one of the distinctive sources of energy as fuel or as an energy carrier in fuel cells. Hydrogen gas can be synthesized from water with low pH, by exploiting the sun and thin films. International standards have been set for drinking water quality, the most important of which is the pH that should be between 7.5 and 8. That play an important role in human health.

In this chapter, in first part the effect of rotational speed on the structural and optical properties of titanium dioxide films deposited on glass substrates is studied. In the last part, the prepared (TiO_2) thin films that have the best properties as a photocatalyst have been used to adjust the pH of the water according to international standards for drinking water in addition to producing hydrogen gas.

IV.2. Experimental details

Titanium (IV) isopropoxide (Ti [OC-H (CH3) $_2$] $_4$) was used as precursors, acetyl acetyl (CH3COCH) was used as a stabilizer and ethanol (C_2H_5OH) was used as a solvent. Sol-Gel deposition solution was formed (spin-painted) by mixing Titanium tetra (IV) isopropoxide and acetyl acetone in ethanol with titanium tetra (IV) isopropoxide acetyl acetone ratio 1: 1. The rotational speed was changed from 1000 rpm to 6000 rpm. The solution was left under the stirrer for 3 hours at 50 ° C. Titanium dioxide (TiO_2) deposited thin films on the glass substrate. The substrate was chemically cleaned before deposition. The films are dried at 250 ° C for 10 min followed by annealing at a temperature of 500 ° C for 2 hours.

IV.3. Results and discussion

IV.3.1. Film thickness

The variation of the film thickness of titanium dioxide (TiO_2) as a function of speed rotation is shown in figure.VI.1. It can be seen, that the film thickness decreases with increasing of rotation speed from 1000 to 4000 rpm . As well known that thickness of a film will depend upon the material concentration and solvent evaporation rate. It can be explain the film thickness variation as follow: rotation of the substrate at a certain speed means that the centrifugal force combined with the surface tension of the solution pulls the liquid coating into

an even covering. During this time, the solvent then evaporates to leave the desired material on the substrate in an even covering. Rotation is continued while the fluid spins off the edges of the substrate, until the desired thickness of the film is achieved. Therefore, the higher the angular speed of spinning, the thinner the film ,which corresponds to the theoretical results [158,159]. It can be observed, a stability of film thickness from 4000 rpm to 6000 rpm. This is due to the balance between the centrifugal force applied to the solution and the solvent evaporation rate that affects the viscosity of the solution. When the solution dries, the viscosity increases so that the radial force of the circulation cannot move the solution on the surface significantly.

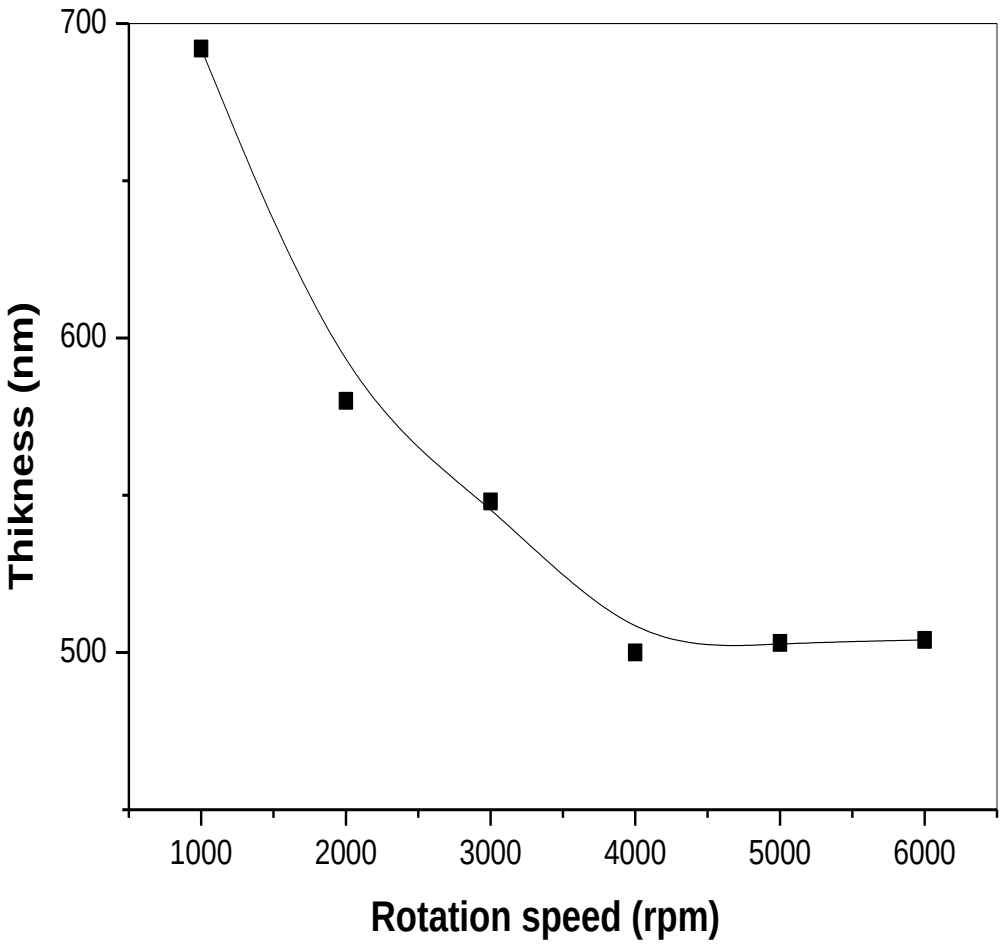

Fig.IV.1 Titanium dioxide (TiO_2) films thickness as a function of rotation speed.

IV.3.2.Structural characteristics

IV.3.2.1.XRD diffraction spectra

To identify the crystal structure of TiO_2, the elaborated films was characterized by X-ray diffraction (XRD). XRD spectra of the TiO_2 thin film prepared by sol-gel (spin coating) method on glass substrates by varying rotational speeds from 1000 to 6000 rpm are shown in Fig. IV.2. There are two peaks at the diffraction angle of $2\theta = 25.41$ and 48.05 °, corresponding with (101) and (200) planes, respectively. All samples has an anatase phase according to [JCPDS 21-1271] [160, 161]. It has a tetragonal structure. It is also found that the peak intensity at (101) plane slightly increases up to 4000 rpm, after that it decreases.

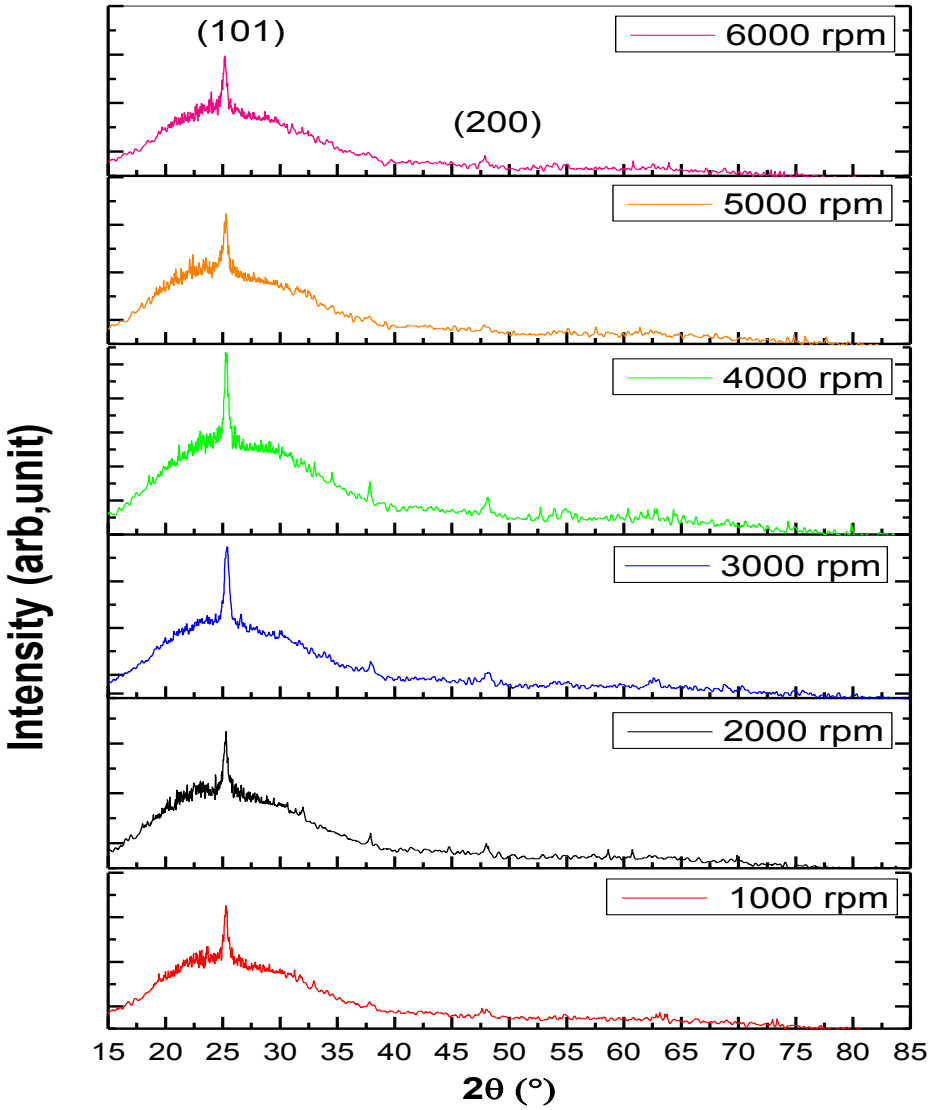

Fig. IV.2 XRD spectra of TiO_2 thin films with different solution concentration.

IV.3.2.2.Grain size (D)

The grain size *D* of the TiO_2 films was measured using the classical Scherrer formula (equation II.7). Where the constant k is the shape factor, λ is the wavelength of X–ray, θ is the Bragg's angle and β is the full width of the half maxima (FWHM).It can be remarked that the grain size increases in the range of rotation speed between 1000 rpm and 4000 rpm and it decreases at rotation speed more than 4000 rpm (see figure.IV.3). It can be explain the increase of grain size with increasing of rotation speed as follow: the solution covers the entire surface of the glass substrate, leading to film formation before complete evaporation of solvent. The TiO_2 thin film deposited in the substrate is increase then the probability to form a crystal in orientation (101) is large, which means improving the crystalline state of films due to raise of nucleation centers after annealing treatment. However, after 4000 rpm, the grain size decreases because the large part of the solution is removed from the substrate where centrifugal force cannot be avoided, this means increased dispersion of the solution therefore 4000 rpm can be considered as a critical speed.

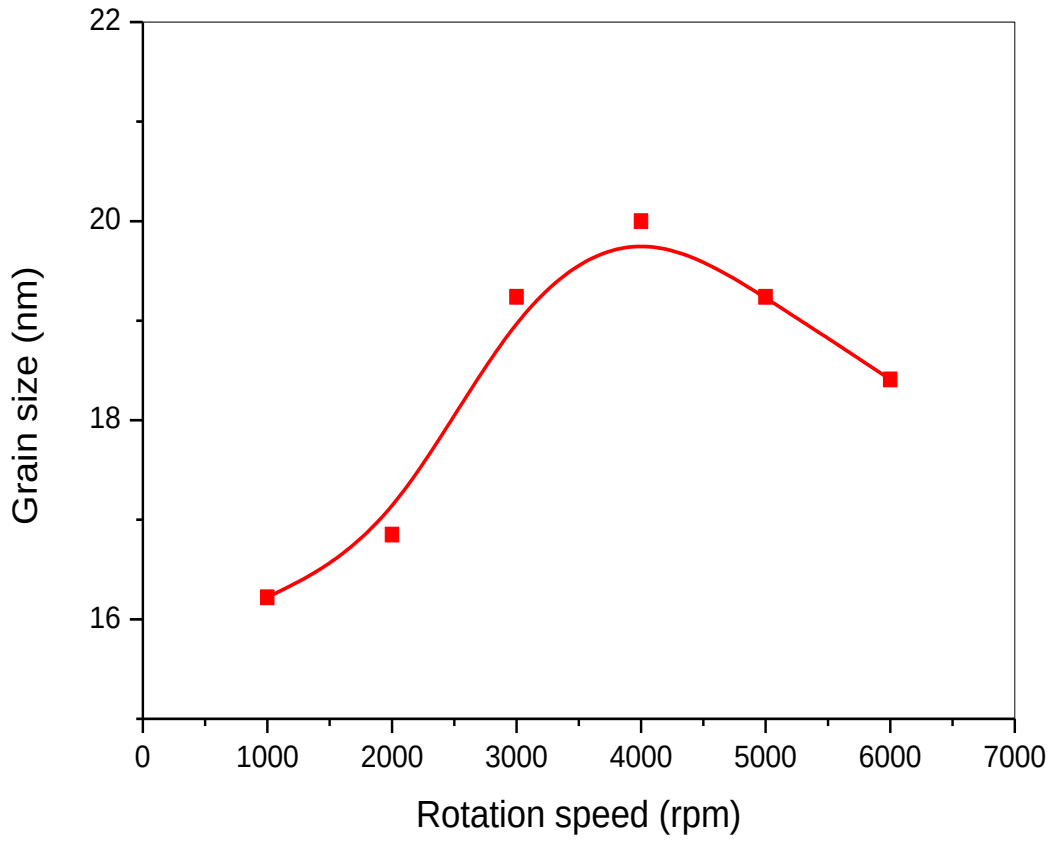

Fig.IV.3 Grain size as a function of rotation speed.

IV.3.3 Raman analysis

Raman spectra of the TiO_2 thin films deposited at various rotation speeds varying from 1000 rpm to 6000 rpm are shown in Figure.IV.4. All samples showed anatase main peak at 143 cm^{-1}, which are due to O–Ti–O symmetric stretching vibrations [162, 163].It can be remarked that the main anatase peak of sample which deposited at 4000 rpm have a minimum full width at half maximum (FWHM). This corroborates the increase in the crystallite size of the anatase phase. After 4000 rpm, full width at half maximum (FWHM) of main anatase peak increases. Therefore, a deterioration of crystalline state of elaborated films (see figure.IV.5).

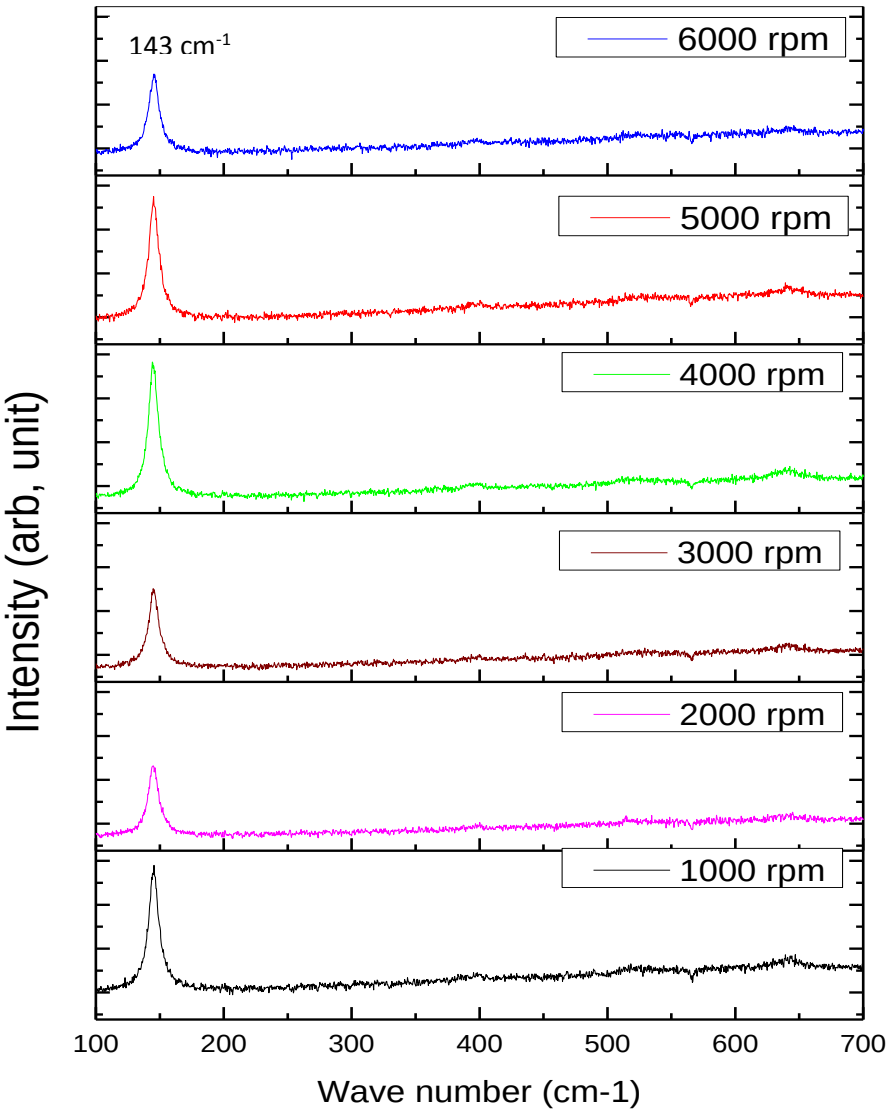

Fig. IV.4 RMN spectra of TiO_2 thin films with different rotation speed.

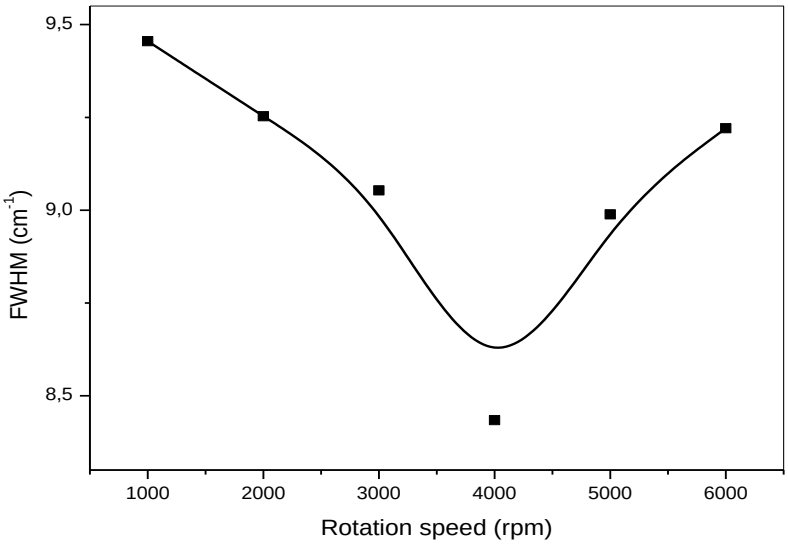

Fig.IV.5 FWHM as a function of rotation speed.

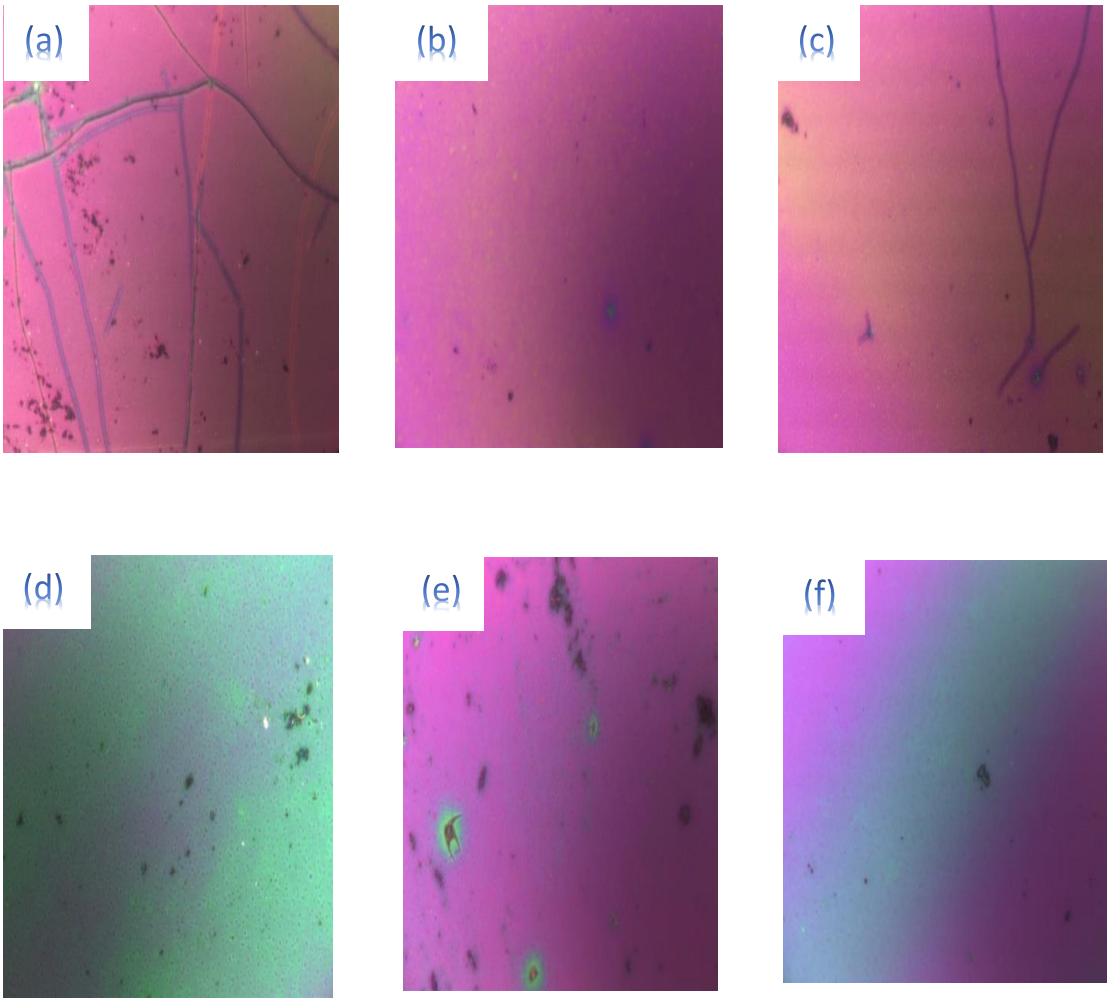

Fig.IV.6 image of samples at various rotation speed such as: a) 1000 rpm, b) 2000 rpm, c) 3000 rpm, d) 4000 rpm, e) 5000 rpm, f) 6000 rpm.

In Figure IV.6, violet color is observed at 1000 rpm, 2000 rpm and 3000 rpm, and then disappears, and green color appears at 4000 rpm. At 5000 rpm, violet color appears with green spots, and at 6000 rpm, both colors appear together. The appearance of violet and green indicates the presence of crystal defects in TiO_2 thin films. Violet color indicates the presence of impurities. These impurities absorb the radiation applied to the samples and then send radiation along the wavelength of the color violet. The appearance of the green color indicates the presence of the oxygen vacancies that absorb the radiation applied to the samples and then send the radiation along the green wavelength. It is concluded that TiO_2 thin films prepared at 1000 rpm, 2000 rpm, 3000 rpm, 5,000 rpm and 6000 rpm contain crystalline defects of impurities with small amounts of oxygen vacancies. At 4000 rpm, the concentration of oxygen vacancies is greater than impurities. These results are supported by result photoluminescence spectra.

IV.3.4. Morphological properties

SEM images of TiO_2 nanoparticles are illustrated in Figure IV.7. It can be seen that the prepared TiO_2 images show morphology like aggregated Plates Island with cracks [164]. this supports the theoretical conclusion obtained by Shigeki Hirasawa and all that says that the continuation of centrifugal force throughout the shrinking process increases film surface undulation [165].

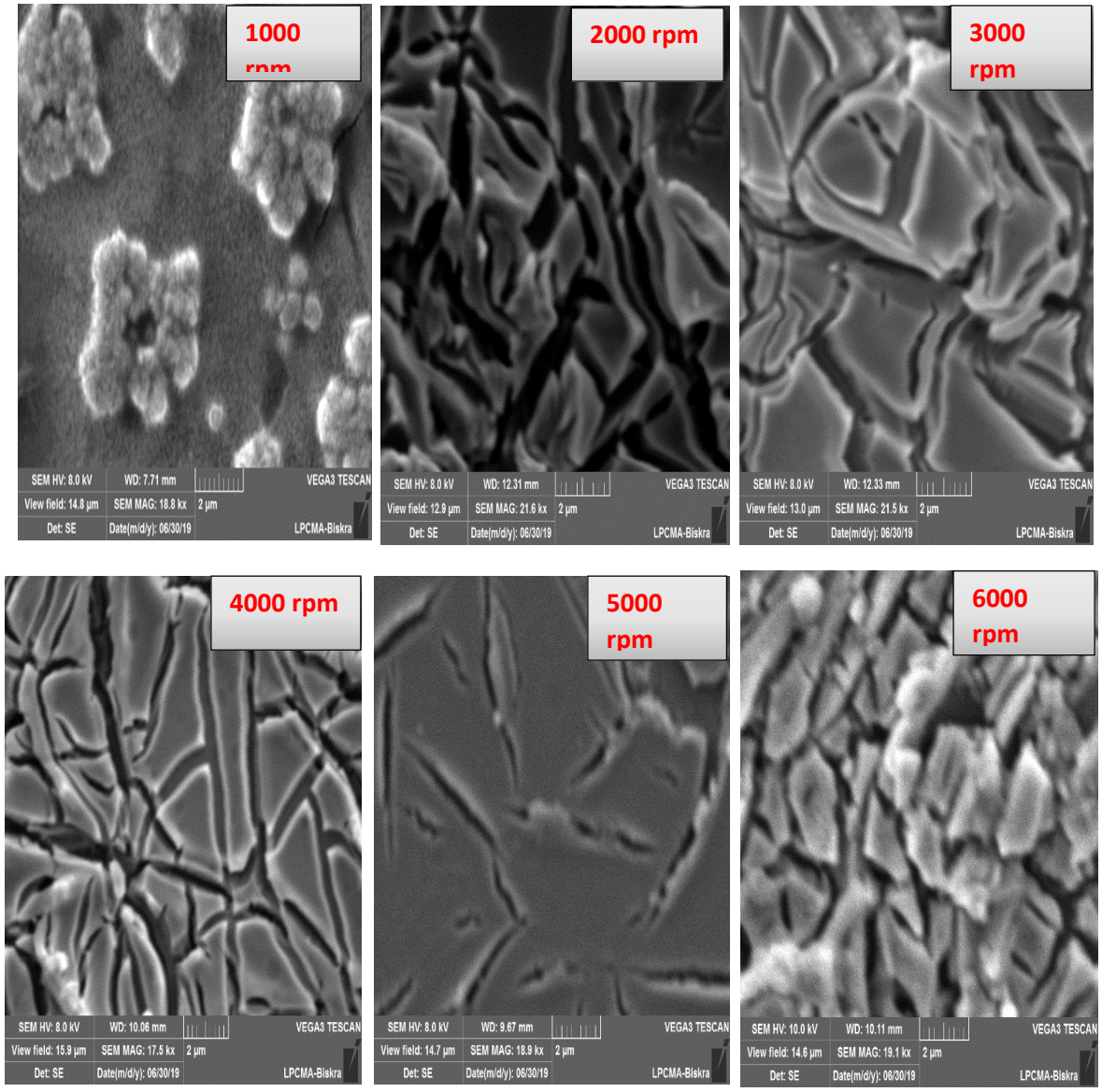

Fig.IV.8 SEM images of TiO_2 thin films deposited at different rotation speed.

IV.3.5. Photoluminescence spectra:

Figure.IV.9 shows the influence of rotation speed on the emission spectrum of TiO_2 thin films. It can be remarked the presence of three strong emission peaks at 371 nm, 456 nm, 525 nm and a shoulder peak at 481 nm. The emission peaks located at 456 nm, 481 nm are attributed to impurities and defects, and the peak at 525 nm is due to oxygen vacancies [162, 164]. The PL intensity is proportional to the rate of e−/h+ recombination. It can be seen from Fig. 9 that the deposited film with 4000 rpm shows the lowest PL intensity, while higher intensities of PL are obtained for films in 6000 rpm. It is assumed that higher e−/h+

recombination of samples 6000 rpm is a consequence of increased of defects due to the deterioration of crystalline state of the elaborated films [162,165].

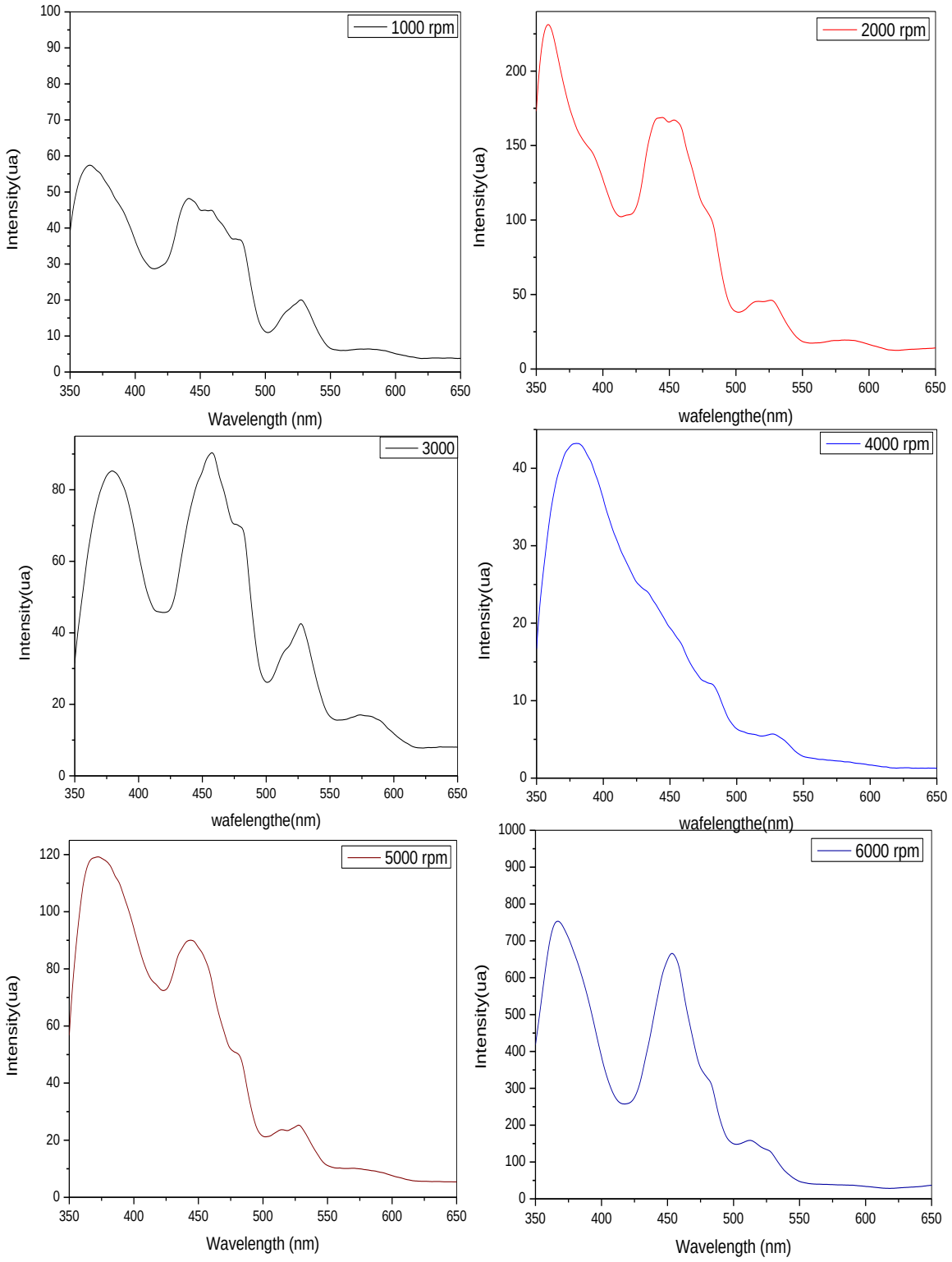

Fig.IV.9 Pl spectrum of TiO_2 thin films.

IV.3.6 Optical properties

IV.3.6.1 Transmittance spectra

The transmittance spectra of TiO_2 thin films versus speed rotation are displayed in figure.IV.10. It can be observed that thin films have a good transmittance in visible rang. It can be seen that the transmittance of TiO_2 films is improved from 1000 rpm to 5000 rpm. It is possible to explain the improvement of the transmittance by the increasing in the grains size, which causes the reduction of the grain boundaries those origins, the decrease of light scattering centers. In 6000 rpm, the reduction in transmittance may be due to the degradation of the crystalline state of the films produced.

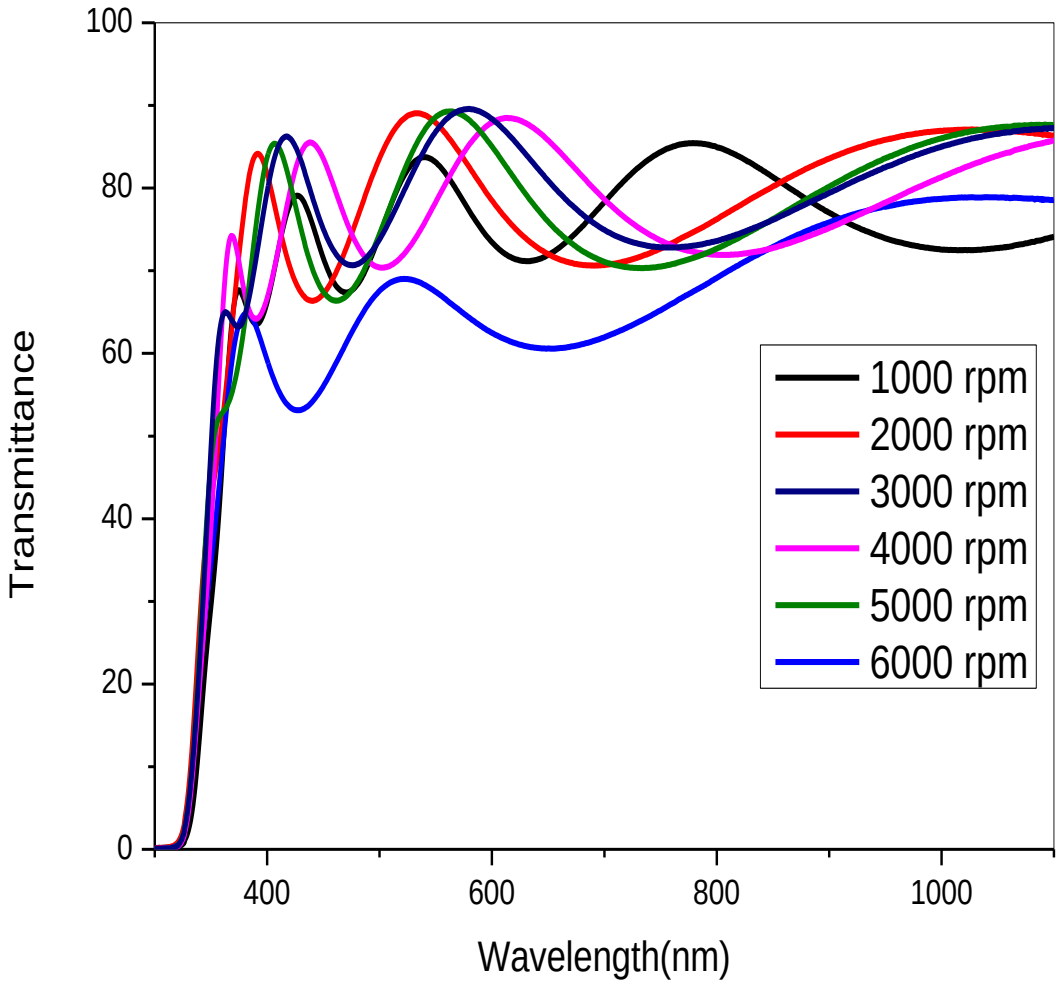

Fig.IV.10 Transmittance spectra of TiO_2 thin films as function of speed rotation.

IV.3.6.2 Optical band gap

The absorption edge corresponds to electron excitation from the valence band to the conduction band, which is determined the value of the direct optical band gap. The incident photon energy $h\nu$ and absorption coefficient are α related through the well-known equation.

Where A is the proportionality constant and Eg is the optical band gap. The direct optical band gap values of thin films are calculated by extrapolating the straight line portion of the $(\alpha h\upsilon)^2 = f\ (h\nu)$ graph (Fig. IV.11 (a)). The value of the band gap is obtained by looking at the intercept with the $h\nu$ axis. It is observed that the sample of TiO_2 deposited whose rotation speed equal to 4000 rpm has a minimum value of optical gap. This confirmed that this condition (4000 rpm) of the rotation speed permits to use it in the photocatalytic field.

The indirect optical band gap values of thin films are calculated by extrapolating the straight line portion of the $\alpha h\upsilon^{1/2} = f\ (h\nu)$ graph (Figure. IV.11 (b)).

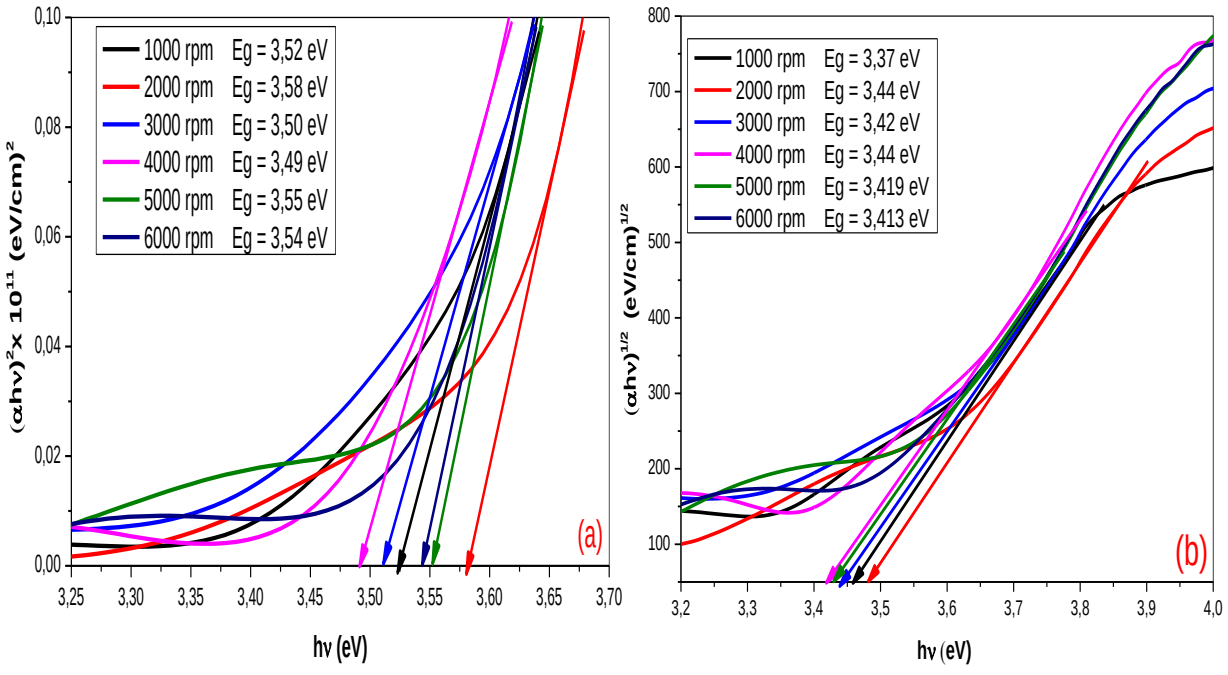

Fig.IV.11 (a)$(\alpha h\upsilon)^2$ plotted versus hυ at different speed rotation. (b) $(\alpha h\upsilon)^{1/2}$ plotted versus hυ at different speed rotation.

IV.3.7 Fourier Transform Infra-Red (FTIR) spectra

Several peaks were observed in all samples (see figure.IV.12). Peak at 597 cm^{-1}, 827 cm^{-1} and 1265 cm^{-1} This is probably due to the vibration of Ti-O-Ti , Ti – O and Ti-O-Ti bonds respectively the TiO_2 [166, 167, 168, 169, 170] while the peak of 1630 cm^{-1} may be due to vibration of O-H bonds [170,171].

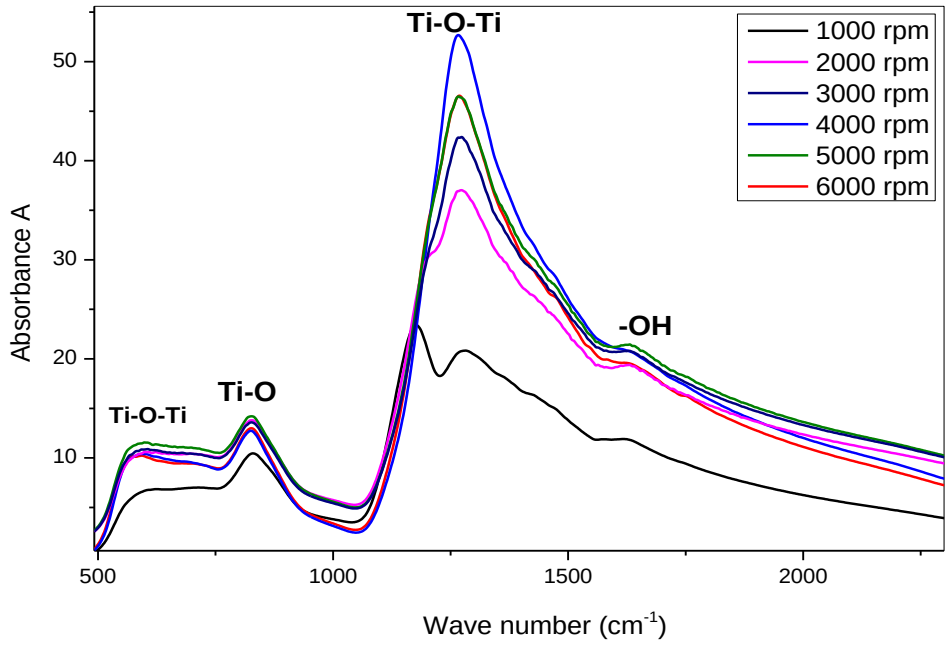

Fig.IV.12 FTIR spectra of TiO_2 versus solution concentration.

IV.4 Photocatalytic activity of TiO_2 films

After the study of speed rotation effect on structural, morphological and optical properties of TiO_2 thin films. It found that the optimal value of speed rotation equal to 4000 rpm. This reason supported to we choose the samples elaborated at 4000 rpm as photocatalysis in modification of water acidity degree (acid rains) and production of hydrogen gaz (H_2).

IV.4.1. Waters acidity

Acidity of waters is typically expressed by the (pH = - log $[H^+]$) as an intensity factor and by acid-neutralizing capacity (ANC), or alkalinity (ALK), as a capacity factor. An acidic water has a pH below 7. Many papers suggest that acidic water should be defined as a water that has a pH below that of pure water in equilibrium [172].

IV.4.2. Photocatalytic experiment

Water acidity measured before immerging the TiO_2 sample. It found the pH = 4.8. Then, TiO_2 samples put in acid water exposed into the sunlight for 4 hours. After 4 hours, the pH of acid water measured again. In this case, it found the pH = 7.4 which corresponding the pH of mineral water.

IV.4.3 Photocatalytic hydrogen production

Increase of the pH indicates a decrease in the concentration of hydrogen ions. This decrease can be explained by the surface of H_2 evolution photocatalyst. The reduction sites transfer the conduction band electrons to hydrogen ions (H^+) to create H_2 [173]. The important reactions for the photocatalytic H_2 production using TiO2 is given as follows [174]:

$$TiO_2 + h\upsilon_{(sun\ light)} \longrightarrow e^- + h^+ \qquad (IV.1)$$

$$H_2O_{Ads} + h^+ \longrightarrow OH^{\bullet}_{Ads} + H^+ \qquad (IV.2)$$

$$2H^+ + 2e^- \longrightarrow H_{2\,(gas)} \qquad (IV.3)$$

The photocatalytic activity efficiency (PCE) of TiO_2 films calculated from the following equation:

$$PCE(\%) = \frac{[H^+]_0 - [H^+]}{[H^+]_0}$$

$[H^+]_0$: Hydrogen ion concentration before immerging the TiO_2 sample.

$[H^+]$: Hydrogen ion concentration after immerging the TiO_2 sample.

Hydrogen ion concentration calculated from the following equation:

$$[H^+] = 10^{-pH}$$

The photocatalytic activity efficiency (PCE) for TiO_2 films equals 99%. Through these results, water pH can be adjusted by thin film TiO_2 using photocatalytic application in addition to hydrogen gas production.

.

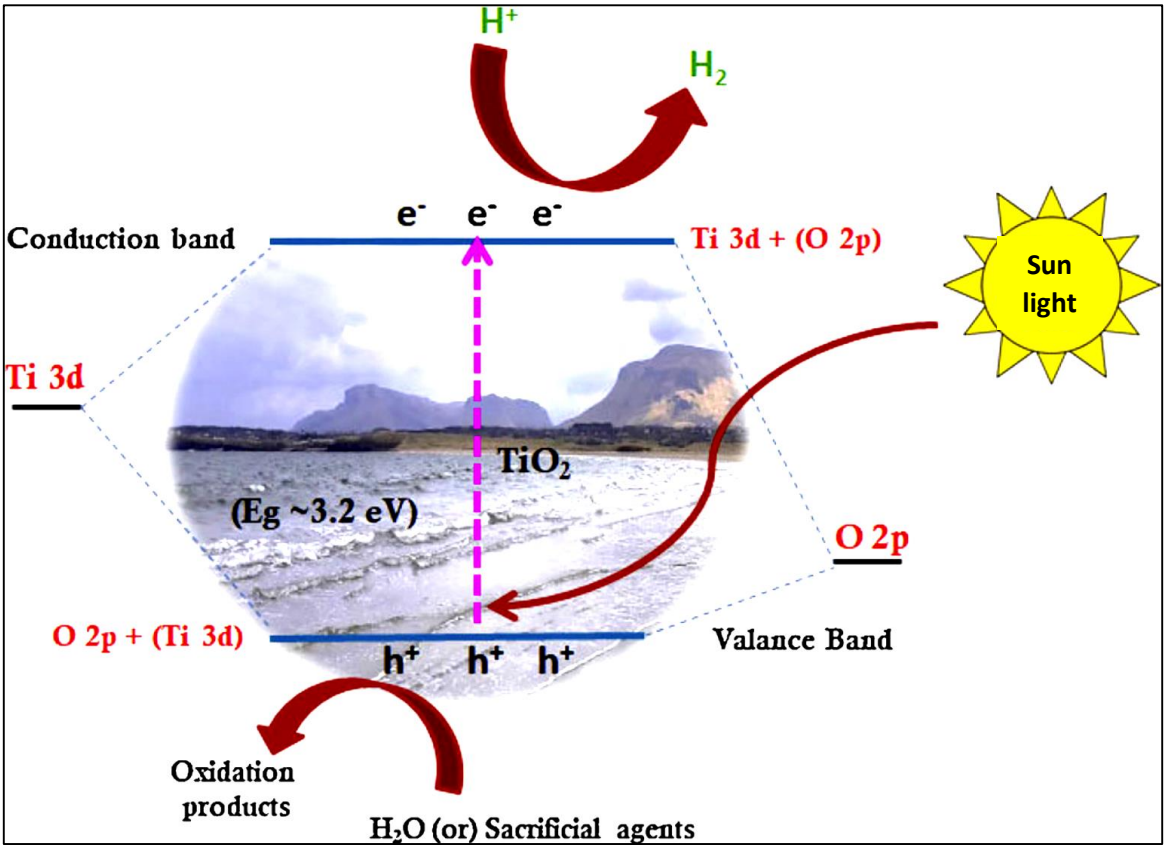

Fig.IV.13 mechanism of H_2 gas production [174].

IV.5 Conclusions

Thin films of TiO_2 were prepared by sol-gel (spin coating). The effect of the rotation speed on the properties of titanium dioxide was investigated. The obtained results show that the deposited films were crystallized into anatase phase which oriented along to (101) plane. Ramen spectra of all samples showed a main peak at 143 cm^{-1}, which are due to O–Ti–O symmetric stretching vibrations of anatase phase. A good transparency in the visible area. The optical band gap around to 3.5 eV. It can be concluded that rotation speed has a significant impact on the structural, morphological and optical properties of TiO_2 thin films. From obtained results, it can be said that the titanium dioxide thin films prepared by sol gel (spin coating) technique are applicable in the photocatalytic applications. It found the best photocatalyst TiO_2 to modify the water acidity from pH = 4.8 to pH = 7.4. In addition, the production of hydrogen gas as a promising fuel for the future which to protect the environment from pollution.

Chapter V

Molar ratio and Gallium doping effect on sol gel TiO_2 thin films properties

V.1.Introduction

The organic pollutants serious problem on human health and environment which are discharged in the environment by industries and houses. Before discharging these harmful organic pollutants must be Environmental pollution is the area of concern and there is need to pay more attention on it. Due to industrial growth, the environmental pollution has been increased and it has attained a level high in developing countries. Photo-oxidation by using TiO_2 photo-catalyst is being widely studied as a relatively new technique of pollution abatement. TiO_2 is a commonly used photo-catalyst because of its stability UV light and water. However, the need of an ultraviolet (UV) excitation source restricts its technological utility for limited applications. For widespread applications, TiO_2 photo catalyst effective in visible radiation or solar light needs to be developed as future generation photo-catalytic material degraded or destroyed [175].

In this chapter, in the first part, thin films of titanium dioxide (TiO2) were prepared by Sol-Gel (spin coating) with varying the molar ratio between the concentration of titanium isopropoxide (IV) ([TTIP]) and acetyle acetone ([AcAc]). The effect of molar ratio y on the structural, optical and photocatalytic properties of TiO_2 thin films is discussed. The lowest photocatalytic degradation was obtained at 84% at 1.1. In order to improve the photocatalytic degradation of this sample, the effect of gallium doping on the photocatalytic properties of titanium dioxide thin films was studied in the last part of this chapter.

V.2 Molar ratio effect on TiO_2 thin films properties

V.2.1 Experimental details

V.2.1.1 Preparation of TiO_2 thin films

Titanium tetra (IV) isopropoxide (Ti [OC-H $(CH_3)_2]_4$) was used as precursor, acetyl acetone (CH_3CH) was used as a stabilizer and ethanol (C_2H_5OH) was used as a solvent. The solution for Sol-Gel (spin-coating) deposition by mixing Titanium tetra (IV) isopropoxide and acetyl acetone in ethanol, the titanium tetra (IV) isopropoxide acetyl acetone. The ratio between titanium tetra (IV) isopropoxide concentration [TTIP] and acetyl acetone concentration [AcAc] was expressed by the following relationship: $y = \frac{[TTIP]}{[AcAc]}$ this ratio varied from 0.5 to 2. The solution was let under agitation to plug closed during 3 h to 50 °C. Titanium dioxide (TiO_2)

thin films were deposited on glass substrate. The substrate were chemically cleaned before the deposition. The films were dried at 250 °C for 10 min followed by annealing in a temperature 500 °C for 2 hours.

V.2.1.2 Photocatalytic experiments

The photocatalytic performance of TiO_2 thin films prepared at different molar ratios using methylene blue (MB) dye in aqueous solution of concentration 15 mg/L as a model pollutant under sun light irradiation. The prepared thin films TiO_2 were settled in methylene blue solution in a closed glass bottle. The solutions were irradiated in sun light for 90 min and 180 min.

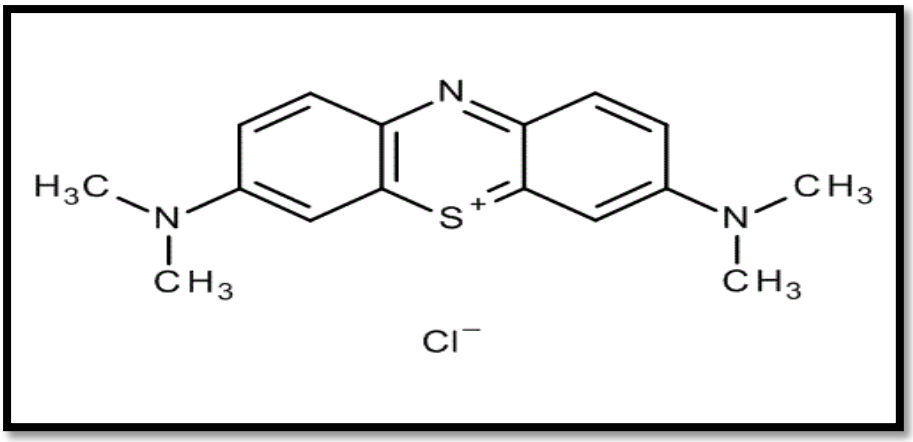

Fig.V.1 The chemical structure of methylene blue.

V.2.2 Results and discussion

V.2.2.1 Structural characteristics

V.2.2.1.1 XRD analysis

FigureV.2 shows the XRD spectra of TiO_2 thin films with different molar ratio and annealing 500 ° C. The peak of XRD is about 2θ = 25.41, 48.05 ° which corresponds to (101), (200) reflections of the anatase phase of TiO_2 according to (JCPDS 21-1271) [8, 9]. The growth along the (101) plane is due to the low free surface energy found in this direction for TiO_2 tetragonale structure.

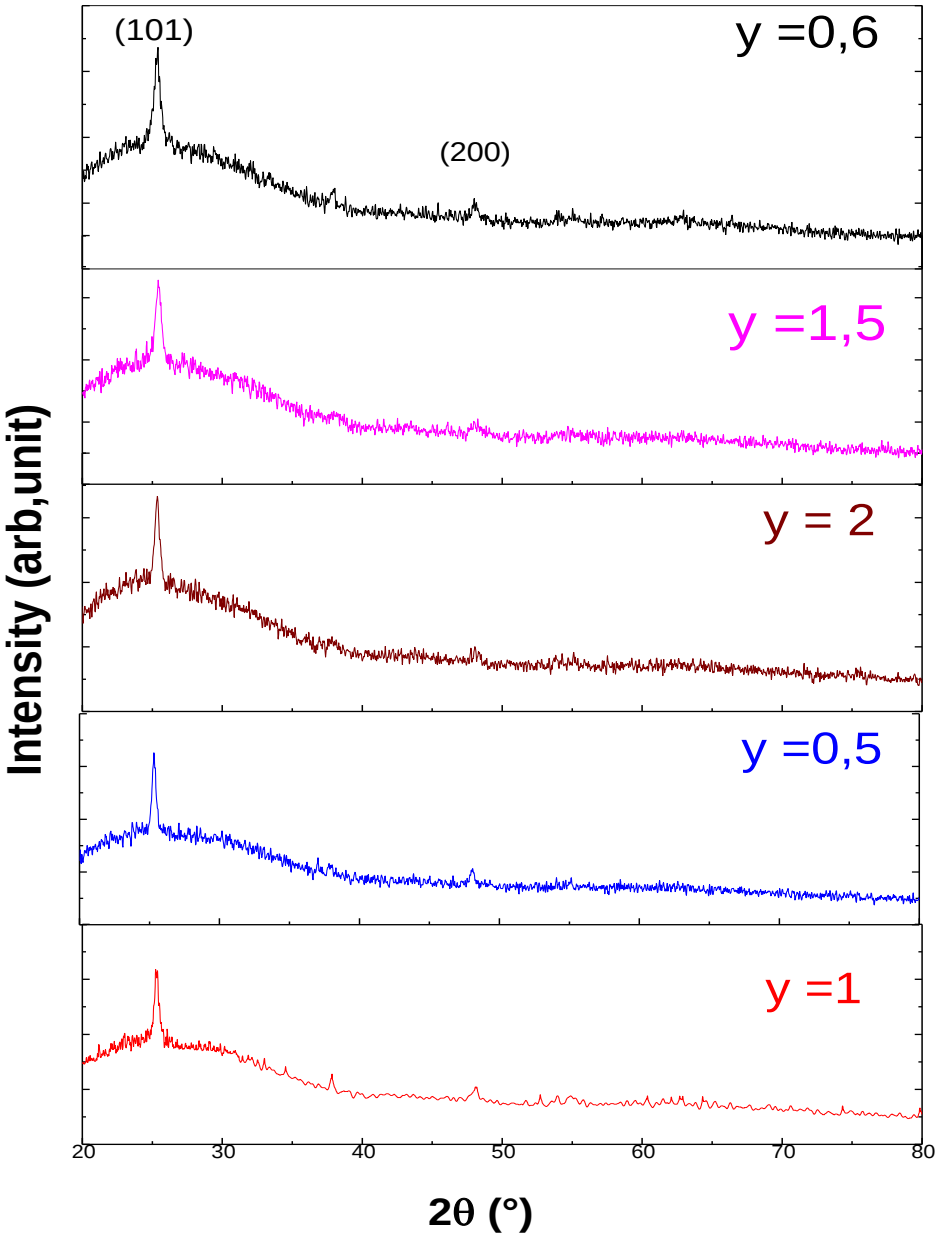

Fig.V.2 XRD spectra of TiO_2 thin films with different molar ratio.

V.2.2.1.2 Grain size and thickness

The grain size *D* of the TiO_2 films was estimated using the classical Shearer formula (equation III.7). The mean crystallite size of the films varies in the range of 20–23 nm. Slight changes in the values of crystallite size are not in correlation with the molar ratio. The results of literature demonstrates that an increase in the amount of the acetylacetonein the precursor solution has no significant effect on the structural properties of TiO_2 thin films, since all the obtained films were annealed at the same temperature 500 C [176,177]. As seen, the higher value of grain size was found at the molar ratio y = 0.5. This indicates an improvement in the

crystalline state of the thin films of titanium oxide. In addition, the lower value of the grain size was found in the ratio y =0.66.

The dislocation density (δ) is defined as the length of dislocation lines per unit volume of the crystal has been calculated by using the Williamson and Smallman (equation III.8).

TableV.1 dislocation density and grain size as a function of molar ratio y.

Molar ratio (y)	D(nm)	$\delta \times 10^{15}$(line/m^3)	Thickness d (nm)
0.5	23	1.8	618
0.6	20	2.7	555
1	22	2	547
1.5	23	1.8	540
2	23	1.8	534

V.2.2.2 Optical properties

V.2.2.2.1 Transmittance spectra

The transmittance spectra of TiO_2 thin films versus molar ratio are displayed in figure.V.3. The optical transmittance spectra of TiO_2 thin films were measured in the spectral region of 300–800 nm for all obtained films are transparent in the visible light region. The transmittance is about 90 % in the spectral region of 400-800nm.It can be observed that an optical transmittance increases with increasing the molar ratio y. According to the interferences fringe, the elaborated films have a smooth surface. It can also be seen that as the molar ratio y increases, the interferences fringe increase, indicating that the surface roughness is decreasing.

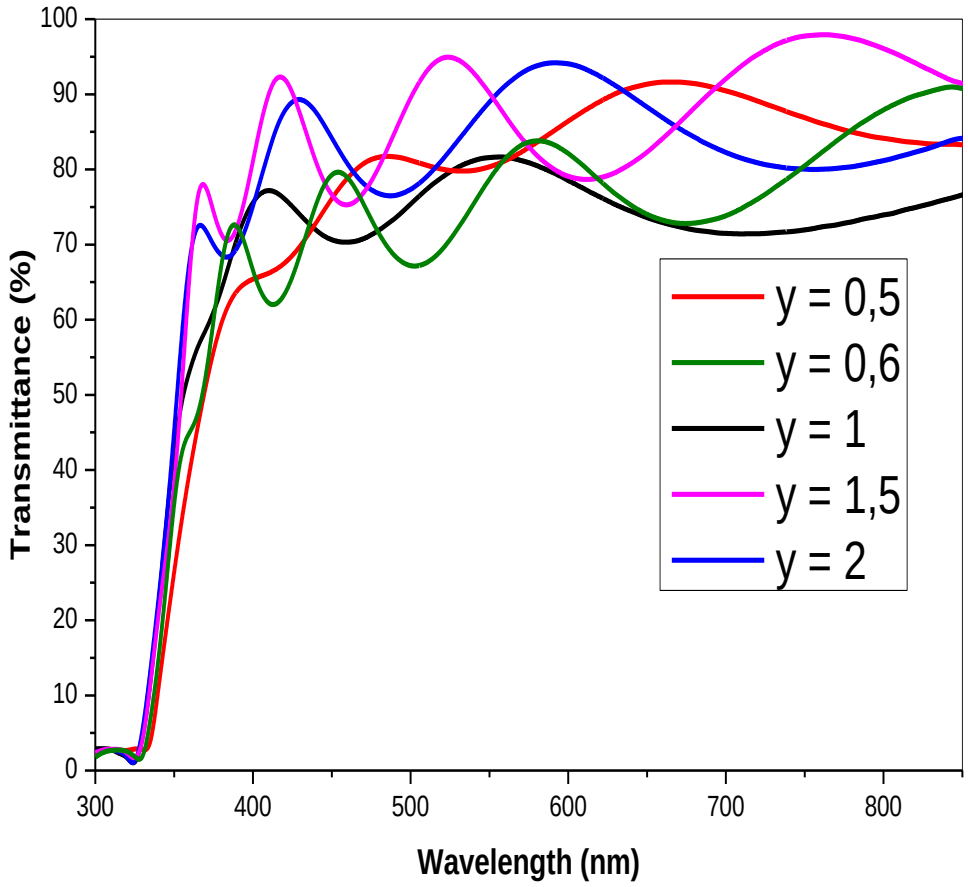

FigV.3 the transmittance spectra of TiO_2 thin films deposited at different molar ratio y.

V.2.2.2.2 Optical band gap Eg

The optical band gap was found using Tauc plot. Since TiO_2 has a direct gap, a plot of $(\alpha h\upsilon)^2 = f(h\upsilon)$ was used (fig.V.4). Table.V.2 shows the band gaps of the obtained TiO_2 thin films as a function of molar ratio.

A minimum value of band gap was found at y = 0.66 (Eg =3.51 eV). TiO_2 has an indirect gap, a plot of $(\alpha h\upsilon)^{1/2} = f(h\upsilon)$ was used (fig.V.5). Table.V.2 shows the indirect band gaps of the obtained TiO_2 thin films as a function of molar ratio. A minimum value of band gap was found at y = 0.66 (Eg =3.38 eV).

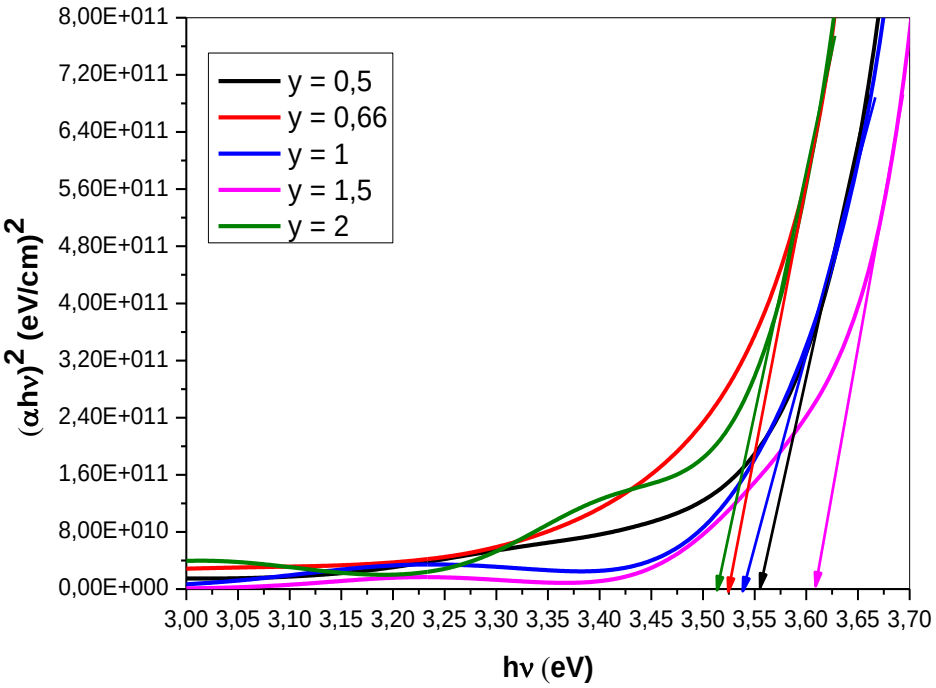

FigV.4 $(\alpha h\upsilon)^2$ versus hυ plotted as a function of molar ratio.

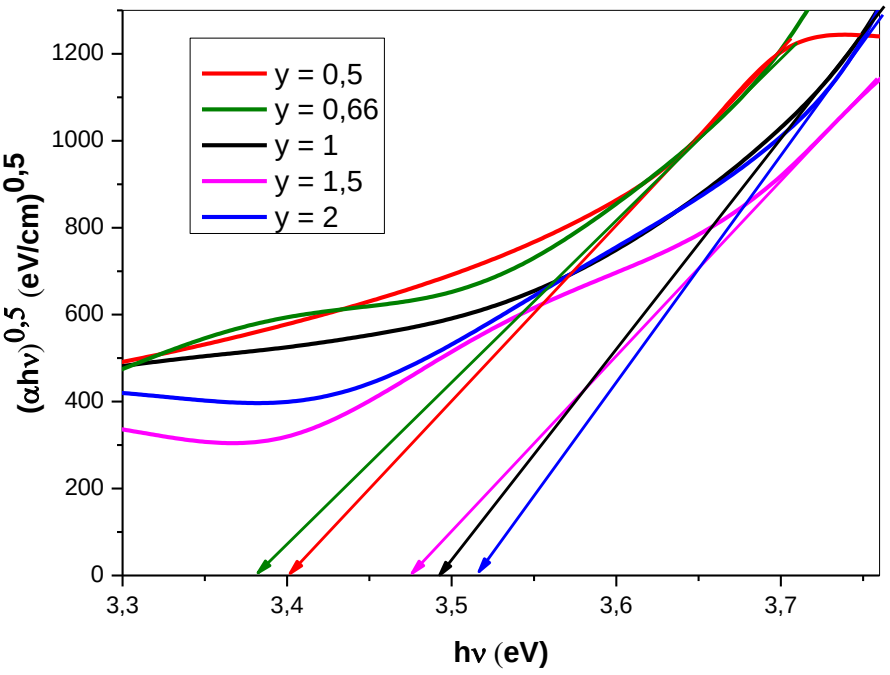

Fig .V.5 $(\alpha h\upsilon)^{0.5}$ versus hυ plotted as a function of molar ratio.

Table V.2 Direct and indirect band gap values as a function of molar ratio y.

Molar ratio y	E_g (direct) (eV)	Eg (indirect) (eV)
0.5	3.52	3.40
0.66	3.51	3.38
1	3.55	3.49
1.5	3.60	3.47
2	3.54	3.51

Overall, it was found that the direct and indirect band gap of the TiO_2 films are not significantly affected by the ratio molar y [177].

V.2.3 Photocatalytic activity studies

V.2.3.1 UV–Vis test of methylene blue by TiO_2/sunlight

The photocatalytic activities of TiO_2 thin films prepared at various molar ratio y varying from 0.5 to 2 was tested by using methylene blue solution as organic pollution.

Fig.V.6 shows UV-Vis absorption spectra of MB solution after reacting with TiO_2 thin films was prepared at different molar ratio in different time (0 min, 90min, and 180min). It is clear from this figure that the intensity of the absorption peaks decreases with the time of sun light radiation exposure, which implies that the MB is degraded. As seen, in all samples a minimum value of peak intensity was found at 180 min.in addition that the absorption peak intensity changed with varying the molar ratio. Fig.V.7 represents the absorption spectra of an aqueous solution of MB in the presence of the TiO_2 thin Films at different molar ratio. It was observed that the lowest value of absorption intensity of methylene blue using TiO_2 thin films with molar ratio y = 0.66. While the maximum value of the absorption intensity is at y = 1. This indicates that the decomposition of methylene blue pigment is significant when using thin films at molar ratio of 0.66.

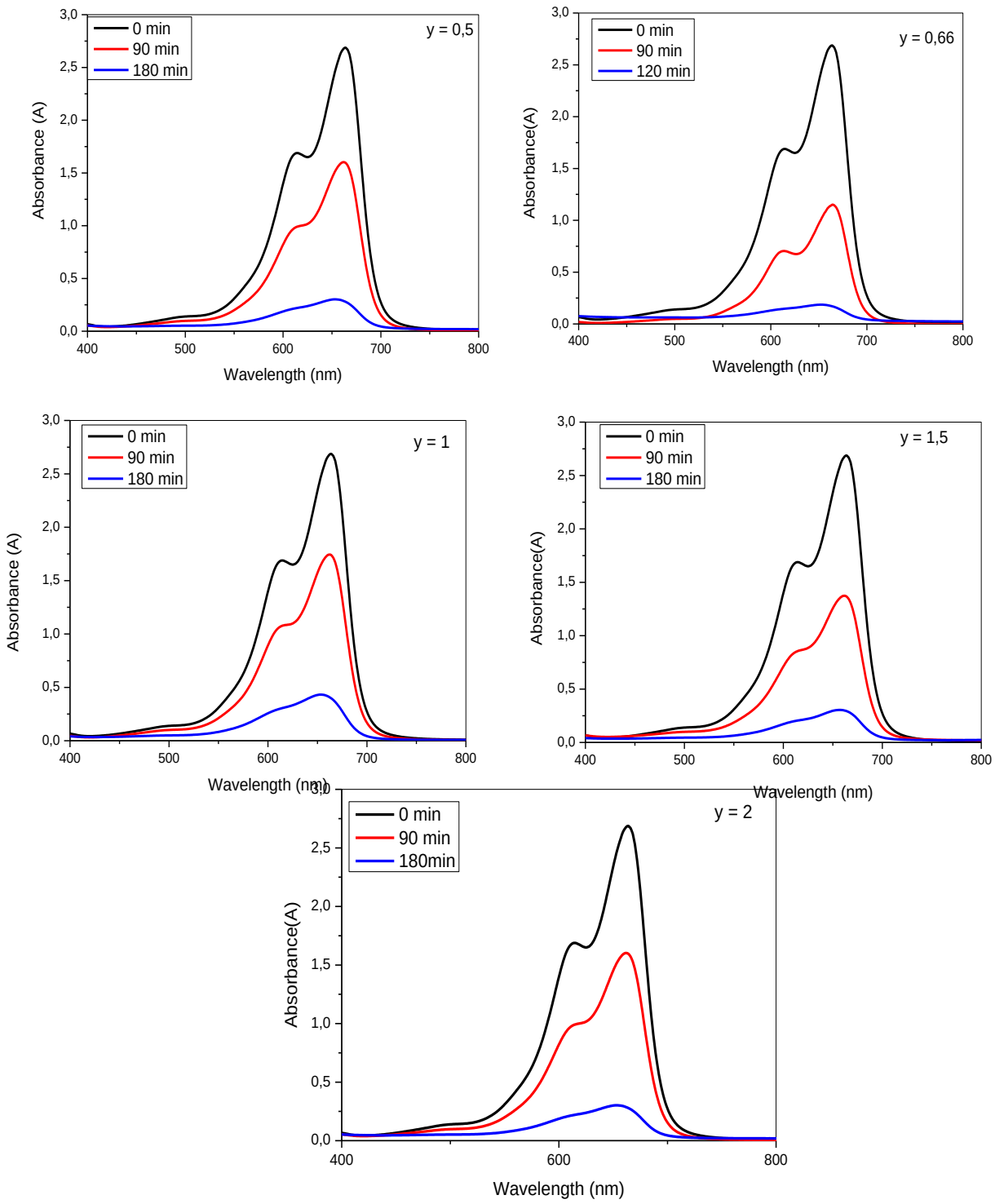

Fig.V.6 UV-Vis absorption spectra of MB solution after reacting with TiO_2 thin films was prepared at different molar ratio in different time (0 min, 90min, and 180min).

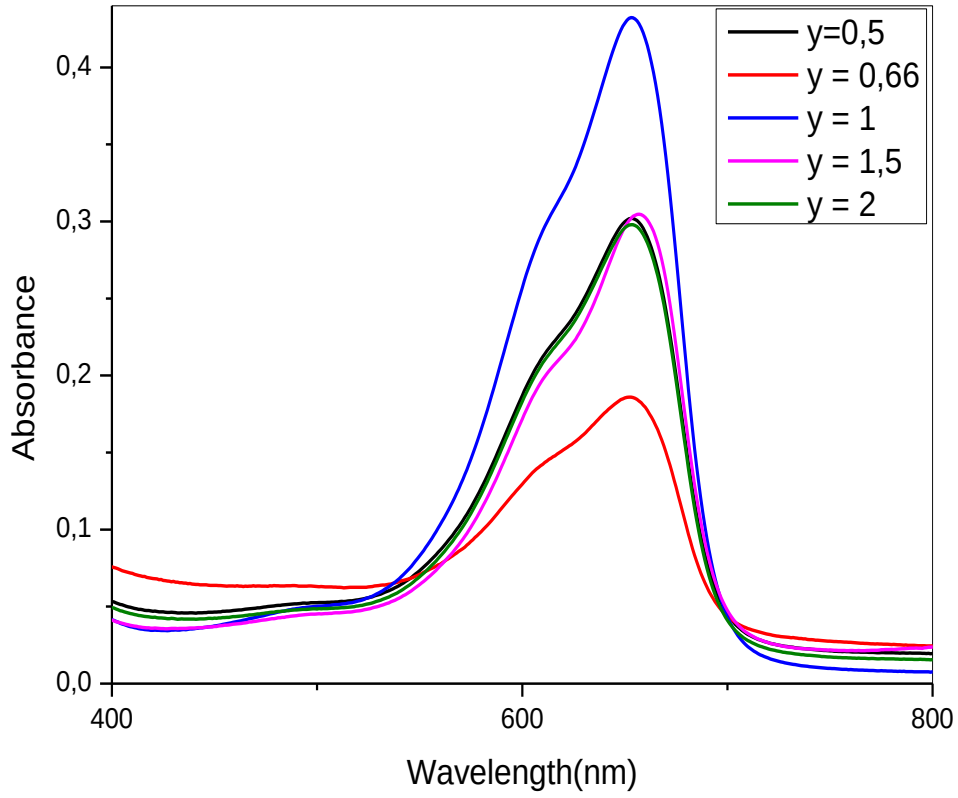

Fig V.7 The absorption spectra of an aqueous solution of MB in the presence of the TiO_2 thin films at different molar ratio.

V.2.3.2 The photocatalytic reaction rate constant (k_{app})

The photocatalytic reaction rate constant (k_{app}) (Kinetics) was determined from the plots represented in Fig. V.8. It was calculated from Langmuir–Hinshelwood kinetics model that express the first order reaction kinetics for the samples. With this approach, it can be inferred that the higher the slope of the linear plot, the higher the degradation reaction rate [178]. The k_{app} parameter indicates the reaction speed. As the k_{app} values increase, the reaction velocity on the surface of the thin layer increases, lead to increased degradation of methylene blue dye. It was also observed that the surface roughness increases with molar ration leading to the increase of the degradation efficiency of dyes. The TiO_2 films with a high rough surface present a higher efficiency of degradation than those with a smoother surface. The porous surface increases the active surface sites, thus enhancing the catalytic activity of the films, as has been established by several authors [179, 180].

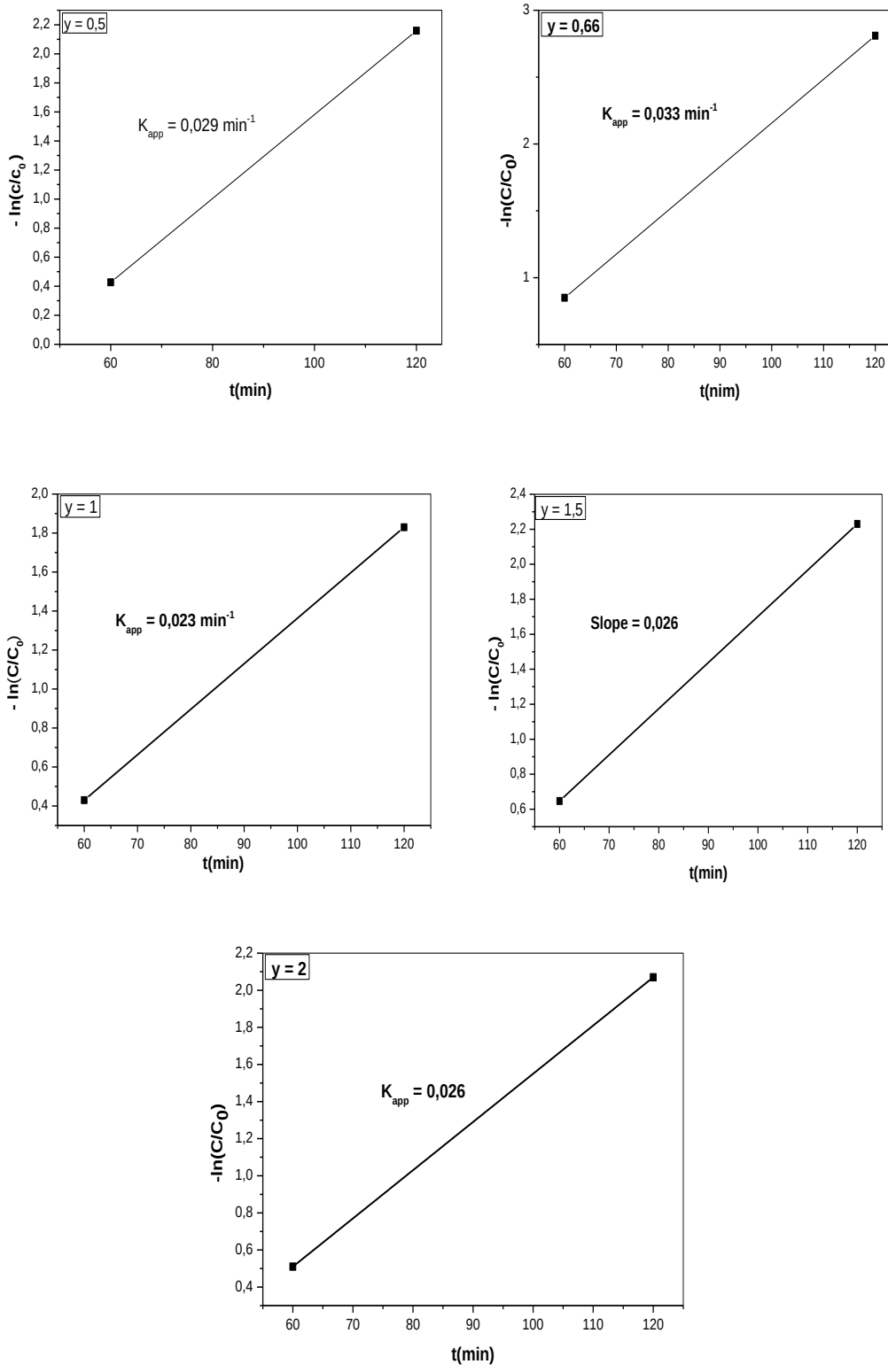

Fig .V.8 Corresponding plots for reaction rate constant (k_{app}) for methylene blue (MB) dye under UV–Vis light irradiation.

V.2.3.3 Photocatalytic degradation rate

The photocatalytic degradation at 90 min and 180 min values as a function of molar ratio y are shown in table.V.3

Table V.3 The photocatalytic degradation at 90 min and 180 min values as a function of molar ratio y

Molar ratio y	Photocatalytic degradation at 90 min	Photocatalytic degradation at 180 min
0.5	40 %	90%
0.66	57%	94%
1	36%	84%
1.5	49%	89%
2	41%	89%

The table V.3 shows that the photocatalytic degradation rate of methylene blue was high, when the molar ratio was not equal to 1. While we achieved the lowest value at molar ratio 1. This means that photocatalytic degradation rate is more effective when the molar concentration of the TTIP is not equal to the molar concentration of the AcAc. TiO_2 thin films were deposited at a molar ratio y = 0.66 exhibited a better photocatalytic degradation rate than those TiO_2 thin films were deposited further, it was found of value photocatalytic degradation rate 94%. In this case the catalytic reaction velocity on the surface is high which is indicated by the value of $K_{app.}$ The change in photocatalytic degradation rate can be explained by existence Ti^{3+} and O^- defect site because charge carriers can be trapped as Ti^{3+} and O^- defect sites in the TiO_2 lattice, or they can recombine, dissipating energy [181,182].

Through the results of structural, it was found that thin films were elaborated with ratio y = 0.66 have the smallest grain size.The smaller the grain size the greater is the surface area for the degradation. Thus, the observed percent photodegradation of MB clearly exhibits that photocatalytic efficiency of films strongly depends on thickness and crystallite size of the titanium dioxide thin films.

M. Danish and all found that as thickness of film decreases the effect of calcination on the films increases leading to an increase in the crystallinity and crystallite size of TiO_2 crystallites and as a consequence the photocatalytic efficiency decreases [183].

V.2.3.4 Mechanism of photocatalytic reactions

The first step involves the adsorption of MB dye molecules on to the surface of nanostructured TiO_2 thin films. When TiO_2 thin film samples with MB dye molecules adsorbed on their surfaces are exposed to sunlight, TiO_2 nanostructures absorb photons leading to the generation of photoexcited electrons in the conduction band and holes in the valance band of TiO_2 (Eq. V.2) [184]. In addition, the MB dye molecules get excited by sun light resulting in the transfer of electrons into the conduction band of TiO_2. The electrons in the conduction band of TiO_2 react with oxygen molecules present at the surface and form super oxide radicals ($O_2^{\bullet -}$) (Eq. V.3). The holes generated in the valance band interact with water molecules to form hydroxyl radicals (OH•) (Eq. V.4). Some of the super oxide radicals react with H^+ to form $HO_2^{\bullet}$, which get converted to hydrogen peroxide (H_2O_2) (Eq.V.6), which leads to an enhancement in the photocatalytic activity.

The highly reactive super oxide and hydroxyl radicals interact with the MB dye molecules adsorbed on the surface of nanostructured TiO_2 thin films and lead to their photocatalytic degradation involving the following reactions [184,185,186].

$$TiO_2 + h\upsilon \rightarrow e_{CB}^- + h_{VB}^+ \quad \text{(V.2)}$$

$$O_2 + \text{é} \rightarrow O_2^{\bullet -} \quad \text{(V.3)}$$

$$H_2O + h_{VB}^+ \rightarrow HO^{\bullet} + H^+ \quad \text{(V.4)}$$

$$O_2^{\bullet -} + H^+ \rightarrow HO_2^{\bullet -} \quad \text{(V.5)}$$

$$2\,HO_2^{\bullet} \rightarrow H_2O_2 + O_2 \quad \text{(V.6)}$$

$$HO^{\bullet} + MB \rightarrow \text{degradation product} \quad \text{(V.7)}$$

$$O_2^{\bullet -} + MB \rightarrow \text{degradation product} \quad \text{(V.8)}$$

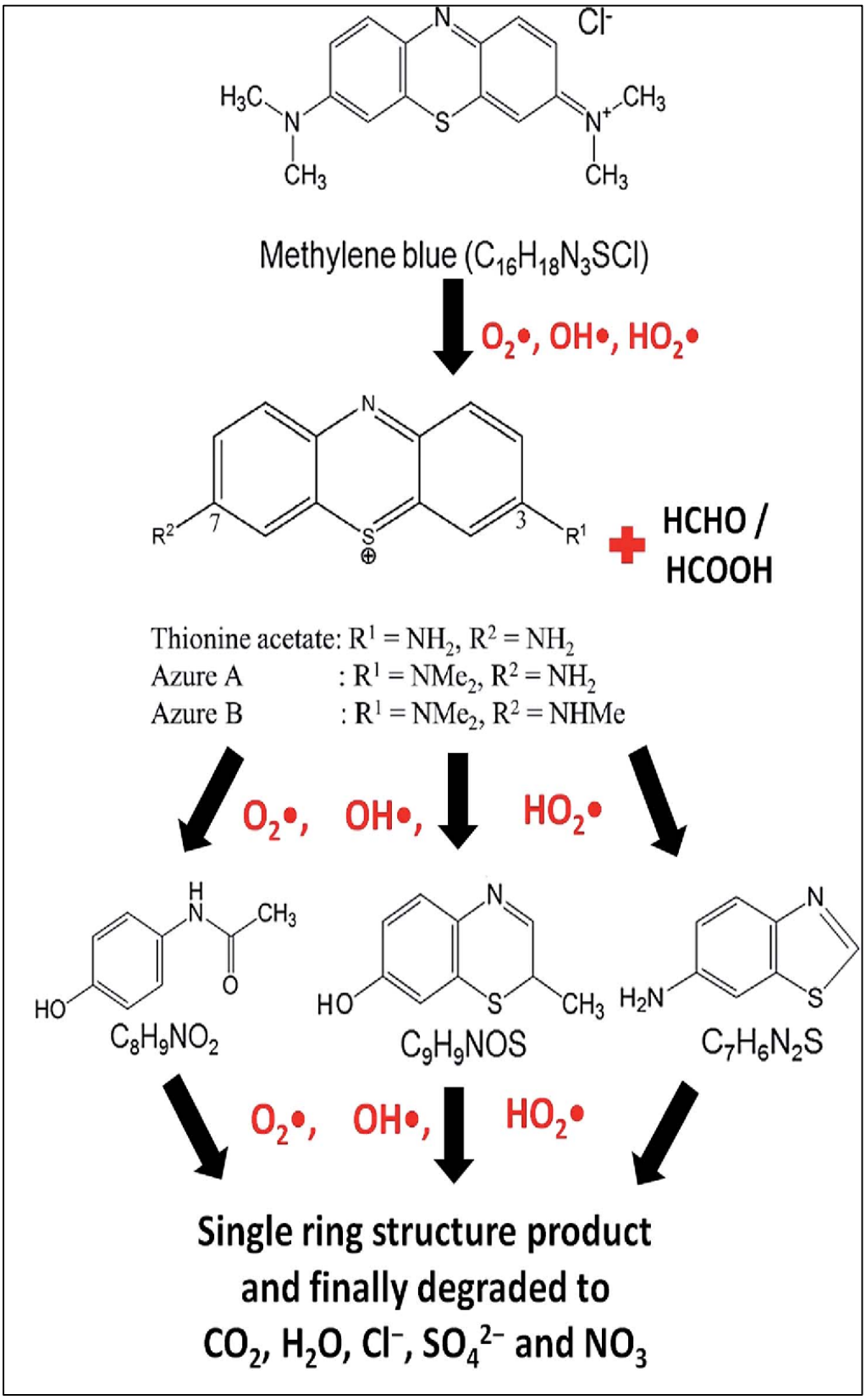

Fig.V.10 Probable reaction steps of MB photocatalytic degradation [187].

V.3 Gallium doping concentration effect on TiO_2 thin films properties

The energy band gap between the VBM and CBM can be reduced by introducing metals or non-metals into the crystalline structure. By reducing the magnitude of the energy band gap, photons of lower energy can be absorbed by the material as well as affecting the recombination rate. Doping generally results in a mixture of doped and non-doped elements in the semiconductor. Important aspects to keep in mind when doping the semiconductor is that the ground state should be lower than the O_2/H_2O level and conduction band higher than the H2/H2O level to enhance the generation of hydroxyl radicals and thereby the photocatalytic activity.

Modification of energy band gap should also allow the mobility of excited electrons and electron-holes across the TiO_2 surface to be able to reach active sites [188].

Among the most important reasons that hinder photocatalysis activity are:

- The speed of recombination of the electron - hole pairs is due to the crystal defects which form the centers of recombination.
- 2- The band gap is large, so it can be reduced by inserting dopants.

V.3.1 Experimental details

$Ti_{1-x}Ga_xO_2$ thin films with x = 0.00 (TG0), 0.02 (TG2), 0.04 (TG4), 0.08 (TG8), and 0.10 (TG10), respectively, have been successfully synthesized by a modified sol-gel process. Gallium nitrate: $Ga(NO_3)_3$ and Titanium tetra (IV) isopropoxide (Ti [OC-H $(CH_3)_2]_4$) were used as Ga and Ti precursors. In beaker, an appropriate amount of $Ga(NO_3)_3$ was dissolved in ethanol (C_2H_5OH).The Ga-solution was added drop wise to the Ti-solution at room temperature while stirring. Stirring was continued to form a homogeneous precursor solution. acetyl acetone (CH_3CH) was used as a stabilizer and ethanol (C_2H_5OH) was used as a solvent mixed and added to the precursor solution. The result and mixture was further stirred for another 3 h. The above process was followed by heating at a constant temperature of 50 C. The films were dried at 250 °C for 10 min followed by annealing in a temperature 500 °C for 2 hours. Thin films prepared were placed inside glass bottles containing methylene blue, then they were exposed to sunlight for four hours.

V.3.2 Results and discussion

V.3.2.1 Structural characteristics

V.3.2.1.1 XRD analysis

The XRD results of $Ti_{1-x}Ga_xO_2$ (x=0, 0.02, 0.04, 0.06, 0.08 and 0.10) thin films shows in fig.V.11. The XRD results confirmed that the Ga-doped TiO_2 exhibits the tetragonal crystal structure with a single anatase phase and are agreed with the standard [JCPDS 21-1271]. The diffraction peak is 2θ = 25.36 indicating preferential crystal growth along the plane (101) [189].

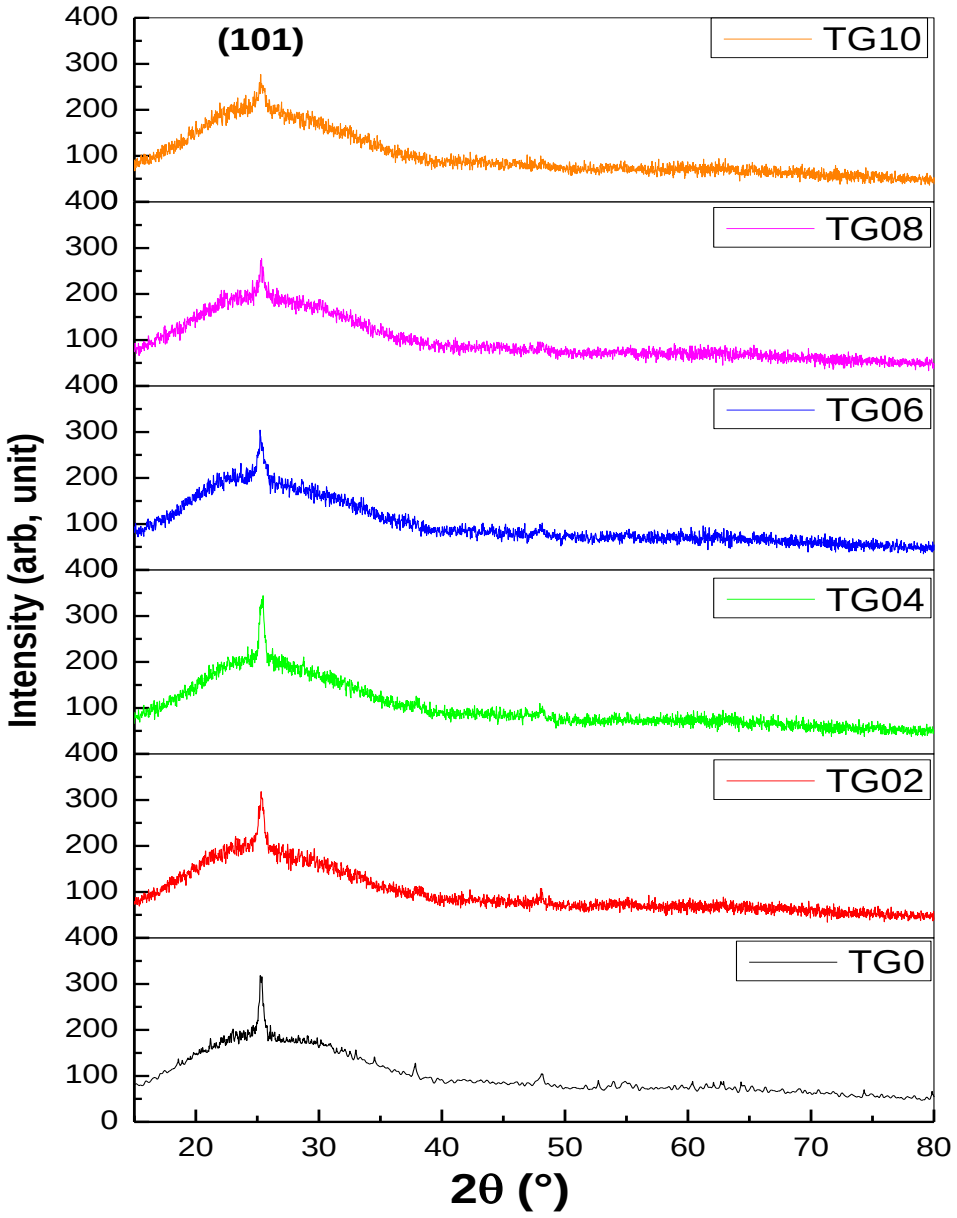

Fig.V.11 XRD spectra of the $Ti_{1-x}Ga_xO_2$ thin films.

V.3.2.1.2 Crystallite size (D)

The crystallite size (D) of $Ti_{1-x}Ga_xO_2$ films was measured using Scherrer's formula (equation II.7). The figure V.12 shows the change of the crystallite size as a function of the gallium doping concentration. The crystallite size increases from 17.77nm to 19.75 nm at x=0.04.After that, it decreases to 9.30 nm with increasing doping concentration. The increase of crystallite size indicates an improvement of crystalline state of $Ti_{1-x}Ga_xO_2$ ($0 \leq x \leq 0.04$) thin films. This is results of Ga^{3+} ions incorporation into Ti^{3+} interstitials sites of TiO_2 lattice. At higher doping ($x > 0.04$), the effect of interstitials is compensated by the effect of substitution (Ti^{4+} by Ga^{+3}) which leads to the decrease of crystallite size [190].

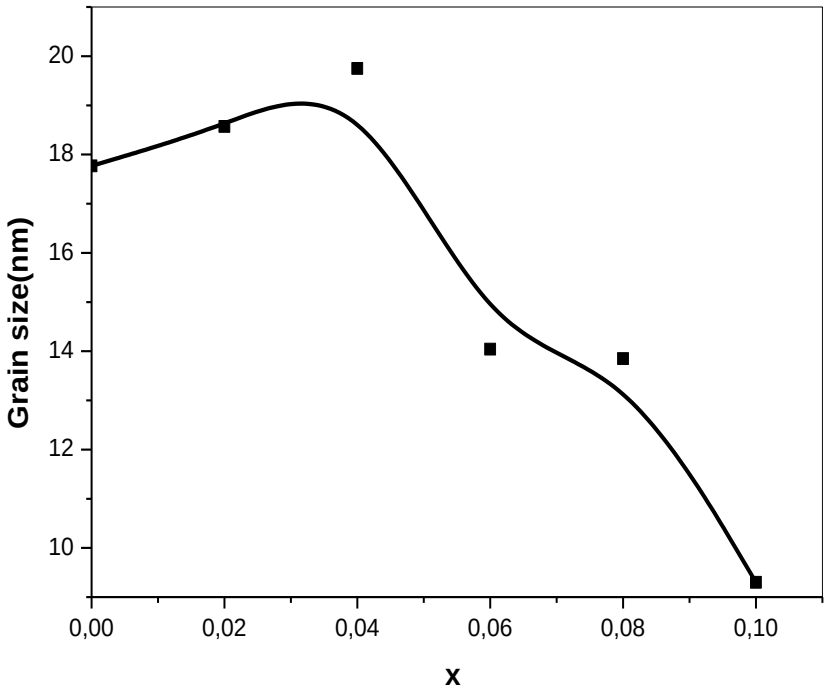

Fig.V.12 Crystallite size as a function of the gallium doping concentration.

The dislocation density (δ) and the thickness shows in the table V.4. It can be seen that the thickness and dislocation density decrease with increasing the gallium doping concentration up to x = 0.04. After that the thickness and dislocation density increase.

Table V.4 Structural parameters of undoped and Ga doped TiO_2 thin films.

samples	2θ	D (nm)	$\delta \times 10^{16}$ (line/m^3)	Film thickness d (nm)
TG0	25.40	17.77	5.62	547
TG02	25.31	18.57	5.38	540
TG04	25.36	19.75	5.06	505
TG06	25.28	14.04	7.12	529
TG08	25.33	13.85	7.22	598
TG10	25.27	9.30	10.6	600

V.3.2.2 Optical properties

V.3.2.2.1 Transmission spectra

The optical transmission spectra of $Ti_{1-x}Ga_xO_2$ thin films shows in Fig. V.13. It can be seen, the $Ti_{1-x}Ga_xO_2$ thin films have the high transmittance at the samples of TG0, TG02, TG04, and TG06, where it reached 86%. This indicates that these samples have a good crystalline state and are consistent with the results obtained from DRX spectra.

After that the transmittance decreases at TG08 and TG10. Whereas a higher concentration of Ga doping leads to a lower transmittance due to the interaction between the light and Ga^{3+} ion. The appearance of interference fringe was observed in the samples TG0, TG02, TG04, and TG06. This indicates that the surface of the samples is smooth. As for other samples, the interference fringe did not appear, which indicates that the surface of the samples is rough.

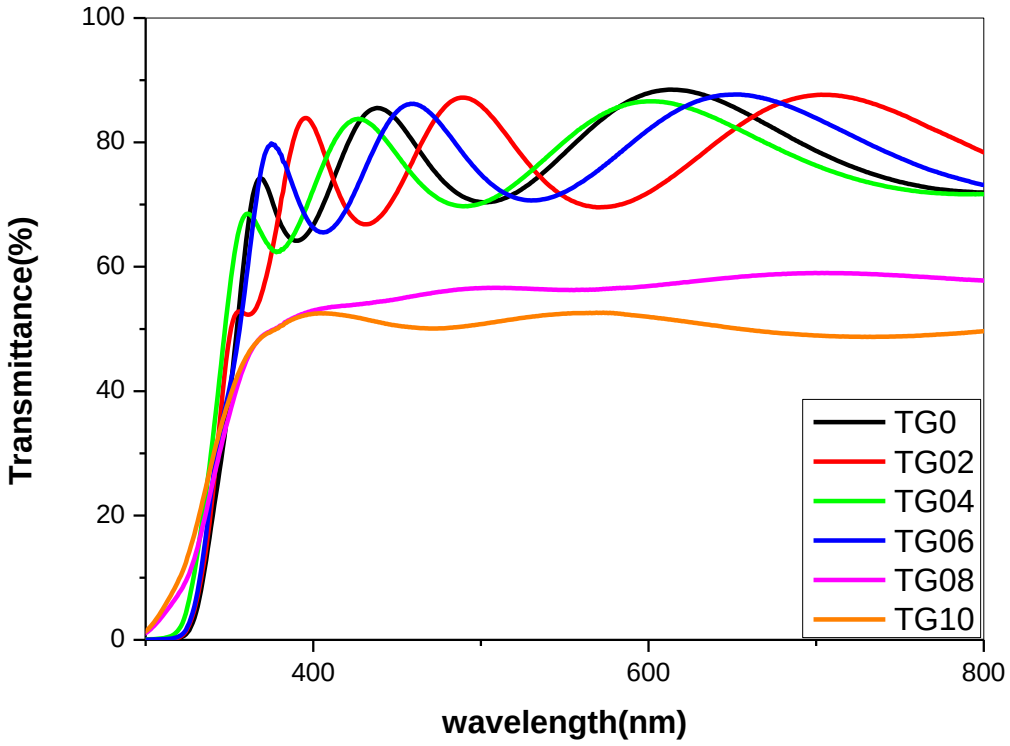

Fig.V.13 Optical transmission spectra of $Ti_{1-x}Ga_xO_2$ thin films.

V.3.2.2.2 Optical band gap Eg

The direct band gab of $Ti_{1-x}Ga_xO_2$ film with different Ga doping concentrations shows in figure V.14. It was observed that the direct band gab decreases with increasing the Ga doping concentration at the sample TG04 and then increasing with increasing Ga doping concentration at the samples TG08 and TG10.In addition, it was observed that the direct band gab of Ga doped TiO_2 films less than of the pure TiO_2 films. This can be explained by the doping of Ga^{3+} ions can form a Ga^{3+} dopant level above the valence band (VB) of TiO_2.The indirect band gab of $Ti_{1-x}Ga_xO_2$ film with different Ga doping concentrations shows in table.V.5.

Table.V.5 Direct and indirect band gap as a function of gallium doping concentration.

samples	direct band gab (eV)	indirect band gab (eV)
TG0	3.55	3.40
TG02	3.30	2.96
TG04	2.99	2.76
TG06	3.38	3.24
TG08	3.46	3.33
TG10	3.44	3.29

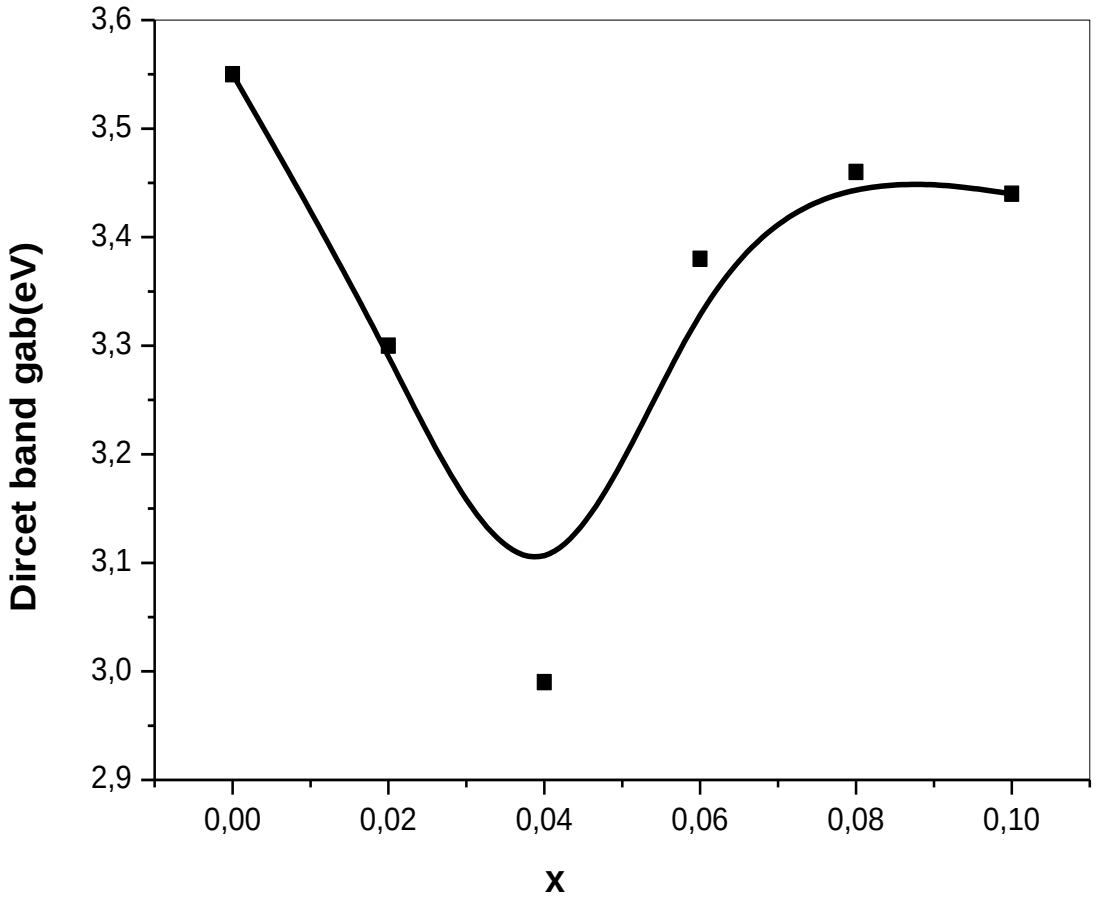

Fig.V.14. Direct band gab of $Ti_{1-x}Ga_xO_2$ film with different Ga doping concentrations

V.3.2.3 Photocatalytic activity of $Ti_{1-x}Ga_xO_2$ films

V.3.2.3.1 UV–VIS test of methylene blue by TiO_2/sunlight

Photocatalytic activity of $Ti_{1-x}Ga_xO_2$ films was evaluated by photodecomposition of MB dye in an aqueous solution of a concentration of 15 mg/L as a model pollutant.Fig.V.15 shows the absorption spectrum of MB solution catalyzed over thin films. It can be seen that the absorption intensity (A) of MB solutions containing Ga- doped thin films is less than that of non-doped. This indicates that the removal of MB dye solution is greater when using the activated slices, while it can be concluded that the Ga doped TiO_2 thin films have an effective role in the effectiveness of photocatalysis.

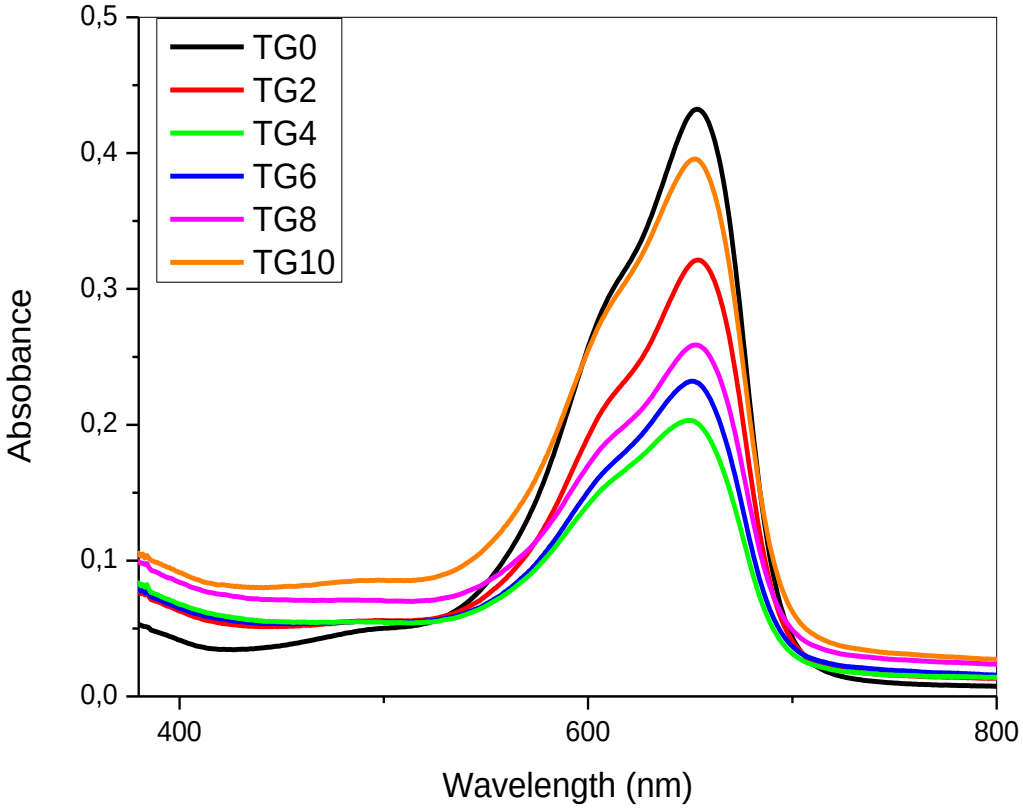

Fig.V.15 UV-Vis absorption spectra of MB solution after reacting with TiO_2 thin films was prepared.

V.3.2.3.2 Photocatalytic degradation rate (PDR)

The results of the photocatalytic degradation rate (PDR) were calculated using the relationship (II.23). The values of photodegradation rate variation of Ga doped concentration are shown in the figure V.16. After 4 h light irradiation, about 95 % of MB molecules are decolorized over the TG04 thin film, while only 84%, 89.2%, 92.2%, 91.2% and 87.3% are decolorized over TiO_2, TG02, TG06,TG08, and TG10 thin films respectively. It was clearly seen that the photodegration rate is increased with Ga-doping concentration, getting more efficient at $Ti_{1-0.4}Ga_{0.4}O_2$ and then decreased gradually due to at a higher concentration the distance between trapping sites decreases and thus increases the probability of recombination rate of the charge carriers [191]. H.J Lin and all [192] and Mathews and all [193].

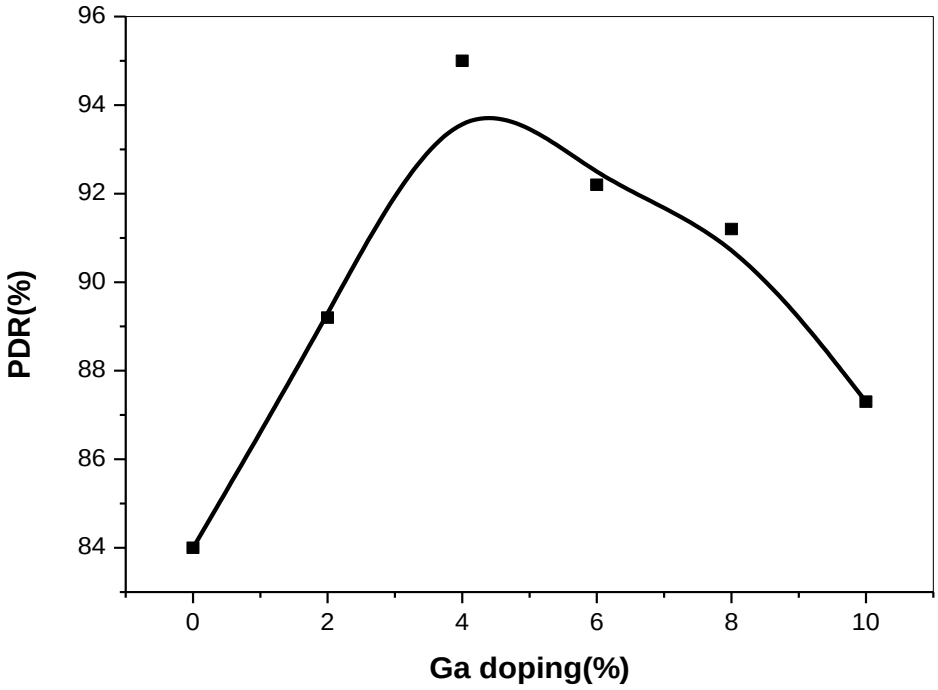

Fig.V.16 Photocatalytic degradation rate as a function of gallium doping concentration.

V.3.2.3.3 Mechanism of photocatalytic reaction

The possible mechanism for enhanced Photocatalytic activity of $Ti_{1-x}Ga_xO_2$ thin films is proposed as follows. When the semiconductor Ga- TiO_2 doped thin films were exposed with suitable light, electrons (e−) are excited to the conductive band (CB) from valance band (VB), thus electron (e−)/ (h+) hole pairs were generated (Eq.V.2). The ionic radius of Ga^{3+} (0.62 Å) being slightly lesser than the ionic radii of the Ti^{4+} (0.68 Å), it is possible for the Ga^{3+} to substitute and occupy Ti^{4+} sites. From the DRX spectra, it found that there is no significant difference of the 2θ on anatas plane (101) between pure TiO_2 and Ga- doped TiO_2 thin films, which also implies that Ga^{3+} can easily enter into the lattice of TiO_2 and substitute for the Ti^{4+} ion [194,195,196,197] . As a result, the substitution of Ga^{3+} to Ti^{4+} ion could create a charge imbalance and then more H_2O/hydroxide ions would be adsorbed onto the surface of TiO_2 catalysts for charge balance. These adsorbed H_2O or OH^- ions on the surface could trap the surface holes and produce highly reactive hydroxide radicals (OH•). [198, 199] which could not only suppress the photo-induced electron-hole pair recombination rate, but also oxidize and adsorb more reactive substrates, and then improved its photocatalytic performance efficiently.

The doped Ga^{3+}ions reduce photoinduced electron-hole pair recombination rate due to the energy level Ga^{3+}/Ga^{4+}. Photo-oxidation process (Eq.V.3) above the VB of anatase TiO_2, develops charge carrier separation. The trapped surface holes in the photooxidation can migrate to the surface adsorbed hydroxyl ions to generate hydroxyl radicals (OH•) (Eq. V.4).

$$Ti_{1-x}Ga_xO_2 + h\nu \longrightarrow Ti_{1-x}Ga_xO_2 + (e^-_{CB} + h^+_{VB}) \quad (V.2)$$

$$Ga^{3+} + h^+_{VB} \longrightarrow Ga^{4+} \quad (V.3)$$

$$Ga^{4+} + OH^-(Ads) \longrightarrow Ga^{3+} + OH^{\bullet} \quad (V.4)$$

Ga^{3+} traps the photoinduced electron to form Ga^{2+} (Eq. V.5), and the trapped electrons transfer to the surface adsorbed O_2 (Eq. V.6) [196, 197]. The energy level of Ga^{3+}/Ga^{2+} below the CB of anatase TiO_2, supporting to enhance the charge carrier separation and resulting in the decline of the (e−)/(h+) pair recombination. The subsequent reactions Eq.V.4 and Eq.V.6 demonstrated that Ga^{3+} could act as electron-hole trapper. As a result, the doping of suitable Ga^{3+} ions is favorable for the decrease of the photoinduced e−/h+ pairs recombination rate and favors the improvement of photocatalytic activity.

$$Ga^{3+} + e^-_{CB} \longrightarrow Ga^{2+} \quad (V.5)$$

$$Ga^{2+} + O_2(ads) \longrightarrow Ga^{3+} + O_2^{\bullet} \quad (V.6)$$

However, at very high doping concentration, unfortunately Ga^{3+} ions can performance as a charge carrier (photoinduced electrons and holes recombination centers Eq.V.7 and Eq.V.8) due to decrease the distance between trapping sites at a high concentration of Ga^{3+} ions and resulting in decline of the Photocatalytic activity.

$$Ga^{4+} + e^-_{CB} \longrightarrow Ga^{3+} \quad (V.7)$$

$$Ga^{2+} + h^+_{VB} \longrightarrow Ga^{3+} \quad (V.8)$$

Schematic illustration for the sunlight photocatalytic process over $Ti_1Ga_xO_2$thin films shows in figure V.17.

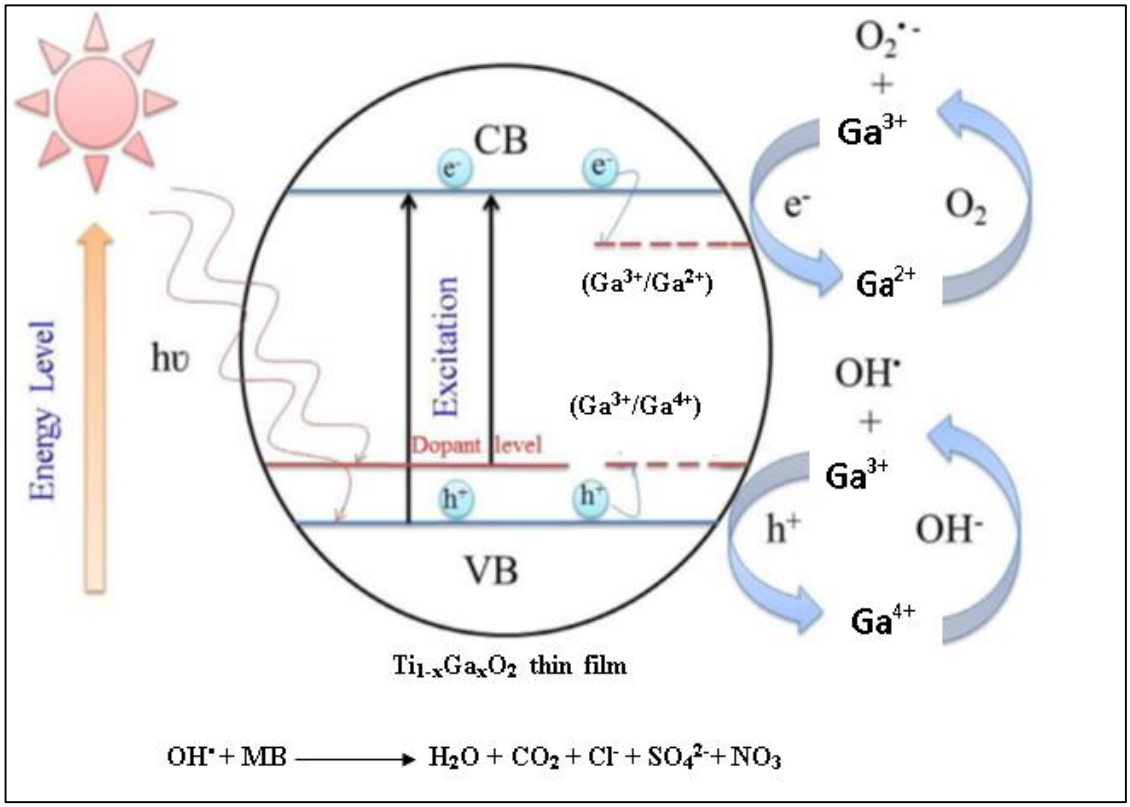

Fig.V.17. Schematic illustration for the sunlight photocatalytic process over $Ti_{1-x}Ga_xO_2$thin films.

V.4 Conclusion

TiO_2 thin films were prepared by sol-gel (spin coating). Firstly, the effect of the molar ratio on the properties of titanium dioxide was studied. Finally, the study of the influence of the gallium doping concentration on the properties of TiO_2 was examined. For the first parameter, i.e. the effect of the molar ratio on the properties of TiO_2. The prepared films are crystallized in the anatase phase. The preferred growth plane is (101).

The average grain size around 23 nm. Good transparency in the visible area. The direct optical band gap varied between 3.5 eV and 3.6 eV. It found the best photodegradation rate of y = 0.66 at t = 180 min. for the last parameter, i.e. the influence of the gallium doping concentration on the properties of TiO_2. the obtained results confirmed that the Ga-doped TiO_2 exhibits the tetragonal crystal structure with a single anatase phase.

The grain size varied from 9.3 nm to 19.75 nm. The direct optical bandgap varied between 2.99 eV and 3.55 eV. It found that the optimum photodegradation rate of 94% at t = 180 min at doping concentration is 4%.

General conclusion and future work

1. General conclusion

Two important aspects of TiO_2 thin films were studied in this work, including the study of the effect of solution concentration, rotation speed, molar ratio and doping by the galuim element on the structural and optical properties of titanium dioxide. For obtaining the best conditions for the preparation of thin layers of TiO_2 used as a photocatalyst with a maximum photodegradation rate of organic pollution (Methylene Bleu was used as a model of organic pollution).

The most important findings are as follows:

1. Thin films of pure TiO_2 with different concentration of solution were prepared by sol gel method (spin coationg). The samples has been shown a tetragonal structure (anatase phase) with a favorable plane of (101). The increased of solution concentration causes the improvement of crystalline state of the samples. A good transmittance in visible rang. Optical band gap varied between 3.09 eV and 3.41 eV. It found at 0.2 M, the samples have a good photocatalytic property with the best photodegradation rate of methylene blue (84%).

2. TiO_2 thin films with different rotation speed were successfully deposited by sol gel (spin coating) method at 500 °C as annealing temperature. The film thickness of samples decreases with increasing of rotation speed from 1000 to 4000 rpm. After 4000 rpm, the film thickness values fixed at 500 nm. The grain size increases in the range of rotation speed between 1000 rpm and 4000 rpm and it decreases at rotation speed more than 4000 rpm. Ramen spectra of all samples show a main peak at 143 cm^{-1}, which are corresponding to O–Ti–O symmetric stretching vibrations of anatase phase. A good transparency in the visible area with optical band gap around to 3.5 eV. It can used the elaborated films (deposited at 4000 rpm) as a photocatalyst to modify the water acidity from pH = 4.8 to pH = 7.4 with produce H_2 gas as a promising fuel for future which to protect the environment from pollution..

3. TiO_2 thin films were deposited with molar ratio y varied from 0.5 to 2. The quantity of acetylacetone in the precursor solution had no significant effect on the optical and structural properties of the TiO_2 thin films. Films consisted of the anatase phase, with a direct band gap in the range of 3.5–3.6 eV and thickness in the range of 534–618 nm. However, the best photodegradation rate reaches to 94 % in y = 0.66 at t = 180 min.

4. Ga-doped TiO_2 thin films have been successfully prepared using a sol-gel method and ethanol as a solvent. It is remarkable that the thin films of $Ti_{1-x}Ga_xO_2$ crystallize in a tetragonal structure (Anatase phase). Optical bandgap narrows to 2.99 eV at 4% of gallium doping concentration. It observed that the Ga doping leads to improving the photocatalysis of TiO_2 thin films, the optimum photodegradation rate is 95% at 4%.

2. Future work

Concerning the findings presented in this thesis, future efforts are suggested as follows:

1. The band gaps of TiO_2 thin films, can be effectively narrowed by galium doping, leading to beneficial visible light absorption. Also, through measuring the degradation speed of MB under visible light, the photocatalytic activities of doped thin films were found to be significantly promoted. Therefore, the practical applications of Ga doped TiO_2 thin films under sunlight should be pursued, e.g. photocatalysis, self-cleaning and water splitting for H_2 production.

2. Co-doping can give rise to gigantic band gap narrowing of TiO_2 through introducing several energy levels/bands next to the CBM with their considerable band width and curvatures result in overlapping of the conduction band. The main absorption of co-doped TiO_2 materials covers the full visible light region and part of the infrared or near-infrared region.

References

[1] C.W. Bunn, The lattice-dimensions of zinc oxide. NATURE VOL. 238 JULY 7 1972

[2] Akira Fujishima, Tata N. Rao, Donald A. Tryk, Titanium dioxide photocatalysis, Journal of Photochemistry and Photobiology C: Photochemistry Reviews 1 (2000) 1–21.

[3]E.Pino, C.Calderón, F.Herrera, G.Cifuentes, G.Arteaga, Photocatalytic Degradation of Aqueous Rhodamine 6G Using Supported TiO2 Catalysts. A model for the removal of organic contaminants from aqueous samples, Frontiers in Chemistry, May 2020, 8, 365.

[4] S. G. Ghugal,D. Vidyasagar, S.G. Ghugal, A.G. Shende, T.Bhoyar, S.S. Umare, Europium Doped TiO2-Ta2O5 Heterostructure for Photodegradation of Dyes, Materials Science inc. Nanomateials & Polymers, *ChemistrySelect* 2020, *5*, 2981 –2984

[5] Q. Sun, Kaijing Li, Songhao Wu, B. Han, L.Sui, L.Dong, Remarkable improvement of TiO_2 for dye photocatalytic degradation by a facile post-treatment, The Royal Society of Chemistry 2020.

[6] D. B. Seong and S. J. Park, J. Nanosci. Nanotechnol., 2019, 19,6247–6255.

[7] V. E. Noval and J. G. Carriazo, Mater. Res., 2019, 22, e20180660.

[8] Y. Benkhetta, Elaboration and characterization of thin layers of zinc oxide (ZnO) deposited by ultrasonic spray for photovoltaic and optoelectronic applications, Thesis, Doctorate, University Biskra, 2019 .

[9] Venables, J. A. Introduction to Surface and Thin Film Processes; Cambridge University Press, 2000.

[10] Pimpinelli, A.; Villain, J. Physics of Crystal Growth; Cambridge University Press, 1999

[11] Freund, L. B.; Suresh, S. Thin Film Materials: Stress, Defect Formation and Surface Evolution; Cambridge University Press, 2003.

[12] Bishop, K. J. M.; Wilmer, C. E.; Soh, S.; Grzybowski, B. A. Nanoscale Forces and Their Uses in Self-assembly. Small 2009, 5, 1600–30.

[13] S. Brochen, electrical properties of ZnO single crystale, doctoral thesis, Grenoble University (2006).

[14] L. Vayssieres. On solar hydrogen and nanotechnology. Wiley (2011).

[15] Q. Deng, band gap tuning and structural engineering of TiO_2 for photocatalysis and solar cells, doctorate these, university of bolton, 2012.

[16] N.Rahimi, R.A. Pax, E.M. Gray, Review of functional titanium oxides. I: TiO_2 and its modifications, Progress in Solid State Chemistry (2016), 07.002.

[17] V.Etacheri, C. D.Valentinc, J.Schneider, D.Bahnemann, S.C. Pillai, Visible-light activation of TiO2 photocatalysts: Advances in theory and experiments, Journal of Photochemistry and Photobiology C: Photochemistry Reviews 25 (2015) 1–29.

[18] I.Ali, M.Suhail, Z.A. Alothmanc , A.Alwarthanc, Recent advances in syntheses, properties and applications of TiO_2 nanostructures, RSC Adv., 2018, 8, 30125.

[19] M.A. Henderson, A surface sciecne perspective on TiO2 photocatalysis. Surf. Sci. Rep. 66,185–297 (2011).

[20] T.L. Thompson, J.T. Yates Jr., Surface science studies of the photoactivation of TiO2-new photochemical processes. Chem. Rev. 106, 4428–4453 (2006)

[21] E.W. McFarland, H. Metiu, Catalysis by doped oxides. Chem. Rev. 113, 4391–4427 (2013).

[22] R.Car, G.Ertl, H.J.Freund, H.Lüth, M.A. Rocca, Defects at Oxide Surfaces,book, Springer Series in Surface Sciences,58,2015.

[23] H. Kamisaka, K. Yamashita, Theoretical study of the interstitial oxygen atom in anatase and rutile TiO2: electron trapping and elongation of the r(O-O) bond. J. Phys. Chem. C 115,8265–8273 (2011)

[24] S. Na-Phattalung, M.F. Smith, K. Kim, M.H. Du, S.H. Wei, S.B. Zhang, S. Limpijumnong,First-principles study of native defects in anatase TiO2. Phys. Rev. B 73, 125205 (2006)

[25] A.G. Hollister, P. Gorai, E.G. Seebauer, Surface-based manipulation of point defects in rutile TiO2. Appl. Phys. Lett. 102, 231601 (2013).

[26] G.H. Enevoldsen, H.P. Pinto, A.S. Foster, M.C.R. Jensen, W.A. Hofer, B. Hammer, J.V.Lauritsen, F. Besenbacher, Imaging of the hydrogen subsurface site in rutile TiO2. Phys. Rev.Lett. 102, 136103 (2009)

[27] Ç. Kılıç, A. Zunger, n-type doping of oxides by hydrogen. Appl. Phys. Lett. 81, 73 (2002)

[28] D.M. Chen, D. Yang, Q. Wang, Z.Y. Jiang, Effects of boron doping on photocatalytic activity and microstructure of titanium dioxide nanoparticles. Ind. Eng. Chem. Res. 45, 4110–4116 (2006).

[29] E. Finazzi, C. Di Valentin, G. Pacchioni, Boron-doped anatase TiO2: pure and hybr DFT calculations. J. Phys. Chem. C 113, 220–228 (2009).

[30] N.D. Feng, A.M. Zheng, Q. Wang, P.P. Ren, X.Z. Gao, S.B. Liu, Z.R. Shen, T.H. Chen,

[31] L. Artiglia, D. Lazzari, S. Agnoli, G.A. Rizzi, G. Granozzi, Searching for the formation of Ti-B bonds in B-doped TiO2-rutile. J. Phys. Chem. C 117, 13163–13172 (2013)

[32] C. Di Valentin, G. Pacchioni, A. Selloni, Theory of carbon doping of titanium dioxide. Chem. Mater. 17, 6656–6665 (2005)

[33] O. Diwald, T.L. Thompson, T. Zubkov, E.G. Goralski, S.D. Walck, J.T. Yates J., Photochemical activity of nitrogen-doped rutile TiO2 (110) in visible light. J. Phys. Chem. B 108, 6004–6008 (2004).

[34] C. Di Valentin, G. Pacchioni, A. Selloni, S. Livraghi, E. Giamello, Characterization of paramagnetic species in N-doped TiO2 powders by EPR spectroscopy and DFT calculations.J. Phys. Chem. B 109, 11414–11419 (2005)

[35] C. Di Valentin, E. Finazzi, G. Pacchioni, A. Selloni, S. Livraghi, M.C. Paganini, E. Giamello, N-doped TiO2: theory and experiment. Chem. Phys. 339, 44–56 (2007)

[36] F. Peng, L.F. Cai, H. Yu, H.J. Wang, J. Yang, Synthesis and characterization of substitutional and interstitial nitrogen-doped titanium dioxides with visible light photocatalytic activity. J. Solid State Chem. 181, 130–136 (2008)

[37] E.A. Reyes-Garcia, Y.P. Sun, K. Reyes-Gil, D. Raftery, 15N solid state NMR and EPR characterization of N-doped TiO2 photocatalysts. J. Phys. Chem. C 111, 2738–2748 (2007)

[38] H. Shen, L. Mi, P. Xu, W.D. Shen, P.N. Wang, Visible-light photocatalysis of nitrogendoped TiO2 nanoparticulate films prepared by low-energy ion implantation. Appl. Surf. Sci. 253, 7024–7028 (2007)

[39] U. Gesenhues, T. Rentschler, Crystal growth and defect structure of Al3+-doped rutile. J. Solid State Chem. 143, 210–218 (1999)

[40] S.T. Martin, C.L. Morrision, M.R. Hoffmann, Photochemical mechanism of size-quantized Vanadium-doped TiO2 particles. J. Phys. Chem. 98, 13695–13704 (1994)

[41] F. Kubec, Z. Šroubek, Paramagnetic resonance of interstitial V4+ in TiO2. J. Chem. Phys. 57, 1660 (1972).

[42] J.A. Wang, R. Limas-Ballesteros, T. López, A. Moreno, R. Gómez, O. Novaro, X.Bokhimi, Quantitative determination of titanium lattice defects and solid-state reaction mechanism iniron-doped TiO2 photocatalysts. J. Phys. Chem. B 105, 9692–9698 (2001).

[43]W.T. Geng, K.S. Kim, Structural, electronic, and magnetic properties of a ferromagnetic semiconductor: Co-doped TiO2 rutile. Phys. Rev. B 68, 125203 (2003).

[44] A. Sasahara, M. Tomitori, XPS and STM study of Nb-doped TiO_2 (110) (1 × 1) surfaces. J. Phys. Chem. C 117, 17680–17686 (2013).

[45] N.O. Gopal, H.-H. Lo, T.-F. Ke, C.-H. Lee, C.-C. Chou, J.-D. Wu, S.-C. Sheu, S.-C. Ke, Visible light active phosphorus-doped TiO2 nanoparticles: an EPR evidence for the enhanced charge separation. J. Phys. Chem. C 116, 16191–16197 (2012).

[46] R.Y. Zheng, L. Lin, J.L. Xie, Y.X. Zhu, Y.C. Xie, State of doped phosphorus and its influence on the physicochemical and photocatalytic properties of P-doped titania. J. Phys. Chem. C 112, 15502–15509 (2008).

[47] R. Long, N.J. English, Energetic and electronic properties of P doping at the rutile TiO_2 (110) surface from first principles. J. Phys. Chem. C 113, 9423–9430 (2009).

[48] T. Ohno, M. Akiyoshi, T. Umebayashi, K. Asai, T. Mitsui, M. Matsumura, Preparation of S-doped TiO2 photocatalysts and their photocatalytic activities under visible light. Appl. Catal. A 265, 115–121 (2004).

[49] X.W. Zhang, L.C. Lei, One-step preparation of visible-light responsive Fe-TiO2 coating photocatalysts by MOCVD. Mater. Lett. 62, 895–897 (2008).

[50] M. Liu, X.Q. Qiu, M. Miyauchi, K. Hashimoto, Energy-level matching of Fe(III) ions grafted at surface and doped in bulk for efficient visible-light photocatalysts. J. Am. Chem. Soc. 135, 10064–10072 (2013)

[51] E. Borgarello, J. Kiwi, M. Gratzel, E. Pelizzetti, M. Visca, Visible light induced water cleavage in colloidal solutions of chromium-doped titanium dioxide particles. J. Am. Chem. Soc. 104, 2996–3002 (1982)

[52] D.H. Kim, K.S. Lee, Y.-S. Kim, Y.-C. Chung, S.-J. Kim, Photocatalytic activity of Ni 8 wt %-doped TiO2 photocatalyst synthesized by mechanical alloying under visible light. J. Am. Ceram. Soc. 89, 515–518 (2006).

[53] S. Kim, S.-J. Hwang, W. Choi, Visible light active platinum-ion-doped TiO2 photocatalyst. J. Phys. Chem. B 109, 24260–24267 (2005)

[54] R. Asahi, T. Morikawa, T. Ohwaki, K. Aoki, Y. Taga, Visible-light photocatalysis in nitrogen-doped titanium oxides. Science 293, 269–271 (2001)

[55] M. Batzill, E.H. Morales, U. Diebold, Influence of nitrogen doping on the defect formation and surface properties of TiO2 rutile and anatase. Phys. Rev. Lett. 96, 026103 (2006).

[56] J.G. Tao, M. Yang, J.W. Chai, J.S. Pan, Y.P. Feng, S.J. Wang, Atomic N modified rutile TiO2(110) surface layer with significant visible light photoactivity. J. Phys. Chem. C 118, 994–1000 (2014)

[57] Y. Ortega, O. Lamiel-Garcia, D.F. Hevia, S. Tosoni, J. Oviedo, M.A. San-Miguel, F. Illas,Theoretical study of the fluorine doped anatase surfaces. Surf. Sci. 618, 154–158 (2013)

[58] A.M. Czoska, S. Livraghi, M. Chiesa, E. Giamello, S. Agnoli, G. Granozzi, E. Finazzi, C. Di Valentin, G. Pacchioni, The nature of defects in fluorine-doped TiO2. J. Phys. Chem. C 112, 8951–8956 (2008).

[59] S.U.M. Khan, M. Al-Shahry, W.B. Ingler Jr., Efficient photochemical water splitting by achemically modified n-TiO2. Science 297, 2243–2245 (2002)

[60] K. Palanivelu, J.S. Im, Y.-S. Lee, Carbon doping of TiO2 for visible light photocatalysis—a review. Carbon Sci. 8, 214–224 (2007)

[61] T. Umebayashi, T. Yamaki, H. Itoh, K. Asai, Band gap narrowing of titanium dioxide by sulfur doping. Appl. Phys. Lett. 81, 454–456 (2002)

[62] T. Umebayashi, T. Yamaki, S. Tanaka, K. Asai, Visible light-induced degradation of methylene blue on S-doped TiO2. Chem. Lett. 32, 330–331 (2003)

[63] S. In, A. Orlov, R. Berg, F. García, S. Pedrosa-Jimenez, M.S. Tikhov, D.S. Wright, R.M. Lambert, Effective visbible light-activated B-doped and B, N-codoped TiO2 photocatalysts. J. Am. Chem. Soc. 129, 13790–13791 (2007).

[64] Q. Xu, Y. Ma, J. Zhang, X.L. Wang, Z.C. Feng, C. Li, Enhancing hydrogen production activity and suppressing CO formation from photocatalytic biomass reforming on Pt/TiO2 by optimizing anatase-rutile phase structure. J. Catal. 278, 329–335 (2011).

[65] B. Zheng, Q. Guo, D. Wang, H. Zhang, Y. Zhu, S. Zhou. Energy-transfer modulation for enhanced photocatalytic activity of near-infrared upconversion photocatalyst. J. Am. Ceram. Soc., 2015, 98(1), 136–140.

[66] F.Huang, A.Yan , H.Zhao, Influences of Doping on Photocatalytic Properties of TiO2 Photocatalyst, Semiconductor Photocatalysis - Materials, Mechanisms and Applications,2016.

[67] B. Thomas, Des nanotitanates de soduim aux dioxydes de titane : électrode négative à base de TiO2 (B) nanométrique pour accumulateur lithium ion, Thèse de Doctorat, Université de Nantes, France (2009).

[68] S. Pardis, "Synthèse de nanoparticules d'oxyde de titane par pyrolyse laser : étude des propriétés optiques et de la structure électronique", Thèse de Doctorat, Université Paris Sud XI, France (2001).

[69]L. Li, C. Liu, Y. Liu. Study on activities of vanadium (IV/V) doped TiO2 (R) nanorods induced by UV and visible light. Materials Chemistry and Physics 113 (2009) 551–557.

[70] J. Zhou, M. Takeuchi, A. K. Ray, M. Anpo, X. S. Zhao. Enhancement of photocatalytic activity of P25 TiO2 by vanadium-ion implantation under visible light irradiation. Journal of Colloid and Interface Science 311 (2007) 497–501

[71] J. C. Wu, C. Chen. A visible-light response vanadium-doped titania nanocatalyst by sol–gel method. Journal of Photochemistry and Photobiology A: Chemistry 163 (2004) 509–515.

[72] K. Bhattacharyya, S. Varma, A. K. Tripathi, A. K. Tyagi. Synthesis and photocatalytic activity of nano V-doped TiO2 particles in MCM-41 under UV–visible irradiation. Journal of Materials Research 25 (2010) 125-133

[73] M. Takeuchi, H. Yamashita, M. Matsuoka, M. Anpo, T. Hirao, N. Itoh, N. Iwamoto. Photocatalytic decomposition of NO under visible light irradiation on the Cr-ion-implanted TiO2 thin film photocatalyst. Catalysis letters 67 (2000) 135-137.

[74] B. Sun, E. P. Reddy, P. G. Smirniotis. Effect of the Cr6+ concentration in Cr-incorporatedTiO2-loaded MCM-41 catalysts for visible light photocatalysis. Applied Catalysis B:Environmental 57 (2005) 139–149.

[75] J. Zhu, Z. Deng, F. Chen, J. Zhang, H. Chen, M. Anpo, J. Huang, L. Zhang. Hydrothermal doping method for preparation of Cr3+-TiO2 photocatalysts with concentration gradient distribution of Cr^{3+}. Applied Catalysis B: Environmental 62 (2006) 329–335.

[76] G. H. Takaoka, T. Nose, M. Kawashita. Photocatalytic properties of Cr-doped TiO2 films prepared by oxygen cluster ion beam assisted deposition. Vacuum 83 (2008) 679–682.

[77] H. Zhu, J. Tao, X. Dong. Preparation and photoelectrochemical activity of Cr-Doped TiO2 nanorods with nanocavities. The Journal of Physical Chemistry C 114 (2010) 28732879.

[78] L. Devi, S. Kumar, B. Murthy, N Kottam. Influence of Mn2+ and Mo6+ dopants on the phase transformations of TiO2 lattice and its photo catalytic activity under solar illumination.Catalysis Communications 10 (2009) 794–798.

[79]S. George, S. Pokhrel, Z. Ji, B. L. Henderson, T. Xia, L. Li, J. I. Zink, A.E. Nel, L. Madler. Role of Fe doping in tuning the band gap of TiO2 for the photo-oxidation-induced cytotoxicity paradigm. Journal of the American Chemical Society 133 (2011) 11270–11278.

[80] M. A. Barakat, H. Schaeffer, G. Hayes, S. Ismat-Shah. Photocatalytic degradation of 2-chlorophenol by Co-doped TiO2 nanoparticles. Applied Catalysis B: Environmental 57(2005) 23–30.

[81] H. Yu, X. Li, S. Zheng, W. Xu, Photocatalytic activity of TiO2 thin film non-uniformly doped by Ni. Materials Chemistry and Physics 97 (2006) 59-63.

[82] G. Colon, M. Maicu, M. C. Hidalgo, J. A. Navio. Cu-doped TiO2 systems with improved photocatalytic activity. Applied Catalysis B: Environmental 67 (2006) 41–51.

[83] G. Shao, Q. Deng, L. Wan, M. Guo, X. Xia, Y. Gao. Molecular design of TiO2 for giganticred shift via sublattice substitution. Journal of Nanoscience and Nanotechnology 10 (2010)1–5

[84] F. Zhang, Z. Cheng, L. Kang, L. Cui, W. Liu, X. Xu, G. Hou, H. Yang. A novel preparation of Ag-doped TiO2 nanofibers with enhanced stability of photocatalytic activity. RSC Adv., 2015, 5, 32088–32091.

[85] K. Gupta, R. P. Singh, A. Pandey, P. Anjana. Photocatalytic antibacterial performance of TiO2 and Ag-doped TiO2 against *S. aureus. P. aeruginosa* and *E. coli*. Beilstein J. Nanotechnol., 2013, 4, 345–351.

[86] H.Xuemin, Ga-Doped Nano-TiO2 Thin Films: Preparation, Optical and Electrical Properties, Article *in* Chinese Journal of Inorganic Chemistry · November 2009.

[87] X.Liua, M.Khana, W.Liua, W.Xianga, M.Guana, P.Jianga, W. Caoa, Synthesis of nanocrystalline Ga–TiO2 powders by mild hydrothermal method and their visible light photoactivity, Ceramics International41(2015)3075–3080.

[88] C.Sarantopoulos**,** photocatalyseurs a base de TiO_2 prepares par infiltration chimique en phase vapeur (cvi) sur supports microfibreux, doctorat theses, Université de Bordeaux, 2007.

[89] F.Scarpelli, T. F. Mastropietro, T. Poerio ,N.Godbert, Mesoporous TiO2 Thin Films: State of the Art, Titanium Dioxide - Material for a Sustainable Environment,2018.

[90] X. Kang, S.Liu, Z.Dai, Y.He, X.Song,Z.Tan, Titanium Dioxide: From Engineering to Applications, Catalysts 2019, 9, 191.

[91] N. H.Salah, Etude de la dégradation photocatalytique de polluants organiques en présence de dioxyde de titane, en suspension aqueuse et en lit fixe, université de Grenoble,2013.

[92] C.M.Teh, A. R.Mohamed, Roles of titanium dioxide and ion-doped titanium dioxide on photocatalytic degradation of organic pollutants (phenolic compounds and dyes) in aqueous solutions, Journal of Alloys and Compounds 509 (2011) 1648–1660.

[93] Dariania, A. Esmaeilia, A. Mortezaalia, S. Dehghanpour,Photocatalytic reaction and degradation of methylene blueon TiO2nano-sized particles, Optik 127 (2016) 7143–7154

[94] D.Komaraiah, E.Radha, J. Sivakumar, M.V. R.Reddy, R. Sayanna, Structural, optical properties and photocatalytic activity of Fe^{3+} doped TiO_2 thin films deposited by sol-gel spin coating, Surfaces and Interfaces 17 (2019) 100368.

[95] M.Ismail, M.Khan, M.A.Khan, A.M. Asiri, Pollution, Toxicity and Carcinogenicity of Organic Dyes and their Catalytic Bio-Remediation, Current Pharmaceutical Design, 2019, 25, 3653-3671

[96] W. Sun, L .Chen, J.Tian, J.Wang, S.He, Degradation of a monoazo dye Alizarin Yellow GG in aqueous solutions by gamma irradiation: Decolorization and biodegradability enhancement. Radiat,Phys Chem 2013; 83: 86-9.

[97] M.G.Khansari, A.M.Bardbori,M.G. Hosseini, Using Janus green B to study paraquat toxicity in rat liver mitochondria. Ann N Y Acad Sci 2006; 1090: 98-107.

[98] A.K.Kushwaha, N.Gupta, M.C.Chattopadhyaya, Removal of cationic methylene blue and malachite green dyes from aqueous solution by waste materials of Daucus carota. J Saudi Chem Soc 2014; 18:200-7.

[99] P.Kumar, M.Govindaraju, S.Senthamilselvi,K Premkumarn Photocatalytic degradation of methyl orange dye using silver (Ag) nanoparticles synthesized from *Ulva lactuca*. Colloids Surf B Biointerfaces 2013; 103: 658-61.

[100] A.Nezamzadeh-Ejhieh, M.Amiri, CuO supported clinoptilolite towards solar photocatalytic degradation of p-aminophenol. Powder Technol 2013; 235: 279-88.

[101] A.Nezamzadeh-Ejhieh, M.Khorsandi, Heterogeneous photodecolorization of Eriochrome Black T using Ni/P zeolite catalyst. Desalination 2010; 262: 79-85.

[102] N.J. Willmott, J.T. Guthrie, G. Nelson, JSDC, 114 (1998) 38-41.

[103] E. Zawlotzki Guivarch, Traitement des polluants organiques en milieux aqueux par procédé électrochimique d'oxydation avancée "Electro-Fenton". Application à la minéralisation des colorants synthétiques, doctorat these, Université de Marne-La Vallée, France (2004).

[104] R.Zuo, G. Du, W.Zhang, L.Liu, Y.Liu, L.Mei, Z. Li, Photocatalytic Degradation of Methylene Blue Using TiO_2 Impregnated Diatomite, Advances in Materials Science and Engineering 2014, 170148, 7.

[105] S. Huang, L.Huijie, Y.Wang, X.Liu, H.Li, Z. Zhan, L.Jia, L.Chen, Monitoring of oxygen using colorimetric indicator based on graphene/TiO2 composite with first-order kinetics of methylene blue for modified atmosphere packaging, Packag Technol Sci. 2018;31:575–584.

[106] H.Khoussa, Elimination des composés organiques par procédés d'oxydation avancée, majesty memory, 2015.

[107] G.W. Ewing, Istumental methods of chemical analysis, NY, MacGraw Hill (1975).

[108] J.M. Herrmann, Heterogeneous photocatalysis : fundamentals and applications to the removal of various types of aqueous pollutants, Catalysis today 53 (1999) 115-129.

[109] C.N. Satterfield, Mass Transfer in Heterogeneous Catalysis, MIT Press,Cambridge, MA (1970) 177–179.

[110] D.F. Ollis, Contaminant degradation in water, Environmental Science and Technology 19 (1985) 480-484.

[111] A. Fernández, G. Lassaletta, V.M. Jiménez, A. Justo, A.R. González-Elipe, J.M.Herrmann, H. Tahiri, Y. Ait-Ichou, Preparation and characterization of TiO2 photocatalysts supported ovarious rigid supports (glass, quartz and stainlesssteel). Comparative studies of photocatalytic activity in water purification, AppliedCatalysis B : Environmental 7 (1995) 49-63.

[112] I. Arslan, I.A. Balcioglu, D.W. Bahnemann, Heterogeneous photocatalytic treatment of simulated dyehouse effluents using novel TiO2 photocatalysts, Applied CatalysisB: Environmental 26 (2000) 193-206.

[113] M. Khairy , W. Zakaria, Effect of metal-doping of TiO2 nanoparticles on their photocatalytic activities toward removal of organic dyes, Egyptian Journal of Petroleum (2014).

[114] A. Aldrin , Preparation and characterization of certain II-VI, I-III-VI2 semiconductor thin films and transparent conducting oxides, PhD thesis, Cochin University of Science and Technology, Kerala, India, 2004.

[115] M. Dahnoun **,**Preparation and characterisation of Titanium dioxide and Zinc oxide thin films via Sol-Gel (spin coating) technique for optoelectronic applications, Doctorate these, University of biskra,2020.

[116] M.Ohring, The Materials Science of Thin Films, book is printed on acid-free paper,1992.

[117] R.Kumar, N. Arorab ,N.Sharmac, Study of spin coated titanium dioxide films, International Journal of Pure and Applied Physics,ISSN 0973-1776 Volume 13, Number 1 (2017),229-231.

[118] L. Yang, Fabrication and characterization of microlasers by the Sol-Gel method", PhD Thesis, California institute of technology, Pasadena, California, USA, (2005).

[119]] A. Yahia **,** Optimization of indium oxide thin films properties prepared by sol gel spin coating process for optoelectronic applications, Doctorate these, University of biskra,2020.

[120] D. Gallagher, TA Ring, Sol-gel processing of ceramics films Chimia, 43 (1989), p. 298.

[121] R. Messemeche, Caractérisation des couches minces d'oxyde de titane (TiO2) obtenue par sol-gel (spin-coating) : L'effet de la concentration de la solution, master memory University of biskra, 2016.

[122] E. Marenna., Sol-Gel Synthesis of functional nanocomposites based on inorganic oxides, Doctorate Thesis, University of Naples Federico II, Italia, (2008).

[123] A.K. Zak, W.H. Majid, M.E. Abrishami, R. Yousefi, X ray analysis of ZnO nanoparticles by Williamson-Hall and size-strain plot methods, Solid State Sci. 13 (2011) 251–256.

[124] J. Solé, L. Bausa, D. Jaque, An introduction to the optical spectroscopy of inorganic solids, John Wiley & Sons, 2005.

[125] R.M. Mohite, Studies of doped and undoped nanostructured zinc oxide thin films for solar cell application, Doctorate Thesis, Solapur University, 2015.

[126] S. Sheth, Synthesis and Characterization of Catalysts for Photo-oxidation of Water, Doctorate Thesis, University of Paris-Sud, 2013.

[127] R. Swanepoel, "Determination of the thickness and optical constants of amorphous silicon", Journal of Physics E: scientific instruments, 16(12), (1983) 1214.

[128] J. Tauc., R. Grigorovici., and A. Vancu, *"Optical properties and electronic structure of* amorphous germanium", Physica Status Solidi (B), 15(2), (1966) 627- 637.

[129] D. Beena., K. J. Lethy., R. Vinodkumar., V. P. Pillai, V. Ganesan., D. M. Phase, S. K. Sudheer, "Effect of substrate temperature on structural, optical and electrical properties

of pulsed laser ablated nanostructured indium oxide films", Applied Surface Science, 255(20) (2009), 8334-8342.

[130] J.I. Pankove, Absorption edge of impure gallium arsenide, Phys. Rev. 140 (1965) A2059.

[131] D. Redfield, Electric fields of defects in solids, Phys. Rev. 130 (1963) 914.

[132] T.P. Rao, M.S. Kumar, Physical properties of Ga-doped ZnO thin films by spray pyrolysis, J. Alloys Compd. 506 (2010) 788–793.

[133] M. Shkir, M. Anis, S. Shafik, M.A. Manthrammel, M.A. Sayeed, M.S. Hamdy, S. AlFaify, An effect of Zn content doping on opto-third order nonlinear characteristics of nanostructured CdS thin films fabricated through spray pyrolysis for optoelectronics, Physica. E 118 (2020) 113955.

[134] I. Sta, M. Jlassi, M. Hajji, M.F. Boujmil, R. Jerbi, M. Kandyla, M. Kompitsas, H. Ezzaouia, Structural and optical properties of TiO2 thin films prepared by spin coating, J. Sol.-Gel. Sci. Technol. 72 (2014) 421–427.

[135] L. urkovic, D. Ljubas, S. Šegota, I. Bacˇic, Photocatalytic degradation of Lissamine Green B dye by using nanostructured sol–gel TiO2 films, J. Alloys Comp. 604 (2014) 309–316.

[136] Y. Benkhetta, A. Attaf, H. Saidi, A. Bouhdjar, H. Bendjedidi, I.B. Kherkhachi, M. Nouadji, N. Lehraki, Influence of the solution flow rate on the properties of zinc oxide (ZnO) nano-crystalline films synthesized by ultrasonic spray process, Optik 127 (2016) 3005–3008.

[137] D. Selma, M. Hassan, Al-Jawad, Effect of Doping on Structural and Electrical Properties of titanium Dioxide (TiO2) Thin Films for Gas Sensor, Int. J.Sci. Eng. Res. 5 (1) (2014) 2171.

[138] I. Joseph Panneerdoss, S. Johnson Jeyakumar, M. Jothibas., Characteristic comparison of TiO2 thin films with an inorganic and organic precursor at different molarities by Spray pyrolysis, Int. J. Eng. Sci. 4 (11) (2014) 15–20.

[139] S. Chelbi, L. Hammiche, D. Djouadi, A. Chelouche, Caractérisations structurale et optique de l'aerogel de TiO2 elabore dans l'ethanol supercritique, Rev. Alg. Phy. 2 (2) (2015) 69–73.

[140] A. Bouhdjer, A. Attaf, H. Saidi, H. Bendjedidi, Y. Benkhetta, I. Bouhaf, Correlation between the structural, morphological, optical, and electrical properties of In2O3 thin films obtained by an ultrasonic spray CVD process, J.Semiconduct. 36 (2015) 082002-1.

[141] D. Nunes, A. Pimentel, L. Santos, P. Barquinha, E. Fortunato, R. Martins, Photocatalytic TiO2 nanorod spheres and arrays compatible with flexible applications, Catalysts 7 (2017) 60.

[142]J. Yan, G. Wu, W. Dai, N. Guan, L. Li, Synthetic Design of Gold Nanoparticles on Anatase TiO2 {001} for Enhanced Visible Light Harvesting ACS Sustainable Chem, Eng. 2 (1940) (2014).

[143] D. Georgescu, L. Baia, O. Ersen, M. Baia, S. Simon, Experimental assessment of the phonon confinement in TiO2 anatase nanocrystallites by Raman spectroscopy, J. Raman Spectrosc. 43 (7) (2012) 876–883.

[144] Zuoli He, Wenxiu Que, Jing Chen, Yucheng He, Gangfeng Wang, Surface chemical analysis on the carbon-doped mesoporous TiO2 photocatalysts after post-thermal treatment: XPS and FTIR characterization, J. Phy. Chem.Solids 74 (2013) 924–928.

[145] Q. Li, C. Zhang, J. Li, Photocatalysis and wave-absorbing properties of polyaniline/ TiO2 microbelts composite by in situ polymerization method, Appl. Surf. Sci. 257 (2010) 944–948.

[146] S. Rahmane, M.S. Aida, M.A. Djouadi, N. Barreau, Effects of thickness variation on properties of ZnO:Al thin films grown by RF magnetron sputtering deposition, Superlattices Microstruct. 79 (2015) 148–155.

[147] M. Shkir, I.M. Ashraf, S. AlFaify, A. Mohamed El-Toni, M. Ahmed, A. Khan, A noticeable effect of Pr doping on key optoelectrical properties of CdS thin films prepared using spray pyrolysis technique for high-performance photodetector applications, Ceramics Int. 46 (4) (2020) 4652–4663.

[148] H. Lin, C.P. Huang, W. Li, C. Ni, S. Ismat Shah, Yao-Hsuan Tseng, Size depende ncy of nanocrystalline TiO2 on its optical property and photocatalytic reactivity exemplified by 2-chlorophenol, Appl. Catalysis B: Environ. 68 (2006) 1–11.

[149] M. Shkir, M. Anis, S. Shafik, M.A. Manthrammel, M.A. Sayeed, M.S. Hamdy, S. AlFaify, An effect of Zn content doping on opto-third order nonlinear characteristics of

nanostructured CdS thin films fabricated through spray pyrolysis for optelectronics, Physica. E 118 (2020) 113955.

[150] H. Águas, N. Popovici, L. Pereira, O. Conde, W.R. Branford, L.F. Cohen, E. Fortunato, R. Martins, Spectroscopic ellipsometry study of Co-doped TiO2 films, P Hys. Stat. Sol. 205 (4) (2008) 880–883.

[151] I. Justicia, G. Garcia, L. Vazquez, J. Santiso, P. Ordejon, G. Battiston, R. Gerbasi, A. Figueras, *Sensors and Actuators B: Chemical*,. 2005, *109*, 52.

[152] B.-H. K. S.-C. Jung, S.-J. Kim, N. Imaishi, Y.-I. Cho,, Chemical Vapor Deposition 2005, 11,137.

[153]S.C.Jong, B.H.Kim, S.J.Kim, N.Imaishi, Y.I.Cho, Characterization of a TiO_2 photocatalyst films deposited by CVD and its photocatalytic activity, Chem. Vap. Deposition 2005, 11, No.3.

[154] D.Komaraiah, E. Radha, M. V. R. Reddy, J. S. Kumar, R. sayanna, structural, optical properties and photocatalytic activity of nanocrystalline TiO2 thin films deposited by sol-gel spin coating, i-manager's Journal on Material Science,. 71 2019.

[155] C. An, S. Peng, and Y. Sun, Facile synthesis of sunlight-driven AgCl:Ag plasmonic nanophotocatalyst, *Advanced Materials*, vol. 22, no. 23, pp. 2570–2574, 2010.

[156] F.-T. Li, Y. Zhao, Y. Liu, Y.-J. Hao, R.-H. Liu, and D.-S. Zhao, "Solution combustion synthesis and visible light-induced photocatalytic activity of mixed amorphous and crystalline MgAl2O4 nanopowders," *Chemical Engineering Journal*, vol. 173, no. 3, pp. 750–759, 2011.

[157] N. C. Castillo, A. Heel, T. Graule, and C. Pulgarin, "Flameassisted synthesis of nanoscale, amorphous and crystalline, spherical BiVO4 with visible-light photocatalytic activity," *Applied Catalysis B*, vol. 95, no. 3-4, pp. 335–347, 2010.

[158] M.D. Tyona, A comprehensive study of spin coating as a thin film deposition technique and spin coating equipment, Advances in Material Research, Vol. 2, No. 4 (2013) 181-193.

[159] M. Teodorescu, L. Schacher, D. Adolphe, I. Gradinaru, I. Zetu, S. Stratulat, Experimental and Theoretical Investigations in Polyamide Spin-Coated Thin Films, MATERIALE PLASTICE 50 No. 3 (2013).

[160]S. Dhanapandian, A. Arunachalam, C. Manoharan, Highly oriented and physical properties of sprayed anatase Sn-doped TiO2 thin films with an enhanced antibacterial activity, Appl. Nanosci. 6 (2016) 387–397.

[161] Xiaoyun Ye, Chan Zheng, Lian Ma, Xingfang Huang, Microemulsion-assisted hydrothermal preparation and infrared radiation property of TiO2 nanomaterials with tunable morphologies and crystal form, Mater. Sci. Semiconduct. Process. 31 (2015) 295–301.

[162] P. Malliga, J. Pandiarajan, N. Prithivikumaran and K. Neyvasagam, Influence of Film Thickness on Structural and Optical Properties of Sol-Gel Spin Coated TiO2 Thin Film, IOSR Journal of Applied Physics (IOSR-JAP), vol. 6, no. 1, pp. 22-28, 2014.

[163] T. Ohsaka, F. Izumi and Y.Fujiki, Raman Spectrum of Anatase, TiO_2, Journal of Raman Spectroscopy, Vol. 7, 6, 1978.

[164] A. Saranya, J. Pandiarajan and N. Prithivikumaran, Synthesis and characterization of TiO_2/PS nano structure for sensor applications, International Journal of Technical Research and Applications e-ISSN: 2320-8163, 2016, PP. 57-60.

[165] S. Hirasawa, Y. Saito, S. Nezu, S. Ohashi and H. Maruyama, Analysis of Drying Shrinkage and Flow Due to Surface Tension of Spin-Coated Films on Topographic Substrates, IEEE transactions on semiconductor manufacturing, vol. 10, no. 4, 1997.

[166]Y. Djaoued, S. Badilescu, P. V. Ashrit and J. Robichaud, Vibrational Properties of the Sol-Gel Prepared Nano- crystalline TiO2 Thin Films, The Internet Journal of Vi-brational Spectroscopy, Vol. 5, Section 4, 2001.

[167] D. C. Bradley, R. C. Mehrotra and D. P. Gaur, “Metal Alkoxides,” Academic Press, New York, 1978.

[168] C. M. Phillippi and S. R. Lyon, “Longitudinal-Optical Phonons in TiO2 (Rutile) Thin-Film Spectra, Physical Review *B*, Vol. 3, No. 6, 1971, pp. 2086-2087.

[169] X.Ye, C.Zheng, L.Ma, X.Huang, Microemulsion-assisted hydrothermal preparation and infrared radiation property of TiO2 nanomaterials with tunable morphologiesand crystal form Materials Science in Semiconductor Processing 31(2015)295–301.

[170] A. J. Haider, Z. N. Jameel, S.Y. Taha, Synthesis and Characterization of TiO2 Nanoparticles via Sol-Gel Method by Pulse Laser Ablation, Eng. &Tech.Journal, Vol.33, Part (B), No.5, 2015.

[171] D. Vasconcelos, V.Costa, E.Nunes, A.Sabioni, M.Gasparon, W. Vasconcelos, Infrared Spectroscopy of Titania Sol-Gel Coatings on 316L Stainless Steel, Materials Sciences and Applications, 2011, 2, 1375-1382

[172] S. A. Norton, Acidification and Acid Rain, book, chapter 9, University of Maine, Orono, ME, USA, 2003.

[173] D.Kong, Y. Zheng, M.Kobielusz, Y.Wang, Z.Bai, W. Macyk, X.Wang , J. Tang, Recent advances in visible light-driven water oxidation and reduction in suspension systems, Materials Today ,Volume 21, Number 8 ,October 2018.

[174] V.Kumaravela , S.Mathewa, J.Bartletta, S.C. Pillaia, Photocatalytic hydrogen production using metal doped TiO2: A review of recent advances, Applied Catalysis B: Environmental 244 (2019) 1021–1064.

[175] D.Chen, Y.Cheng, N.Zhou, P.Chen , Y.Wang, K.Li,S.Huo, P.Cheng, P.Peng, R.Zhang, L.Wang, H.Liu,Y.Liu, R.Ruan, Photocatalytic degradation of organic pollutants using TiO2-based photocatalysts: A review, Journal of Cleaner Production 268 (2020) 121725.

[176] A.O.Juma, I.O. Acik, V.Mikli, A.Mere, M. Krunks, Effect of solution composition on anatase to rutile transformation of sprayed TiO2 thin films. Thin Solid Films 2015, 594, 287–292.

[177] J.Spiridonova, A.Katerski, M.Danilson, M.Krichevskaya, M.Krunks , I.O.Acik, Effect of the Titanium Isopropoxide:Acetylacetone Molar Ratio on the Photocatalytic Activity of TiO_2 Thin Films, Molecules **2019**, 24, 4326.

[178] M.Yurddaskal, M.Yurddaskal, T.Dikici, H.Durmus, effect of annealing temperatures on the crystallization and photocatalytic activity of micro-nanoporous TiO_2 films produced by electrochemical anodization, JOTCSA. 2018, 5, 85-92.

[179] Wua C-Y, Leeb Y-L, Lob Y-S, Lina C-J, Wua C-H ,Thickness-dependent photocatalytic performance of nanocrystalline TiO2 thin films prepared by sol–gel spin coating. Appl Surf Sci ,2013, 280:737–744.

[180] Aprile C, Corma A, Garcı´a H ,Enhancement of the photocatalytic activity of TiO_2 through spatial structuring and particle size control: from subnanometric to submillimetric length scale. Phys Chem Chem Phys, 2008, 10:769–783

[181] L.B.Xiong, J.L.Li, B.Yang, Y.Yu, Ti^{3+} in the Surface of Titanium Dioxide: Generation, Properties and Photocatalytic Application, Journal of Nanomaterials 2011, 2012,

[182] M.Seery, N.Nolan, M.Pelaez, A.G. Kontosd, A Review on the Visible Light Active Titanium Dioxide Photocatalysts for Environmental Applications, Applied Catalysis B 125 (2012) 331– 349.

[183] M. Danish, S.Ambreen, A.Chauhan, A.Pandey, Optimization and comparative evaluation of optical and photocatalytic properties of TiO2 thin films prepared via sol–gel method, Journal of Saudi Chemical Society (2015) 19, 557–562.

[184] H. A. Le, L. T. Linh, S. Chin, and J. Jurng, Photocatalytic degradation of methylene blue by a combination of TiO2- anatase and coconut shell activated carbon, Powder Technology, vol. 225, (2012) 167–175.

[185] R.-J. Wu, C.-C. Chen, C.-S. Lu, P.-Y. Hsu, and M.-H. Chen, Phorate degradation by TiO2 photocatalysis: parameter and reaction pathway investigations, Desalination, vol. 250, no. 3 (2010) 869–875

[186] G. Wang, F. Wu, X. Zhang, M. Luo, and N. Deng, Enhanced TiO2 photocatalytic degradation of bisphenol E by β- cyclodextrin in suspended solutions, Journal of Hazardous Materials, vol. 133, no. 1–3, pp. 85–91, 2006.

[187] S.Mondal, Ma. E. De Anda Reyes, U.Pal, Plasmon induced enhanced photocatalytic activity of gold loaded hydroxyapatite nanoparticles for methylene blue degradation under visible light, *RSC Adv*, 14, (2017) 8633-8645.

[188] H.Persson, Photocatalytic oxidation for VOC abatement, MSc Thesis Project, Department of Chemical Engineering and Technology, 2015.

[189] R.Messemeche, H.Saidi, A.Attaf, Y.Benkhetta, S.Chala, R.Nouadji, R.Azizi, Elaboration and characterization of nano-crystalline layers of transparent titanium dioxide (Anatase-TiO_2) deposited by a sol-gel (spin coating) process, Journal de Surfaces and Interfaces 19 (2020) 100482.

[190] N.Khatun, S.Tiwari, C. P. Vinod, C.M.Tseng, S.W.Liu, S.Biring, S.Sen, Role of oxygen vacancies and interstitials on structural phase transition, grain growth, and optical properties of Ga doped TiO_2, Journal of Applied Physics 123, 245702 (2018).

[191] T. Ali, P. Tripathi, A. Azam, W. Raza, A.S. Ahmed, A. Ahmed, M. Muneer, Photocatalytic performance of Fe-doped TiO2 nanoparticles under visible-light irradiation, Mater. Res. Express 4 (1) (2017) 015022.

[192] H.-.J. Lin, T.-.S. Yang, M.-.C. Wang, C.-.S. Hsi, Structural and photodegradation behaviors of Fe3+-doping TiO2 thin films prepared by a sol–gel spin coating, J. Alloys Compd. 610 (2014) 478–485.

[193] N.R. Mathews, M.A.C. Jacome, E.R. Morales, J.A.T. Antonio, Structural and spectroscopic study of the fe doped TiO2 thin films for applications in photocatalysis, Phys. Status Solidi (c) 6 (S1) (2009) S219–S223.

[194] T. Okajima, T. Yamamoto, M. Kunisu, S. Yoshioka, I. Tanaka, and N. Umesaki, Jpn. J. Appl. Phys. 45, 7028 (2006).

[195] A. N. Banerjee, S. W. Joo, and B.-K. Min, J. Nanomater. 2012, 1 (2012).

[196] J. Chae,J.Lee,J.H.Jeong,M.Kang,Hydrogen production from photo splitting of water using the Ga-incorporatedTiO2 prepared by a solvothermal method and their characteristics ,Bull.KoreanChem.Soc 30 (2009)302–308.

[197] A.N.Banerjee,S.W.Joo,B.K.Min,Photocatalyticdegradationof organic dyebysol–gel-derived Gallium-doped anatase titanium oxide nanoparticles for environmental remediation, J. Nanomater. (2012).

[198] J. Zhu, W. Zheng, B. He, J. Zhang, M. Anpo, Characterization of Fe-TiO2 photocatalysts synthesized by hydrothermal method and their photocatalytic reactivity for degradation of XRG dye diluted in water, J. Mol. Catal. A 216 (2004) 35–43.

[199] J. Zhu, F. Chen, J. Zhang, H. Chen, M. Anpo, Fe^{3+}-TiO2 photocatalysts prepared by combining sol–gel method with hydrothermal treatment and their characterization, J. Photochem. Photobiol. A 180 (1–2) (2006) 196–204.

Abstract

Elaboration and characterization of undoped and doped titanium dioxide thin layers by sol gel (spin coating) for photocatalytic applications.

Titanium dioxide thin films were deposited by sol-gel spin coating technique using titanium tetra-isopropoxide, absolute ethanol and acetylacetone as precursor solution, solvent and catalyzer, respectively. The effect of the solution concentration, rotation speed, molar ratio and gallium doping concentration on the structural, morphological, optical and photocatalytic properties of TiO_2 thin films was studied. All films were characterized by multiple techniques such as X-ray diffraction (XRD), UV-Visible spectroscopy, scanning electron microscope (SEM), photoluminescence (PL) spectroscopy and Fourier transform infrared (FTIR) spectroscopy to investigate the physical properties of titanium dioxide films. X-ray diffraction analysis shows that all films are oriented preferentially along to (101) plane. SEM images show that the films are homogenous, uniform and dense with some holes and cracks. The optical transparency of TiO_2 films around to 90% in visible range which related to good crystalline state of the films. The direct band gap was varied between 2.99 and 3.6 eV. The photoluminescence analysis revealed mainly three emission peaks (ultraviolet, blue and green) corresponding to the near band edge (NBE) and defect levels (DL) emissions. It found at 0.2 M, the samples have a photocatalytic property with the photodegradation rate reach to 84%. The latter is improved used galuim doping TiO_2 which became equal to 95%. Whereas, the photodegradation rate reaches to 94 % at t = 180 min in undoped TiO_2 films with molar ratio y = 0.66. The elaborated films (deposited at 4000 rpm) as a photocatalyst to change the water acidity from pH = 4.8 to pH = 7.4 with produce H_2 gas. The latter used as a promising fuel for the future that protects the environment from pollution.

Key words:

Thin layers, sol-gel, titanium dioxide, photocatalytics, gallium doping, Methylene bleu, structural properties, optical properties, organic pollution.

Résumé :

Elaboration et caractérisation de couches minces de dioxyde de titane non dopées et dopées par sol gel (spin coating) pour des applications photocatalytiques.

Des films minces de dioxyde de titane ont été déposés par une technique de revêtement par centrifugation sol-gel en utilisant du tétra-isopropoxyde de titane, de l'éthanol absolu et de l'acétylacétone comme solution précurseur, solvant et catalyseur, respectivement. L'effet de la concentration de la solution, de la vitesse de rotation, du rapport molaire et de la concentration de dopage au gallium sur les propriétés structurales, morphologiques, optiques et photocatalytiques des couches minces de TiO2 a été étudié. Tous les films ont été caractérisés par plusieurs techniques telles que la diffraction des rayons X (XRD), la spectroscopie UV-visible, le microscope électronique à balayage (MEB), la spectroscopie par photoluminescence (PL) et la spectroscopie infrarouge à transformée de Fourier (FTIR) pour étudier les propriétés physiques du dioxyde de titane des films. L'analyse par diffraction des rayons X montre que tous les films sont orientés préférentiellement le long du plan (101). Les images SEM montrent que les films sont homogènes, uniformes et denses avec quelques trous et fissures. La transparence optique des films de TiO_2 autour de 90% dans le domaine du visible qui est liée au bon état cristallin des films. La bande interdite directe variait entre 2,99 et 3,6 eV. L'analyse de photoluminescence a révélé principalement trois pics d'émission (ultraviolet, bleu et vert) correspondant aux émissions de bord de bande proche (NBE) et de niveaux de défaut (DL). On constate qu'à 0,2 M, les échantillons ont une propriété photocatalytique avec un taux de photodégradation atteignant 84%. Ce dernier est amélioré utilisé galuim dopant TiO2 qui est devenu égal à 95%. Alors que le taux de photodégradation atteint 94% à t = 180 min dans des films de TiO2 non dopés avec un rapport molaire y = 0,66. Les films élaborés (déposés à 4000 tr / min) en tant que photocatalyseur pour changer l'acidité de l'eau de pH = 4,8 à pH = 7,4 avec du gaz H_2. Ce dernier est utilisé comme un carburant prometteur pour l'avenir qui protège l'environnement de la pollution.

Mots clés:

Couches minces, sol-gel, dioxyde de titane, photocatalytique, dopage au gallium, bleu de méthylène, propriétés structurales, propriétés optiques, pollution organique.

الملخص

تحضير وتوصيف طبقات رقيقة من ثاني أكسيد التيتانيوم غير المطعم والمطعم بواسطة تقنية الطرد المركزي سائل – هلام من أجل تطبيقات التحفيز الضوئي.

تم ترسيب الأغشية الرقيقة من ثاني أكسيد التيتانيوم بواسطة تقنية الطرد المركزي سائل-هلام باستخدام التيتانيوم رباعي الأيزوبروبوكسيد ، والإيثانول والأسيتيل الأسيتون كمصدر، مذيب ووسيط ، على التوالي. تم دراسة تأثير تركيز المحلول، سرعة الدوران، النسبة المولية وتركيز التطعيم بعنصر الغاليوم على الخواص التركيبية والمورفولوجية والبصرية والتحفيز الضوئي للشرائح الرقيقة لثاني أكسيد التيتانيوم. تم توصيف جميع الشرائح بعدة تقنيات مثل مطيافية انعراج الأشعة السينية، مطيافية الأشعة فوق البنفسجية - المرئية ، المجهر الإلكتروني الماسح، مطيافية التألق الضوئي و مطيافية الأشعة تحت الحمراء (FTIR) لدراسة الخصائص الفيزيائية لشرائح ثاني أكسيد التيتانيوم المحضرة. يوضح تحليل طيف انعراج الأشعة السينية أن نمو جميع الشرائح يتم بشكل تفضيلي على طول المستوى (101). تظهر صور المجهر الإلكتروني الماسح أن الأفلام متجانسة وموحدة وكثيفة مع بعض الثقوب والشقوق. تبلغ الشفافية الضوئية لشرائح ثاني أكسيد التيتانيوم حوالي 90٪ في المجال المرئي المرتبط بالحالة البلورية الجيدة للشرائح. كما تتراوح قيم فجوة النطاق الممنوع المباشرة بين 2.99 الكترون فولط و3.6 الكترون فولط. كشف تحليل مطيافية التألق الضوئي بشكل أساسي عن ثلاث قمم انبعاث (فوق بنفسجي، أزرق وأخضر) توافق الانبعاثات من حافة النطاق القريب ومستويات العيوب. ويلاحظ أنه عند 0.2 مولارية، تتمتع العينات بخاصية تحفيز ضوئي بمعدل تحلل ضوئي يصل إلى 84٪. تم تحسين هذا المعدل باستخدام التطعيم بواسطة عنصر الغاليوم والذي أصبح يساوي 95 ٪. بينما وصل معدل التحلل الضوئي إلى 94٪ في مدة 180 دقيقة في الشرائح الرقيقة لثاني أكسيد التيتانيوم المحضرة بنسبة مولارية 0.66 = y . في حين وجد ان الشرائح الرقيقة (المحضرة عند 4000 دورة في الدقيقة) يمكن استخدامها كمحفز ضوئي لتغيير حموضة الماء من PH =4.8 إلى PH= 7.4 مع انتاج غاز ثنائي الهيدروجين و الذي يستخدم في المستقبل كوقود واعد يحمي البيئة من التلوث.

الكلمات الدالة:

الطبقات الرقيقة، سائل-هلام، ثاني أكسيد التيتانيوم، التحفيز الضوئي، التطعيم بالغاليوم، أزرق الميثيلين، الخصائص البنيوية، الخصائص البصرية، التلوث العضوي.